STREAMING BIREFRINGENCE AS A HYDRODYNAMIC RESEARCH TOOL

Thesis by

Salvatore Philip Sutera

In Partial Fulfillment of the Requirements

For the Degree of

Doctor of Philosophy

California Institute of Technology

Pasadena, California

1960

ACKNOWLEDGEMENTS

The author wishes to express his gratitude to Professor J. H. Wayland, who directed this research. His enthusiasm toward the work was always encouraging, and without his cooperation this thesis could not have been completed when it was.

Thanks are also due to Professors W. D. Rannie and J. K. Knowles for many helpful discussions of certain aspects of the work.

This work was partially supported by the Engineering Sciences Division of the National Science Foundation under contract Number G-2400. Approximately one-third of the work represented here was conducted while the author was holder of the Shell Oil Company Fellowship.

Finally, the author is deeply appreciative of the labor invested in this thesis by his wife, Celia. In addition to spending many hours at the calculating machine, she typed both the original and final drafts of this thesis.

ABSTRACT

An optical system capable of providing precise pointwise measurements of streaming birefringence (SBR) was used to explore the flow of dilute solutions of tobacco mosaic virus between rotating eccentric cylinders. The local relationship between the observed optical anisotropy and the rate of strain tensor calculated from the theoretical solution for the particular flow field was studied. The relationship is apparently in accord with the conclusions of the orientation theory for a sufficiently dilute solution of rigid macromolecules in generalized two-dimensional flow.

The general problem of using streaming birefringence of colloidal solutions to visualize two-dimensional laminar flows is considered. The conclusion is reached that a clear and unambiguous kinematic interpretation of SBR in such fluids is possible only for a restricted class of flows. If the flow is such that the angle between the streamline and the principal rate of strain axes is not less than 35°, then to a good approximation SBR can give the magnitude and direction of the principal strain rates. This information, it is shown, is sufficient to permit calculation of the entire velocity field if the velocity is known on all boundaries.

In the most general flow situations, SBR of colloidal solutions cannot indicate the orientation of the rate of strain tensor. SBR in certain birefringent pure liquids may yield the necessary information even in the most general flows. These pure liquids hold promise of being valuable flow visualization agents.

TABLE OF CONTENTS

TABLE OF CONTENTS (Cont'd)

1.0 Introduction

During the past thirty to forty years a considerable amount of attention has been given to the problem of visualizing complex flow situations by means of doubly refracting fluid systems. The phenomenon of streaming birefringence or flow double refraction, which certain liquids and colloidal systems are found to exhibit when set in motion, has an undeniable appeal as a possible tool for hydrodynamic research. The use of such a tool, requiring only the passage of a beam of polarized light through the test flow field, appears at first sight to be free of any distorting influence on the flow which is being observed. In several instances streaming birefringence has already proven itself invaluable to studies of transition to turbulence and flow separation. Such studies are, however, of a qualitative nature, and the utility of this optical technique for the execution of precise quantitative velocity measurements had not been effectively demonstrated when this research program was initiated.

The basic literature on the subject of streaming birefringence is dominated by efforts aimed at gaining an understanding of the microhydrodynamics which govern the optical phenomenon. Some of the more important of these writings will be briefly discussed in the second part of this thesis. In addition a few noteworthy experimental programs have been reported in which attempts were actually made to construct flow patterns of varying generality from observed interference patterns. Unfortunately the latter works have not been based on microhydrodynamical theories but rather

on hypotheses or physical arguments of a macroscopic sort. The results of these experimental programs could not be called encouraging for the use of streaming birefringence as a hydrodynamic research tool.

The measuring techniques employed in the aforementioned experimental investigations are almost exactly those of the method of photoelasticity. The optical method of stress analysis known as photoelasticity also experienced its development over the past thirty or so years; but by 1940 this tool, which might be called the solid-state analog of streaming birefringence, had definitely outgrown the formative stage in which its results were only of a qualitative nature, and had achieved the full stature of a powerful technical instrument of quantitative stress analysis in two dimensions. As such, it exceeds all other methods in reliability, scope, and practicability. It is not at all derogatory toward the experimentalists in the field of applied streaming birefringence to suggest that, in a majority of instances, the highly advanced techniques of photoelasticity have exerted an influence on their approach to the application of the phenomenon to hydrodynamic analysis.

But if the success of photoelasticity has to some degree motivated investigations into the use of flow birefringence as a hydrodynamic research tool, it might also be that the influence of photoelasticity has in certain respects hindered the advance of its fluid state sister. The desire to establish a stress-optic law for the birefringent fluids, just as has been done for the photoelastic solid, is evident in previous attempts to analyze flow fields from

photographs of interference patterns. The author firmly believes that to attempt the formation of a correlation between streaming birefringence and photoelasticity on such a basic point is incorrect and illogical, and in the long run will only serve to confuse the issue and thereby retard the progress of streaming birefringence as an experimental tool.

The stress-optic law of photoelasticity is based on experimental evidence accumulated over a long period of time by many notable physicists who measured the effect of stresses on the velocity of light in crystalline substances. This law governs a static or quasi-static situation. The situation in a flowing fluid is, on the contrary, a dynamic one. Furthermore, streaming birefringence, when it occurs, can be due to entirely different causes in one kind of system than in another. Theory and experiment agree quite well on the fact that birefringence in flowing colloidal solutions is due to orientation of anisotropic particles under the combined action of fluid stresses acting on the particle surfaces and thermal diffusion. This is obviously not the case in pure liquids and at this writing there is no satisfactory theory for birefringence in pure liquids. In concentrated polymeric solutions, network stresses seem to be responsible for streaming birefringence while in dilute polymer solutions it may be molecular distortion. It is easy to understand why any generalization concerning a basic law for streaming birefringence is dangerous.

The experimental work covered in this thesis deals solely with the flow birefringence of very dilute colloidal solutions, the solvent

of which is a Newtonian liquid. Recently a theory for the orientation of rigid ellipsoidal particles in a general two-dimensional flow has been completed by Wayland [1]. The theory is essentially an extension of the highly successful orientation theory of Peterlin and Stuart [2], [3] for simple shear flow to the more complicated general two-dimensional flow. This orientation theory is fundamentally important to the interpretation of birefringence measurements made within general two-dimensional flows. It deals with the validity of simple Couette flow calibrations of the birefringent medium for application to the general flow. It tells in quantitative terms where such a calibration might be applied to the general flow with reasonable accuracy.

The primary purpose of the experimental work reported in this thesis is to test this extended orientation theory by making birefringence measurements within a known two-dimensional flow of a general type. To this end, it was necessary to construct an experimental apparatus capable of providing the controlled flow, and an optical system of instrumentation capable of yielding precise localized measurements of flow birefringence at any desired position in the flow field.

The second objective of the thesis is to study the problem of reconstructing a general two-dimensional velocity field from the information which, according to the orientation theory, is provided by birefringence measurements. A satisfactory solution to this problem is as fundamentally important as the establishment of a foundation theory to the basic question of the utility of streaming birefringence for flow visualization.

2.0 Review of Previous Work

The literature on theories of streaming birefringence is quite extensive. Two excellent and complete reviews of this literature may be found in the articles by Cerf and Scheraga [2], and by Jerrard [3]. Specific attention will be drawn here only to a few of these theories, those pertinent to the development of the particular problem of this thesis. The reports by investigators who attempted to apply streaming birefringence to hydrodynamic analysis are comparatively few in number.

In 1923 Humphrey [4] used a solution of vanadium pentoxide to demonstrate qualitatively a few examples of laminar and turbulent flow. He said, however, that his experiments were only preliminary and offered no interpretation of the observed effect.

Alcock and Sadron [5] in 1935 attempted quantitative velocity measurements in flows of sesame oil, a pure liquid. Assuming that the birefringence of the pure liquid was proportional to the stresses existing in the liquid, they made use of the Newtonian stress-strain-rate relation to relate birefringence to the velocity gradient in steady, parallel laminar flow. In such a flow the only component of the velocity gradient is normal to the streamlines. Yet an application was made to the flow through a slightly diverging channel without any apparent consideration for the component of the velocity gradient along the streamlines. In this particular case velocity profiles were constructed for several positions along the channel, and the integrals of these profiles across the channel sections only differed by about 4 per cent. However, a value for the actual

volumetric flow rate through the channel was not given. Velocity profiles were also constructed for laminar flow between straight parallel walls and reasonable agreement with theory was obtained. To measure the rather small effects produced by sesame oil the investigators used these birefringences to modify the birefringence of a gypsum full wave plate. By measuring the shift in the interference fringe of the wave plate with a spectrometer, they arrived at the liquid birefringence.

The possibilities of using bentonite solutions for visualizing complex two-dimensional flows were discussed in two notes by Hauser and Dewey [6], [7]. Dewey [8] made a detailed study of the problem in his doctoral dissertation in 1941. In it he listed certain factors considered to be responsible for streaming double refraction, either singly or in combination, and stated that no satisfactory theoretical formulae had been developed to relate the flow variables to the optical phenomenon. He hypothesized furthermore that a Couette cell calibration could take the place of theory and relate the local birefringence measurements in a complex flow to the streamline direction and the velocity gradient normal to the streamline. Utilizing both still and motion photography, Dewey examined the interference patterns due to flow normal to a circular cylinder as well as that past several automobile models. In the former case he initiated a quantitative interpretation of his optical measurements but did not attempt an integration to get the velocity field.

Weller et al [9], [10] did some work similar to that of Dewey. Again a "photoviscous law" directly analogous to the stress-optic

law of photoelasticity was assumed to hold, but only a pure shear type of velocity gradient was included in the law. Some photographs were presented of the flow of very viscous polymer solutions around obstacles and through channels, but no attempts to construct the velocity fields were made. Ullyott [11] used vanadium-pentoxide solutions to demonstrate the aspects of flows past certain obstacles. In a discussion following Ullyott's article, R. T. Knapp wrote that it seemed possible, although somewhat involved, to obtain quantitative results from photographic records of interference patterns in two-dimensional flows.

Rather effective qualitative applications of streaming birefringence to problems of flow separation and transition to turbulence have been reported by Leaf [12], Binnie [13], Binnie and Fowler [14], and Lindgren [15], [16], [17]. Leaf for example observed the flow of a birefringent solution through a transparent model of a locomotive firebox. On the basis of his observations he recommended design changes aimed at eliminating erosion of boiler tubes due to the suspension of solid ash in the actual gas flow.

Rosenberg [18] presented a study of fluid flow analysis by means of streaming birefringence in 1952. In it he discussed the construction of a general flow pattern, due perhaps to flow past an obstacle, based on the hypothesis that the birefringence data can be interpreted to give streamline direction and the velocity gradient component which is normal to the streamlines. This interpretation would be performed by means of a Couette cell calibration of the birefringent fluid. He also included a layout of a test facility for

model studies which purportedly was under construction at the time at the David Taylor Model Basin. Actually this facility was never built.

Rosenberg then went on to consider the orientation of long slender rod-like particles in a general two-dimensional flow. Assuming only that the particles rotate with the fluid while not disturbing the fluid motion, he was led to raise some questions concerning the motion of the particles in divergent flow. However, he neglected the effect of Brownian diffusion in his treatment and any discussion of stability which does not include this effect is not complete and lacks physical significance.

In a subsequent section of his report Rosenberg turned to the question of hydrodynamic studies utilizing doubly refracting pure liquids. Stating that double refraction in such systems is due primarily to deformation rather than orientation of molecules (which is not a generally accepted theory), he expected a close analogy between the flow birefringence and photoelasticity to hold. The assumption followed that "the birefringence is a maximum along the plane of maximum shear and the magnitude of the birefringence is proportional to the maximum shear." Whether the term "shear" is meant to refer to shear stress or shear rate is not clear from this statement, but it probably refers to the former since the notation τ_{max}, conventionally applied to maximum shear stress, appears farther on in the text. In any event, it is assumed that birefringence data can give the maximum shear (stress) and the orientation of the plane of maximum shear (stress) with the aid of a Couette cell calibration.

Since in the final analysis Rosenberg wanted to deal with the kinematic properties of the flow, velocity gradients and eventually velocities, he was faced with the problem of converting his assumed stress-optical calibration into a rate of strain-optical calibration. This he solved by assuming that the particular liquid was Newtonian, i. e., that it was characterized by a simple linear stress-rate of strain relationship. Based on this assumption the calibration and the birefringence data could be interpreted to give the maximum rate of shear strain, and the orientation of the plane of maximum rate of shear strain. In summary, an assumption that a birefringent pure liquid is governed by a stress-optic law was coupled with an assumption that the same liquid is Newtonian in order that birefringence data could be translated into kinematic quantities. The former assumption has not been established. In fact the only notable theoretical treatment of the pure liquid case by Tolstoi [19] supports an orientation type theory even for the pure liquid. The validity of the latter assumption would of course depend on the particular liquid.

Finally Rosenberg proposed a method for numerically integrating the rate of strain components which would be derived from the birefringence measurements to get the streamlines and velocities throughout the unknown flow field. The method involves the introduction of the stream function and the integration of a second order partial differential equation for this function. The integration problem is an important one and a later section of this thesis is devoted to it. It will be shown therein that the integration of the strain-rate components, if they are known, to get the velocity field

can be effected in a manner much more straightforward than that proposed by Rosenberg.

In his doctoral research Young [20] set out to make quantitative measurements in flows around submerged bodies using aqueous solutions of milling yellow dye [21], [22], [23], [24], a colloidal system possessing very strong optical activity. Young also accepted the idea that the flow double refraction can be simply related to the fluid stresses. He used a Hele-Shaw type of apparatus which confines the flow between closely spaced parallel plates, and the polarized light ray passed through the flow in a direction normal to these plates. Young found that he could readily obtain the isoclinic patterns in flows around submerged bodies, but the isochromatic patterns were generally absent.* Thus with only a part of the optical data in hand he was incapable of even attempting to construct a flow field. Furthermore the observed isoclinic patterns did not agree with the theoretically predicted ones. Young believed that this discrepancy could be attributed either to non-Newtonian effects or to the fact that the optical phenomenon was not governed by a stress law. However, his hypothesis that the velocity gradient in the direction parallel to the light beam would not affect the angle of isocline was not supported by a satisfactory demonstration, theoretical or experimental. A method for predicting flow patterns was also proposed in the thesis. It is essentially the same as that proposed by Rosenberg [18], and will be discussed in a later section.

---

* The isoclinic patterns tell essentially the orientation of the principal optical axes throughout the field while the isochromatic patterns give the retardation or birefringence everywhere. This is true for any doubly refracting system, be it a photoelastic solid or a birefringent fluid.

The contribution of Prados [25] is also based on an assumed, but not proven, stress-optical relationship. His basic assumption was that the interference patterns produced by flow double refraction give the magnitude and direction of the maximum shearing stress at each point in the flowing liquid. He proposed that a Couette flow calibration of a given liquid could provide (1) the value of the maximum shearing stress corresponding to any particular isochromatic, and (2) the angle between the maximum shear stress plane and the axis of polarization of the incident light along any isoclinic. Following Rosenberg, Prados then converted his stress-optical calibration into a rate-of-strain-optical calibration by assuming that the maximum shear stress is directly proportional to the maximum rate of deformation (the principal value of the rate of strain matrix), the factor of proportionality being the coefficient of viscosity.

Using the technique of photoelasticity, Prados analyzed four two-dimensional flow situations: straight parallel flow, simple converging flow, simple diverging flow, and flow normal to a circular cylinder. In the first three cases Prados either knew or assumed he knew the streamlines throughout the flow, and hence the normal curves as well. Knowing the radii of curvature of the two orthogonal curves plus the maximum rate of deformation at any point, Prados was able to calculate the local velocity gradient normal to the streamline direction at the point. Using this, he integrated velocities along the normal curves starting from some bounding wall where the velocity was zero. In the case of the straight parallel streamlines the integrated velocity profile was

compared to a theoretical parabolic profile. A flow rate computed by integrating the calculated velocity profile over the channel section was also compared to a measured flow rate. The method gave quantitative agreement to within ± 10 percent.

The results obtained for the converging and diverging flows were checked by comparing flow rates only. Here the quantitative agreement was found to be ± 15 percent.

The streamlines were unknown in the case of flow normal to the circular cylinder. Here Prados followed the method proposed by Rosenberg to obtain values of the stream function at the corners of a square grid which he superposed on the photographs of the isoclinic and isochromatic patterns. This method requires numerical integration of a second order partial differential equation for the stream function. In order to carry out the integration Prados needed a measured flow rate, and consequently he could not use this information as a check on his velocity distribution. There were no existent theoretical treatments corresponding to the actual bounded flow against which Prados might have compared his derived streamline pattern. Hence he was not able to assess the validity of his integration, nor could he define any error limits for his results in this most interesting case of two-dimensional flow with streamlines unknown a priori.

Wayland [26] reported some interesting measurements in 1954. Using both colloidal solutions and pure liquids he examined the flow between rotating concentric cylinders at speeds above and below the transition to Taylor vortex flow. In such a shear flow he found that

the birefringence in a pure liquid appears to depend on the mean velocity gradient even in the turbulent regime.

Notable in Wayland's work is his use of a new technique for making precise localized birefringence measurements at points within the flow field. He used a very narrow well-collimated beam of light which could be translated across the gap between the cylinders. Measurements were possible as close as 0.1 mm to a wall. In addition, quite small birefringences, much less than one full wave length retardation, could be measured with great accuracy and relative ease. With such a technique one no longer needs to analyze the rather coarse interference patterns which result from the photographic method previously mentioned. Even slow flows of very weakly birefringent systems can be analyzed precisely with this optical system, even if a full wave length retardation is achieved nowhere in the flow field. The optical system employed in the current research program is in principle the same as the Wayland system. It will be described in more detail in a later section of this thesis.

3.0 The Orientation Theory for General Two-Dimensional Flow

Wayland [1] treats the streaming birefringence due to the orientation of a population of rigid axi-symmetrical ellipsoidal particles in a general two-dimensional laminar flow. The concentration of particles in the flowing liquid is taken as sufficiently small to permit the neglect of interactions between particles. Initially the treatment is confined to a monodisperse population, i.e., one in which all the particles are identical in size as well as shape. The semi-axes of the particles are $a_1 \neq a_2 = a_3$, and these lengths are taken to be small compared to the spatial scale of variation of the flow. The minimum particle dimension is restricted to be greater than 10 Angstrom units, thereby permitting application of continuum fluid mechanics to the solvent flow.

The orientation state of the particle population is described by means of an orientation distribution function $F(\theta, \varphi)$, where θ and φ are the polar and azimuthal angles respectively in some appropriate reference frame XYZ. The physical significance of the function F is most easily represented by a distribution of points on the surface of a unit sphere (Figure 1). The orientation (θ, φ) of the major or symmetry axis of each particle is represented by a point P having the angular coordinates θ and φ on the unit sphere surface. The number of such points contained within the elemental solid angle, θ to $\theta + \delta\theta$, φ to $\varphi + \delta\varphi$, per unit solid angle is defined as the orientation density or distribution function F at θ, φ. Strictly speaking F is also a function of time so that the above definition should be rephrased to read that $F(\theta, \varphi, t)$ is defined as

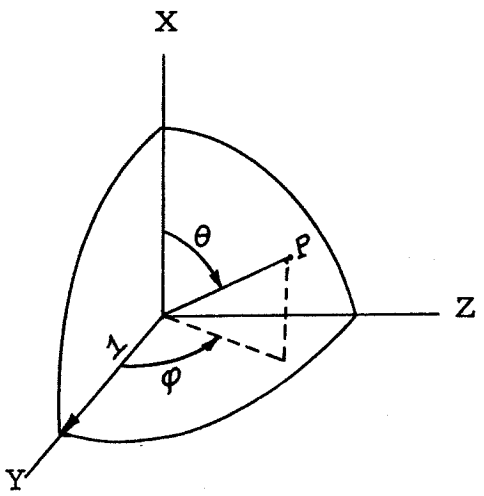

Figure 1

the number of points in the elemental solid angle per unit solid angle at the particular instant t. Thus it is seen that F, being defined as the ratio of a number to a solid angle, is a dimensionless scalar quantity.

In the absence of all orienting influences, such as flow of the solvent liquid, all orientations are equally probable, and normalization yields $F = \frac{1}{4\pi}$ for such an isotropic state. This isotropy, or lack of orientation, is maintained by rotational diffusion, a manifestation of Brownian movement, as long as no orienting field is imposed. The law governing this diffusion says that the flux of points at a position θ, φ on the unit sphere due to the existence of a distribution gradient there, is given by

$$\underset{\sim}{i}_{dif} = -D \nabla F \qquad (1)$$

where D is known as the rotary diffusion constant. Thus, if no other effect is present, this diffusion always acts to even out any non-uniformities in the function $F(\theta, \varphi, t)$.

The role played by the hydrodynamic field in creating a non-isotropic suspension is based on Jeffery's solution [27] for the motion of ellipsoidal particles in an arbitrary laminar viscous flow. Jeffery assumed that the particle motion is entirely due to

surface forces exerted by the fluid, and that for slow relative motions the angular accelerations, and hence the net moment acting on the particle, are always zero. He then was able to calculate the angular velocity of the particles due to the hydrodynamic forces. Wayland applies this procedure to the following specific case.

Take the XYZ coordinate system as fixed in direction but having an origin which moves with the center of mass of a particle. The flow is two-dimensional, parallel to the YZ plane (Figure 2), so that the velocity component u = 0, and both v and w are independent of X. A second coordinate system, xyz, is fixed in the particle with origin also at the center of mass and the x axis coincident with the symmetry axis of the particle (Figure 2). The orientation of the particle is described by the Euler's angles θ, φ, and ψ (Figure 2), where θ and φ are the polar and azimuthal angles made by the axis of symmetry with the XYZ directions. The angle ψ accounts for the spin of the particle about its axis of symmetry. However, it is further assumed that the x axis is an axis of symmetry with regard to the particle's optical properties as well, so that ψ does not enter into the final expressions for the birefringence.

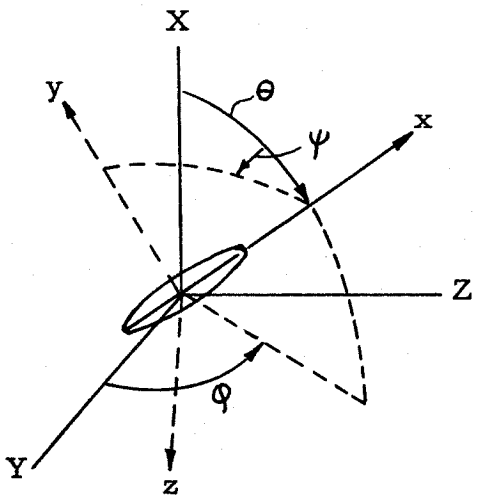

Figure 2

For the angular velocities $\dot{\theta}$ and $\dot{\varphi}$ of the particle's symmetry axis in this two-dimensional flow Wayland obtains

$$\dot{\theta} = b \sin\theta \cos\theta \left[e_{YY} \cos 2\varphi + e_{YZ} \sin 2\varphi \right] \qquad (2)$$

$$\dot{\varphi} = \frac{1}{2}\xi - b \left[e_{YY} \sin 2\varphi - e_{YZ} \cos 2\varphi \right] \qquad (3)$$

where

$$b = \frac{a_1^2 - a_2^2}{a_1^2 + a_2^2}$$, a shape parameter;

$$e_{YY} = \frac{\partial v}{\partial Y}$$

$$e_{YZ} = \frac{1}{2}\left(\frac{\partial v}{\partial Z} + \frac{\partial w}{\partial Y} \right)$$

and

$$\xi = \left(\frac{\partial w}{\partial Y} - \frac{\partial v}{\partial Z} \right),$$ the component of the rotation $(\nabla \times V)$ normal to the plane of flow.

ξ is, in fact, the only non-zero rotation component for the flow as defined.

It is important to understand that $\dot{\theta}$ and $\dot{\varphi}$ make up the instantaneous angular velocity of the particle when it is situated at a point in the flow where the kinematic parameters are ξ, e_{YY}, and e_{YZ}. The flow is taken as stationary, that is, it does not vary with time at any fixed point in space. The particle, however, is moving and sees a different state of flow at each

succeeding instant. The hypothesis is implicit here that the particle orientation is always perfectly adjusted to the ξ, e_{YY}, and e_{YZ} which it sees instantaneously. This is equivalent to assuming that relaxation or retardation of orientation is absent, an assumption which is consistent with Jeffery's original hypothesis that the angular acceleration of the particle is always zero. In order that this be so, the particle's inertia to rotation must be zero. Thus the results are expected to be valid only for very small particles in flows which are not too fast. In other words the treatment is a Stokesian one, good only for sufficiently low particle Reynolds numbers.

With a knowledge of the angular velocities $\dot{\theta}$ and $\dot{\varphi}$, it is possible to write an expression for the transport flux of particle orientations, or points on the unit sphere, at any position θ, φ on the unit sphere.

$$\underset{\sim}{i}_{str} = F\dot{\theta}\,\underset{\sim}{e}_{\theta} + F\dot{\varphi}\sin\theta\,\underset{\sim}{e}_{\varphi} \qquad (4)$$

where $\underset{\sim}{e}_{\theta}$ and $\underset{\sim}{e}_{\varphi}$ are unit vectors for the angular variables θ and φ. Now the net efflux of points per unit solid angle at any position on the unit sphere is given by the divergence of the sum of $\underset{\sim}{i}_{str}$ and $\underset{\sim}{i}_{dif}$ taken at the particular position. The rate of accumulation of particles having a particular orientation θ, φ is thus given by the general equation

$$\frac{\partial F}{\partial t} = -\nabla \cdot (\underset{\sim}{i}_{str} + \underset{\sim}{i}_{dif}) \qquad (5)$$

At a fixed position in the stationary flow the orientation distribution achieves a steady state, so that $\frac{\partial F}{\partial t}$ vanishes there. The steady state rotational diffusion equation may then be integrated to give the distribution function $F(\theta, \varphi)$ at the particular position. In terms of the spherical coordinates this equation takes the following form:

$$\nabla \cdot (F\dot{\theta}\, \underset{\sim}{e}_\theta + F\dot{\varphi} \sin\theta\, \underset{\sim}{e}_\varphi) - D\nabla^2 F = 0 \qquad (6)$$

At this stage Wayland makes a change in one of the independent variables which results in considerable simplification of the expressions for the angular velocities $\dot{\theta}$ and $\dot{\varphi}$, (Eqs. 2 and 3). Instead of referring the projection of the particle axis in the flow plane to the YZ axes which do not rotate (Figure 2), he wishes to refer it to the local principal rate of strain axes. Consider a fixed observation point O in the steady flow field (Figure 3). Since the flow is steady, there is a definite pair of orthogonal directions, the principal axes or eigenvectors of the rate of strain tensor, which lie in the plane of flow and can be used as reference axes. Call the principal axes p and q. These lie in the YZ plane and are inclined at some angle β to the YZ frame. Since the directions of the Y and Z axes are not changing, and since the state of flow at any fixed point

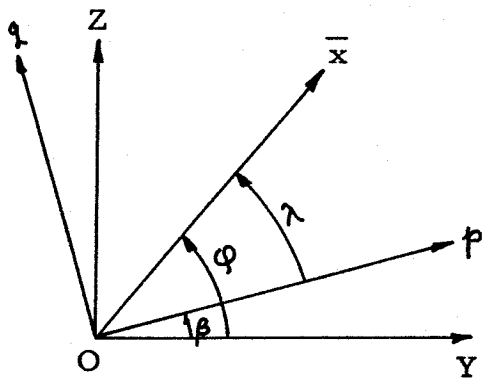

Figure 3

is not varying with time, β is seen as a constant angle by a stationary observer at O. To an observer moving with the particle, however, p and q rotate with respect to YZ, and β is consequently a function of time to such an observer. Let $\bar{x}$ represent the projection of the particle's axis of symmetry into the plane of flow. Then the instantaneous direction of this projection with respect to p and q is given by the new angle λ where

$$\lambda = \varphi - \beta \tag{7}$$

The angle β is fully determined at any point by a knowledge of the components of the strain-rate matrix with respect to the YZ axes. Taking advantage of the continuity relation, $e_{YY} + e_{ZZ} = 0$, one can show in a straightforward manner that

$$\sin 2\beta = \frac{e_{YZ}}{E}, \quad \cos 2\beta = \frac{e_{YY}}{E} \tag{8}$$

where

$$E^2 = e_{YZ}^{\ 2} + e_{ZZ}^{\ 2} \tag{9}$$

The quantity +E is one of the principal values (eigenvalues) of the rate of strain matrix. The other principal value is -E. When referred to principal coordinates, the rate of strain matrix assumes the simplified normal form

$$S = \begin{pmatrix} E & O \\ O & -E \end{pmatrix} \tag{10}$$

Substitution of $\varphi = \lambda + \beta$ into Eqs. 2 and 3 for the angular velocity components results in

$$\dot{\theta} = E\, b \sin\theta \cos\theta \cos 2\lambda \qquad (11)$$

$$\dot{\varphi} = \frac{1}{2}\xi - E\, b \sin 2\lambda \qquad (12)$$

The angular velocity $\dot{\varphi}$ is an absolute angular velocity. If the streamlines of the flow are curved, the particle motion will include a "solid body rotation" due to the mere curvature of the streamlines. With regard to the unit sphere used earlier as a means of illustrating the significance of the distribution function, the effect of this solid body rotation is to rotate the entire sphere about its polar axis (X in Figure 1). It contributes nothing to the migration of points on the sphere's surface, i.e., to the creation of a non-uniform distribution; hence it must be subtracted out of $\dot{\varphi}$. In performing this subtraction Wayland introduces a third coordinate system, $x'y'z'$, which is also convected with the particle, but which rotates with the streamline. The $y'z'$ axes lie in the flow plane and always retain the same orientation relative to the streamline along which the particle is being transported.

Figure 4 shows a particular observation point where the $y'z'$ axes coincide with the YZ axes. The velocity of a particle there is V and the streamline (s) has a radius of curvature ρ. By definition the $y'z'$ frame has an angular velocity

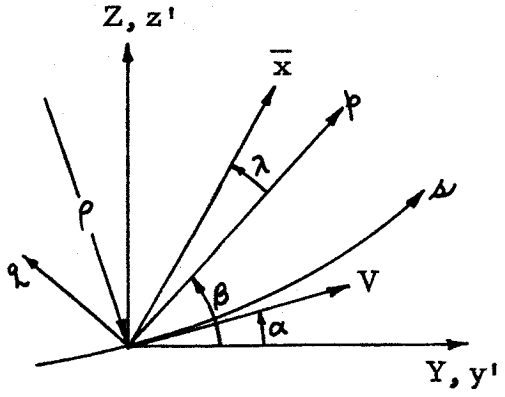

Figure 4

$$\Omega = \frac{V}{\rho} = \frac{\sqrt{v^2 + w^2}}{\rho} \tag{13}$$

at the point. It is this angular velocity which must be subtracted from $\dot{\varphi}$ before the transport flux $\underset{\sim}{i}_{str}$ can be correctly calculated.

If tan α is the slope of the streamline at the observation point referred to the YZ coordinate system, then

$$\Omega = V \frac{d\alpha}{ds} = V \frac{d}{ds} (\tan^{-1} \frac{w}{v}) \tag{14}$$

where ds is taken along the streamline. Performing the calculation, Wayland finds

$$\Omega = \frac{1}{2} \xi + E \sin 2(\beta - \alpha) = \frac{1}{2} \xi + E \sin 2\Lambda_o \tag{15}$$

The angle $\beta - \alpha = \Lambda_o$ is just that between the principal strain rate axis and the streamline direction at the point of observation. The angular velocity components referred to the rotating y'z' frame now become

$$\dot{\theta}' = \dot{\theta} = E b \sin\theta \cos\theta \cos 2\lambda \tag{16}$$

$$\dot{\varphi}' = \dot{\varphi} - \Omega = -E (b \sin 2\lambda + \sin 2\Lambda_o) \tag{17}$$

In terms of the variables θ and λ and the corrected angular velocities the transport flux ; Eq. 4, becomes

$$\begin{aligned} \underset{\sim}{i}_{str} &= F\dot{\theta}' \underset{\sim}{e}_\theta + F \dot{\varphi}' \sin\theta \underset{\sim}{e}_\lambda \\ &= E\Big[F b \sin\theta \cos\theta \cos 2\lambda \, \underset{\sim}{e}_\theta \\ &\quad - F(b \sin 2\lambda + \sin 2\Lambda_o) \sin\theta \underset{\sim}{e}_\lambda\Big] \end{aligned} \tag{18}$$

Inserting this into the steady state diffusion equation Wayland finally obtains

$$\nabla^2 F = \sigma \amalg F \tag{19}$$

in which $\sigma = \frac{E}{D}$ and $\amalg$ is a differential operator defined by

$$\amalg F = -3b^2 \sin^2\theta \cos 2\lambda \cdot F + b \sin\theta \cos\theta \cos 2\lambda \cdot \frac{\partial F}{\partial \theta}$$

$$- (\sin 2\Lambda_o + b \sin 2\lambda) \frac{\partial F}{\partial \lambda} \tag{20}$$

The parameter σ indicates the relative importance of hydrodynamic distortion and Brownian movement in influencing the orientation. To obtain a solution for F, Wayland assumes that for sufficiently small values of σ, F can be represented by an infinite series in powers of σ:

$$F = \sum_{j=0}^{\infty} \sigma^j F_j \tag{21}$$

Substituting this series into the differential equation, Eq. 19, it is found that each of the F_j must satisfy

$$\nabla^2 F_{j+1} = \amalg F_j \qquad j = 0, 1, 2, \ldots \tag{22}$$

Each of the F_j is expanded in a series of Legendre polynomials and associated Legendre functions:

$$F_j = \sum_{n=0}^{j} a_{no,j} P_{2n}(\cos\theta)$$

$$+ \sum_{n=1}^{j} \sum_{m=1}^{n} (a_{nm,j} \cos 2m\lambda + b_{nm,j} \sin 2m\lambda) P_{2n}^{2m}(\cos\theta) \tag{23}$$

The normalization condition on F requires that

$$F_0 = \frac{1}{4\pi}$$

Starting with F_0 it is possible to solve successively for F_1, F_2, F_3, and so on from Eq. 22. Wayland has worked out the first five F_j (including F_0). These are given in his paper [1] and need not be listed here. The results of his calculations for the angle of isocline and the amount of birefringence are more directly pertinent to the thesis subject, and these will be discussed more thoroughly.

Before leaving the derivation of the distribution function it should be mentioned that the expansion procedure described above is somewhat classic in theories on streaming birefringence. Peterlin [28] gave such a solution for F in 1938, but his was a series in powers of the shape parameter b whose magnitude is bounded between +1 and -1. This solution was utilized by Peterlin and Stuart [29] in their orientation theory for simple shear flow. They gave the form of F for small σ out to three terms. In a treatment of the combined effect of an electrostatic field and a shear flow on rigid particle orientation, Demetriades [30] obtained a series solution for the distribution function in powers of

a parameter which contained the velocity gradient and the electric field intensity.

3.1 Calculation of the Angle of Isocline and the Amount of Birefringence From the Distribution Function

The theory governing the optical behavior of the oriented suspension is very clearly outlined in Jerrard's review paper [3]. The theory is due to Peterlin and Stuart [29] and has been extended by Snellman and Bjornstahl [31]. The latter took into account the effect of absorption of light by the particles and dealt in more detail with the internal electric field.

A monodisperse system showing no optical activity is assumed in which the particles are taken to be identical, uncharged, rigid, homogeneous ellipsoids of revolution. In order that the influence of the electric field of the incident light wave may be treated quasi-statically the largest particle dimension is restricted to be less than 1000 A. This restriction is set for the particles when in solution, since in some cases the size of the "dry" particles will be different because of possible changes due to solvation or swelling. The principal geometrical axes of the particles, the principal axes of dielectric susceptibility, and the principal axes of the absorption indices are all assumed coincident. The solution is assumed to be so dilute that interaction effects are negligible; hence the total effect of all the particles is just the sum of the effects produced by the individual particles.

The optical behavior of the oriented medium is determined by the induced polarization of the system in the electric field of

the incident light wave. This polarization has to be related to such macroscopic quantities as index of refraction and particle concentration in order that an expression for the birefringence can be reached. Following Sadron [32], [33], Bjornstahl and Snellman take the total induced polarization of the medium to result from the induced dipole moments on the particles and the isotropic polarization of the solvent. The calculation of the polarization leads to a dielectric permittivity tensor for the oriented suspension.

The isoclinic axes are the principal axes of this dielectric permittivity tensor. For quasi-stationary conditions the components of this tensor are proportional to the squares of the components of the refractive index tensor. Because of the two-dimensionality of the flow, the particles are oriented symmetrically with respect to the flow plane. Consequently one of the principal axes of permittivity is normal to the flow plane and the other two lie in it. The acute angle between the principal permittivity axes and the principal axes of rate of strain at the point of observation is called χ. This angle of isocline is related to the distribution function through the following integral relationship [3], [29]:

$$\tan 2\chi = \frac{\int_0^{\pi}\int_0^{2\pi} F \sin^3\theta \sin 2\lambda \, d\lambda \, d\theta}{\int_0^{\pi}\int_0^{2\pi} F \sin^3\theta \cos 2\lambda \, d\lambda \, d\theta} \qquad (24)$$

Substituting his results for F into Eq. 24, Wayland obtains

$$\chi = -\frac{\sigma \sin 2\Lambda_o}{6}\left[1 - \frac{\sigma^2}{27}\left(\sin^2 2\Lambda_o + \frac{24b^2}{35}\right) + O(\sigma^4)\right] \quad (25)$$

The negative sign appears because of the direction convention chosen for angles measured in the flow plane. Figure 3 shows that positive angles are measured counter clockwise from the p axis. Thus if the isoclinic axes are rotated from the pq frame in a clockwise sense, χ will be negative.

The flowing suspension exhibits three principal indices of refraction and is thus said to behave as a biaxial crystal. One of these principal indices pertains to the direction normal to the flow plane, which means that it is important only to a light ray whose electric vector vibrates normal to the flow plane. With the usual method of observation (to be explained in detail in a later section on experimental technique) the exploring light ray travels along the normal to the flow plane, and consequently only the difference between the other two principal indices can be measured. In Figure 5 is shown the relationship between the isoclinic axes, 1 and 2, and the principal strain rate axes at the observation point O. If the plane of polarization of the incident light ray is parallel to 01, then the velocity with which the light travels through the medium is determined by n_1, and similarly for the direction 02.

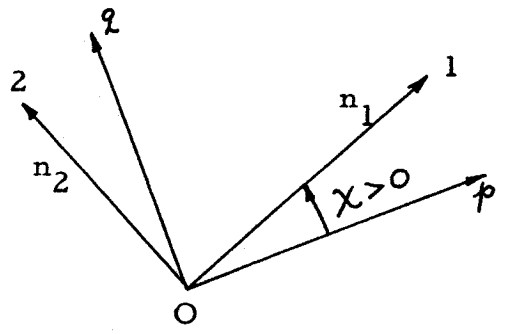

Figure 5

The amount of birefringence is $\Delta n = n_1 - n_2$, and according to the quasi-static optical theory [3], [29] Δn consists mainly of an optical anisotropy factor $(g_1 - g_2) = G$ and an orientation factor $f(\sigma, b, \Lambda_o)$:

$$\Delta n = 2\pi c \cdot \frac{G}{n} \cdot f(\sigma, b, \Lambda_o) \tag{26}$$

where c is the volume concentration of particles and n is the mean index of refraction of the solution. The optical factor contains the optical and geometrical properties of the particles. This factor is entirely independent of the flow state and the consequent orientation distribution. The orientation factor on the other hand is derived from the distribution function F through another integral formula:

$$f(\sigma, b, \Lambda_o) = \left\{ \left[\int_0^{\pi} \int_0^{2\pi} F \sin^3\theta \sin 2\lambda \, d\lambda \, d\theta \right]^2 + \left[\int_0^{\pi} \int_0^{2\pi} F \sin^3\theta \cos 2\lambda \, d\lambda \, d\theta \right]^2 \right\}^{1/2} \tag{27}$$

For this Wayland obtained

$$f(\sigma, b, \Lambda_o) = \frac{2\sigma b}{15} \left[1 - \frac{\sigma^2}{18} \left(\sin^2 2\Lambda_o + \frac{6b^2}{35} \right) + O(\sigma^4) \right] \tag{28}$$

From which

$$\Delta n = \frac{4\pi}{15} \cdot \left(\frac{G}{n} \right) cb\sigma \left[1 - \frac{\sigma^2}{18} \left(\sin^2 2\Lambda_o + \frac{6b^2}{35} \right) + O(\sigma^4) \right] \tag{29}$$

If in Eqs. 25 and 29 σ is replaced by $\frac{E}{D}$, it is possible to write

$$\chi = -\frac{\gamma_s}{12D}\left[1 - \frac{1}{27D^2}\left(\frac{\gamma_s^2}{4} + \frac{24b^2}{35}E^2\right) + \ldots\right] \quad (30)$$

$$\Delta n = \frac{4\pi}{15}\left(\frac{G}{n}\right)\frac{cEb}{D}\left[1 - \frac{1}{18D^2}\left(\frac{\gamma_s^2}{4} + \frac{6b^2}{35}E^2\right) + \ldots\right] \quad (31)$$

where $\gamma_s = 2E \sin 2\Lambda_o$ is just the rate of shear along the streamlines.

For a pure shear flow (Couette flow) $\Lambda_o = 45^o$ and Eqs. 25 and 29 reduce to the classical solution of Peterlin and Stuart. In a general two-dimensional flow the angle between the streamline direction and the principal strain rate axis may differ from 45^o. The results indicate that this will affect the angle of isocline no matter how small the principal strain rate E. It will not, however, influence the amount of birefringence until Δn ceases to be linearly dependent on E.

Wayland also considered the effect of polydispersity on and Δn. He concluded that a simple correspondence between optical measurements taken in Couette flow and those taken in a general flow is maintained as long as χ and Δn depend linearly on σ. Beyond the linear region there is no simple connection between the two cases unless $\Lambda_o = 45^o$. These remarks will be significant to the subject of the succeeding section of the thesis, viz. the problem of calibration.

It is necessary at this point to draw attention to a matter of nomenclature. So far the name "isoclinic axes" has been applied

to the principal axes of the dielectric permittivity tensor of the oriented medium. Reference has also been made to the principal indices of refraction which implies the existence of three principal "index of refraction" directions. The two sets of principal axes are actually the same. These principal directions, two of which lie in the flow plane and one normal to the flow plane, have to do with the direction of vibration of the dielectric displacement vector and not with the direction of the light ray. In this respect these directions might be most appropriately called "principal vibration directions", and in certain textbooks on optics they are so named. While most descriptive this last appellation is somewhat cumbersome. For the sake of convenience and simplicity, the name "principal optical axes", and often simply "optical axes", will be used quite frequently in the following sections of the thesis. This practice may conflict slightly with the accepted terminology of crystal optics wherein a "biaxial" crystal, having two "optic axes" of crystallographic significance, has three principal vibration directions. The thesis matter, however, deals solely with streaming birefringence in two-dimensional flowing systems so that this convention is expected to cause little or no confusion to the reader.

4.0 The Problem of Calibration of a Birefringent Colloidal Solution

In the preceding section the Wayland orientation theory for general two-dimensional flow was discussed. The essential conclusions of this theory are represented by Eqs. 25 and 28 which relate the orientation of the principal optical axes and the orientation factor at a fixed point in a steady two-dimensional laminar flow to the local kinematics of the flow. It was pointed out that the amount of birefringence is proportional to the orientation factor and that the factor of proportionality is dependent upon the optical and geometrical properties of the particles as well as the index of refraction of the solvent liquid. Furthermore both the quantities χ and f are expressed in terms of the parameter σ and not directly in terms of the principal strain rate. σ, it will be recalled, is defined as the ratio of E, the principal rate of strain, to D, the rotary diffusion constant. Perrin [34] has calculated the rotary diffusion constant for ellipsoids of revolution, and Jerrard [3] lists Perrin's results in an appendix. According to these results

$$D = \frac{kT}{\eta_o V} \varphi(r)$$

where

k is Boltzmann's constant

T is the absolute temperature

η_o is the solvent viscosity

V is the particle volume

and $\varphi(r)$ is a shape factor, a function of r, the particle's axial ratio. Theoretically φ for a prolate ellipsoid is different from φ for an oblate ellipsoid.

The point of the preceding remarks is that quantitative interpretation of the optical effect by means of Eqs. 25 and 28 requires a precise knowledge of the internal and external characteristics of the particle. Methods exist in the fields of chemistry and biology for learning a remarkable amount about the structure of macromolecules; but instances are rare if existent at all, when complete and precise agreement can be found on all of the necessary information. The system chosen for the present research program was tobacco mosaic virus (TMV). A great deal is known about its properties, but distinct disagreement still persists between the value of the rotary diffusion constant deduced from streaming birefringence measurements and that deduced from the transient Kerr effect (electric birefringence).

Another complication which is always present to some degree is the lack of perfect monodispersity in the particle population. In any real population there will always be a distribution of particle sizes centered about some mean size. The sharpness of the size distribution about the mean size is an indication of how monodisperse the population is, and one reason for the choice of TMV in the present experiments was that highly monodisperse populations would be available on the Institute campus. Wayland [1] has considered the effect of polydispersity and finds that for small values of σ the linear dependence of χ and f on σ is maintained. For larger values of σ the effect of polydispersity becomes too involved to describe qualitatively.

One possible way of compensating for these deficiencies in the exact knowledge of the particle properties and of circumventing the complication of polydispersity is calibration. Calibration of the particular solution in a known flow situation which can be varied in a controlled manner could conceivably provide the behavior of χ and Δn, the birefringence, over an arbitrarily large range of E, the principal rate of deformation, from which σ differs only by a constant factor. Provided a complete calibration could be carried out, the results therefrom could then be applied to the analysis of an unknown two-dimensional flow.

At this point it must be emphasized that the suggested recourse to calibration does not in any way detract from the theory, nor does it replace the theory. It is only as a result of the conclusions of the theory that one has a basis for the design of a calibration experiment, as well as for a logical choice of the independent variable or variables of the calibration. As stated earlier, Dewey [8] hypothesized that calibration in the flow between concentric rotating cylinders (Couette flow) could take the place of a theory. In contradiction with the theory presented in this thesis Dewey took the streamline direction and the velocity gradient normal to the streamline as his independent variables. Similarly Rosenberg [18] and Prados [25] based their thinking on a Couette cell calibration which, they hypothesized, could relate the observed optical effects to the maximum shear stress and the direction of the plane of maximum shear stress. Rosenberg, however, correctly recognized a certain important ambiguity

associated with calibration in Couette flow, due to the fact that, in Couette flow, the streamline direction coincides with the direction of the maximum shear rate, and the magnitude of the principal rate of strain just differs by a factor of two from that of the velocity gradient normal to the streamlines. Thus in Couette flow the invariant properties, principal rate of strain (E) and the maximum shear-rate direction, become confused with the variants, streamline direction and the velocity gradient normal to the streamline.

A very significant aspect of the conclusions of the general orientation theory can now be appreciated. Examination of Eqs. 25 and 28 reveals that, in addition to their dependence on the invariant principal rate of strain (through the parameter σ), χ and f are influenced by another quantity Λ_o which represents the local angle between the principal strain-rate axis and the streamline. Even for small values of E, such that χ and f depend linearly on σ, the orientation of the principal optical axes is seen to be affected by this angle. The appearance of Λ_o, or equivalently, the appearance of the streamline direction in the orientation theory raises a serious question: Can a complete, useful calibration be performed in Couette flow?

In order to demonstrate clearly how this question arises, and to answer it, it is necessary to review briefly the essential characteristics of Couette flow. Rigorously, the name "Couette flow" is applied to the flow depicted in Figure 6. The fluid is confined between two plane parallel walls of infinite extent normal

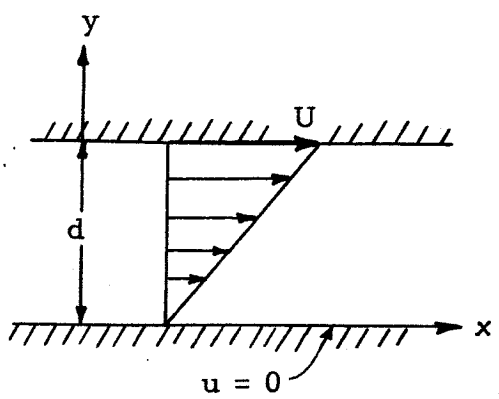

Figure 6

to the plane xy. The planes are separated by a distance d. The lower plane (y = 0) remains at rest while the plane at y = d translates parallel to itself at a constant velocity U. Because the fluid is viscous there is no relative motion between the walls and the fluid in contact with them. Thus the motion of the upper wall causes the fluid to be sheared, and a shear stress is transmitted to the wall which is at rest.

Taking the fluid to be incompressible and Newtonian, and to have constant properties throughout, the equations of motion can be readily solved in this case to give the velocity profile across the gap. The velocity in the y direction is zero everywhere and no changes occur in the x direction, the direction of flow. Hence the momentum equations for the y and x coordinates respectively reduce to

$$\frac{dp}{dy} = 0$$

$$\frac{d^2u}{dy^2} = 0$$

Thus it is seen that the pressure is uniform throughout and that

$$u(y) = c_1 y + c_2$$

Inserting the two boundary conditions into this last result, one finds that

$$u(y) = \frac{U}{d} y \qquad (32)$$

The velocity varies linearly across the gap as shown in Figure 6. The rate of strain components can now be calculated; they are

$$e_{xx} = e_{yy} = 0 \qquad e_{xy} = e_{yx} = \frac{1}{2}\frac{du}{dy} = \frac{1}{2}\frac{U}{d}$$

The principal rates of strain are just $E = \pm \frac{1}{2}\frac{U}{d}$; and the orientation of the principal axes of rate of strain with respect to the streamline is given by

$$\tan \Lambda_o = \frac{+\frac{1}{2}\frac{U}{d}}{-e_{xy}} = \pm 1$$

The principal rate of strain axes are inclined at 45^o and 135^o to the streamline direction.

Thus it is seen that in Couette flow:

(a) the principal rate of strain is constant and equal in magnitude to one-half the velocity gradient $\frac{U}{d}$;

(b) the principal strain-rate axes are always rotated by 45^o from the streamline direction;

(c) the maximum rate-of-shear occurs along the streamline direction.

By locating the optical axes and measuring the amount of birefringence for various values of U/d, two calibration curves can be constructed which would give χ and Δn as functions of E. But these calibrations would be valid only for $\sin 2\Lambda_o = 1$, and there is no possible way for the Couette flow to provide informa-

tion on how the calibration curves would change for values of Λ_o different from 45^o. Couette flow cannot therefore provide a complete calibration.

A practical consideration which might have some bearing on the problem must be injected here. The Couette flow as described above, due to the relative motion of two infinite parallel planes, is not conveniently achievable in the laboratory. To obtain a steady flow closely approximating the ideal Couette flow one usually resorts to the flow between rotating concentric cylinders. The fluid is contained in the gap between a pair of concentric cylinders and a pair of end-plates perpendicular to the cylinder axes. One or the other of the two cylinders is driven. If the ratio of the gap width to the mean radius of curvature is very small, say on the order of 10^{-3}, then the effect of curvature is practically negligible, and the flow is very near to a true Couette flow. End effects due to the confining plates are minimized by making the cylinder lengths great compared to the gap width. Such an arrangement is often referred to as a "Couette cell". This nomenclature will also be used in this thesis.

Due to its true curvature the shear flow between the concentric cylinders differs in certain respects from the flow between the plane parallel walls. The momentum equations in the simple two-dimensional case reduce to

$$\frac{dp}{dr} = \rho \frac{v^2}{r} \quad , \quad \frac{d^2v}{dr^2} + \frac{1}{r}\frac{dv}{dr} - \frac{v}{r^2} = 0$$

where r and θ are plane polar coordinates shown in Figure 7.

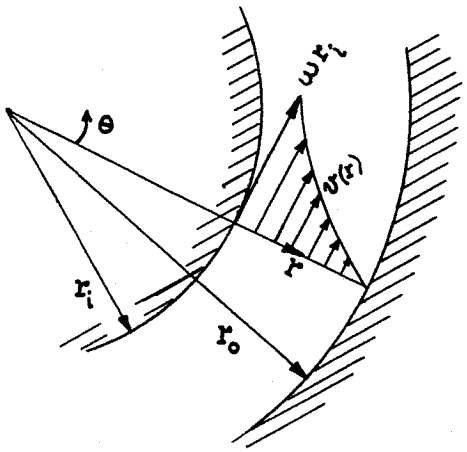

Figure 7

The first equation just gives the radial pressure gradient while the velocity profile v(r) can be found by integrating the second equation. This results in

$$v = c_1 r + \frac{c_2}{r} \qquad (33)$$

Introducing the boundary conditions $v(r_o) = 0$, $v(r_i) = \omega r_i$, which corresponds to an arrangement with internal cylinder rotating, one obtains

$$v(r) = \omega r \frac{\frac{1}{r^2} - \frac{1}{r_o^2}}{\frac{1}{r_i^2} - \frac{1}{r_o^2}} \qquad (34)$$

The velocity profile is curved as shown in Figure 7.

The rate of strain components are

$$e_{rr} = e_{\theta\theta} = 0 \qquad e_{r\theta} = \frac{1}{2} r \frac{d}{dr}\left(\frac{v}{r}\right) = - \frac{\omega}{\left(\frac{r_o}{r_i}\right)^2 - 1} \left(\frac{r_o}{r}\right)^2$$

and the principal rates of strain are

$$E = \pm \frac{\omega}{\left(\frac{r_o}{r_i}\right)^2 - 1} \cdot \left(\frac{r_o}{r}\right)^2 \qquad (35)$$

In the curved Couette flow E varies across the gap, but just as in the linear Couette flow the principal rate of strain axes are inclined at 45^{o} and 135^{o} to the streamline direction. The streamlines still coincide with the maximum rate of shear direction.

For a Couette cell with external cylinder rotating, internal cylinder stationary, the boundary conditions to be applied to Eq. 33 are

$$v(r_o) = \omega r_o, \qquad v(r_i) = 0$$

The resulting velocity distribution is

$$v(r) = \omega r \frac{\frac{1}{r_i^2} - \frac{1}{r^2}}{\frac{1}{r_i^2} - \frac{1}{r_o^2}} \tag{36}$$

In this case

$$e_{r\theta} = + \frac{\omega}{1 - \left(\frac{r_i}{r_o}\right)^2} \cdot \left(\frac{r_i}{r}\right)^2$$

differing only in sign from $e_{r\theta}$ for the flow due to internal cylinder rotating. The principal strain rate is the same also.

$$E = \pm \frac{\omega}{1 - \left(\frac{r_i}{r_o}\right)^2} \cdot \left(\frac{r_i}{r}\right)^2 \tag{37}$$

The principal strain-rate axes are again rotated by 45^{o} from the streamline direction.

The following conclusion can be made: It is not possible to perform a complete calibration of a birefringent colloidal system for application to the interpretation of a general two-dimensional flow, either in rectilinear Couette flow or in a cylindrical Couette flow. In Couette flow $\Lambda_o = 45^o$ always, so that this type of flow cannot show the dependency of the optical effects on this angle.

At first sight this fact seems to represent a serious limitation to the use of streaming birefringence in hydrodynamic analysis. Actually, if the general orientation theory is correct, a much more fundamental limitation exists, and the whole question of calibrability becomes academic. This fundamental limitation lies in the dependency of the angle χ on two variables, viz. E and Λ_o, instead of just one, even when the birefringence varies linearly with E.

This problem is easily understood by first assuming that a hypothetical calibration experiment has been performed which was capable of supplying the functions $\chi(E, \Lambda_o)$ and $\Delta n(E, \Lambda_o)$ over arbitrarily large ranges of E and Λ_o. The theory says that, for E sufficiently small, Δn depends essentially on E alone while χ still depends upon both E and Λ_o. Now consider an unknown general flow which is slow enough so that $\Delta n = \Delta n(E)$ everywhere therein. Optical measurements are made which give Δn and locate the principal optical axes at any point in the flow. With the measured value of Δn one can go to the calibration, and from it determine the E which exists at the point. But knowing E is not enough to permit deduction of χ, since χ also depends on Λ_o, and Λ_o is still unknown. Hence one is left with a knowledge only of the principal

strain rate at the point. The orientation of the principal strain rate axes is not determined.

A subsequent section of the thesis is devoted to the problem of calculating the velocity field from birefringence measurements. The import of the fundamental indeterminacy in the angle χ to this broader problem of analysis will be amplified in that section.

5.0 The Experimental Program

To test the conclusions of the orientation theory it was necessary to design and construct an apparatus capable of yielding precise measurements of birefringence and isocline orientation in some general two-dimensional laminar flow. A hydrodynamic problem was sought for which a theoretical solution was either available or could be carried out. One portion of the experimental apparatus had then to provide the flow to be studied; the rest consisted of optical instrumentation for making the required measurements.

The decision was made to study the flow between two cylinders, eccentrically situated with respect to one another, due to the rotation of the inner cylinder. The geometry will be recognized as that of the journal bearing, but this feature was only a minor reason for its choice. A solution to the problem of viscous flow between infinitely long rotating eccentric cylinders due to Jeffery [35] was found in the literature. His solution is an "exact" one insofar as he neglected only the acceleration terms in the Navier-Stokes equations.

The eccentric cylinder arrangement gives a variety of flow conditions. Regions can be found wherein the flow is parallel, divergent, and convergent. Jeffery's theoretical solution even predicted a zone of reversed flow with a stagnation envelope. Furthermore a pressure gradient would naturally be present if provision could be incorporated into the design to retain it.

As mentioned earlier, it was decided to use tobacco mosaic virus (TMV) as the orientable system, since a fair amount is

known about its properties and good quality samples were available through the Biology Division of the Institute. However, only small quantities, on the order of 100 milligrams or less, could be considered reasonable requests at any one time. This amount, used at the desired concentration levels, would suffice for as many as 50 to 100 cubic centimeters of solution. Thus a rather stringent volume requirement was imposed upon the device which would provide the flow situation to be studied. Physical or chemical contamination of the TMV solutions posed a serious threat to the quality of the optical measurements obtainable. Such could result from the excessive inclusion of dust and/or undissolved air, and contact with certain chemically active metals. Hence for two reasons, viz. the volume limitation and the need for great cleanliness, a test section styled after a conventional water tunnel, with an external pumping circuit, did not appear at all feasible.

Finally, the aforementioned resemblance between the eccentric cylinders and the journal bearing promised to be of real value in the event of a future research program on the lubrication possibilities of high polymer solutions. Many such solutions are transparent and highly birefringent as well; and optical measurements made in the eccentric cylinder flow could conceivably provide information on the presence and magnitude of normal stresses generated by non-Newtonian effects.

In summary then, the flow between eccentric rotating cylinders was chosen as the problem to study because:

(a) a theoretical solution for the problem was available;

(b) the single arrangement provided a variety of interesting flow conditions;

(c) such a test section could be accommodated by a small volume of liquid;

(d) sources of possible contamination of the test suspensions of TMV were minimized; and

(e) it offered the possibility of future lubrication studies with high polymer solutions.

As mentioned previously, a system of optical instrumentation was selected which would be capable of making precise localized measurements at any desired position in the test flow. The system as finally realized is similar to, but differs in certain important details from that used by Wayland [26]. It will be described more fully in the next section.

Before proceeding to the detailed discussion of the experimental program and its results, the author feels compelled to remark that a very significant portion of his physical effort was given to the design, construction, and development of the apparatus. Because of the precision required and the general nature of the experiments, the basic characteristic of the apparatus was one of great delicacy. This fact necessitated painstaking care throughout the construction phase of the work as well as a continual sequence of tedious, but very vital, adjustment and readjustment operations. It is perhaps unfortunate that it is not the custom, even in dissertations on predominantly experimental research, to include a

full detailed account of design and development of the apparatus. In the author's opinion, the story of his long hard struggle against the perversity of matter would introduce a moving human element that theses usually lack.

5. 1 Description of the Apparatus

The experimental apparatus is best described as consisting of two major systems: (1) the experimental cell which contains the solution of interest and produces in it the hydrodynamic situation to be investigated, and (2) the optical system which permits the measurement of the optical properties of the flowing solution at discrete positions within the flow. These major systems are made up of several operating components each of which performs a specific function in the experimental procedure.

In order to achieve a maximum of compactness and rigidity, the entire assembly was built onto an integral steel frame which serves as a combination supporting structure and work bench. A complete view of the configuration is given by Figure 8a. Except for certain auxiliary equipment, such as the power supply and cooling system for the light source, and the control panel for the cell drive, all components are mounted on the basic frame. To facilitate possible future relocation of the experimental apparatus, the frame is equipped with wheels. During operation, however, the entire system is supported on four heavy leveling screws which rest on wooden blocks.

5. 1. 1 The Experimental Cell

The experimental cell design is a variation on the conventional Couette cell (or Maxwell cell) with internal cylinder

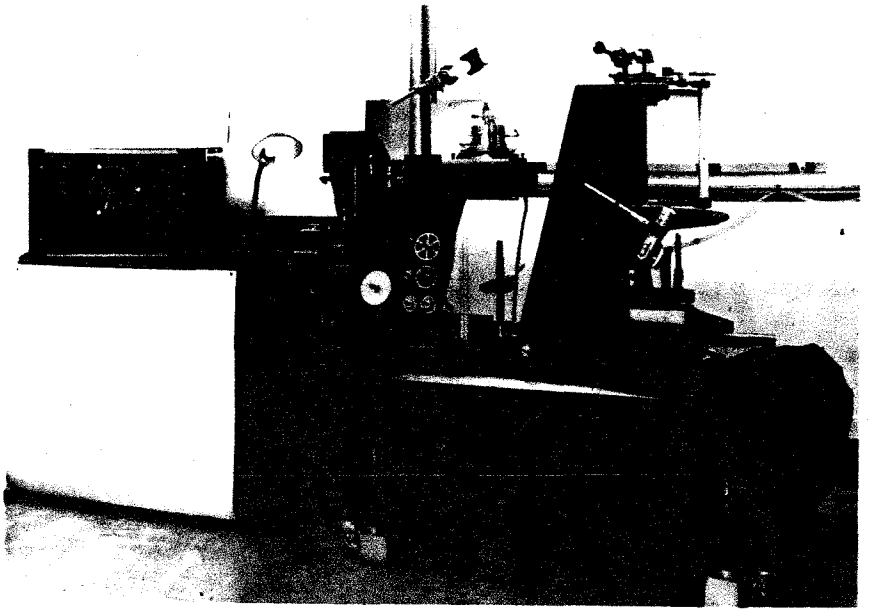

(a) Overall View of Apparatus with Cell in Position.

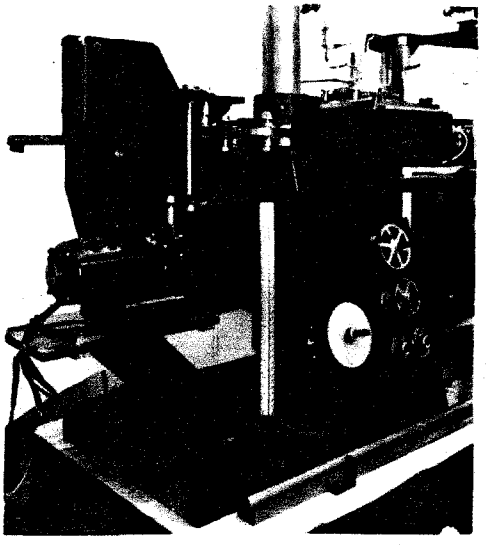

(b) Drive System for the Cell Rotor.

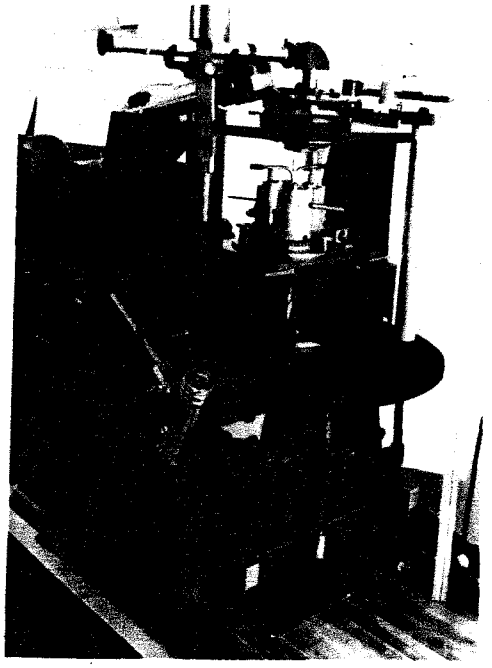

(c) Polarimeter and Cell in Operating Position

Figure 8

rotating. There are two external cylinders of the same internal diameter (nominally 5.4 cm), one of which was bored concentrically to the bearing system of the rotating cylinder, and the other of which was bored eccentrically to the rotor. The eccentricity in the latter case was designed to be about 0.1 cm. There are two rotors, the same in every respect save for their diameters which are nominally 5.0 cm and 5.2 cm.

A conventional Maxwell cell having a uniform gap width of 0.1 cm is obtained when the 5.2 cm rotor is assembled within the concentric stator, while a uniform gap width of 0.2 cm can be obtained by use of the 5.0 cm rotor. Use of the 5.0 cm rotor in conjunction with the eccentric stator results in a gap whose width varies gradually from a minimum of 0.1 cm to a maximum of 0.3 cm (see Figure 9c). The wetted length of the rotors and the stators in both concentric and eccentric arrangements is approximately 5.0 cm.

Figure 9d shows a fully assembled view of the experimental cell. It can be seen from the photograph that the top cover plate contains six window ports that are regularly spaced at 60° intervals. These ports are matched by similar ports on the bottom cover plate. Slotted mounting holes in the cover plates permit rotation of the viewing positions so that any angular coordinate in the non-uniform gap may be studied. The circular glass windows are mounted in stainless steel cartridges which are inserted into the ports. In order to minimize any delay due to possible breakage of a window, extra cartridges were fabricated and outfitted with windows.

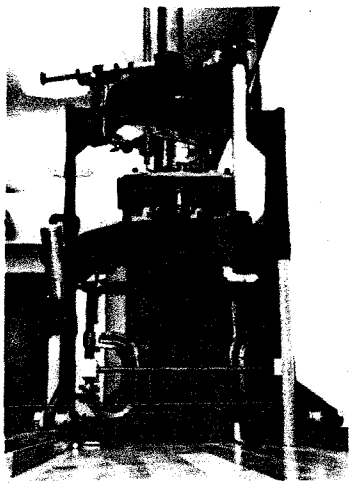

(a) View Showing Deflector Plate and Quarter-Wave Plate Holder.

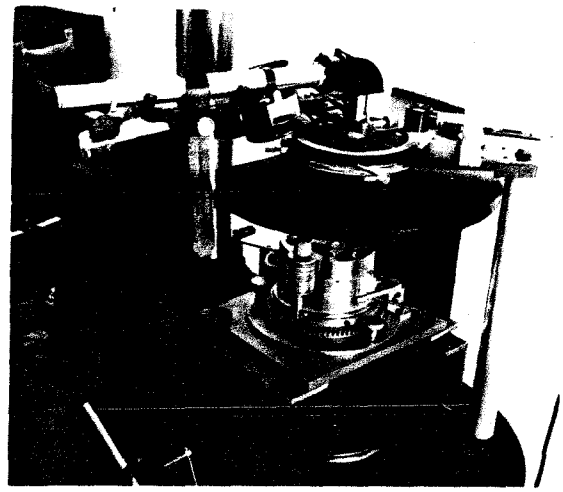

(b) View of Analyzer Head Showing Graduated Circles and Clamping Arrangement.

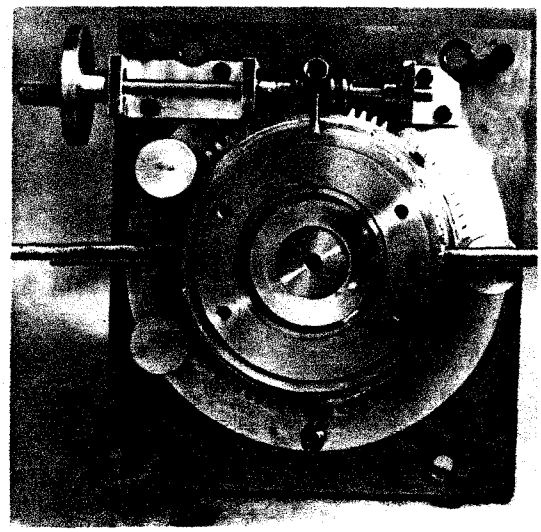

(c) Partial Assembly of Cell Showing Eccentric Gap and Positioning Device.

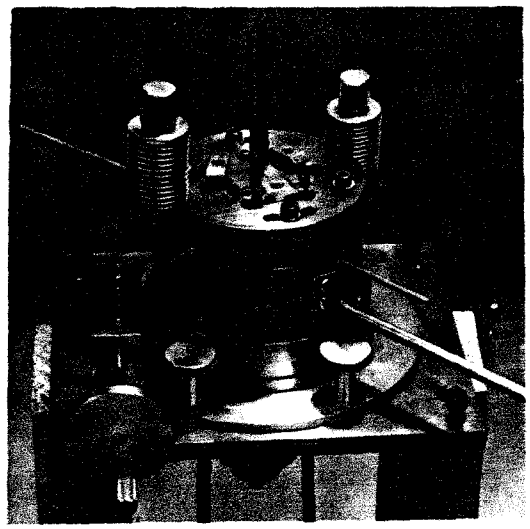

(d) Experimental Cell with Concentric External Cylinder.

Figure 9

The lack of good strain-free glass for windows was for a long time a very serious impediment to the initiation of experiments. The need for strain-free windows is an essential one. Without them it is impossible to begin making accurate birefringence measurements. It is always expected that some residual birefringence will be present in the glass, but this should be sufficiently small so that the total birefringence due to two windows, stacked one against the other, is not measurable by the particular optical instrumentation. Many specimens of purportedly well-annealed windows were examined with no success until a contact was established with the Hayward Scientific Glass Corporation of Whittier, California. Hayward was able to supply a satisfactory lot of windows which were machined from one of their high grade annealed blanks. The actual polishing work was subcontracted by Hayward to the Penn Optical Company of Costa Mesa, California.

Mounting and sealing of windows in such a way that no strains are induced in the glass is another problem that must be contended with in any streaming birefringence apparatus. The windows required in the present work were rather small, in the form of discs about 1/4 inch in diameter and 1/8 inch thick, so that satisfactory mounting and sealing was not too difficult to accomplish. The windows were held in place with a compound called "Sealit" made by the Fisher Scientific Company. Further tests were conducted to determine whether the pressures developed in the eccentric cell were great enough to induce strain-birefringence in the windows, and it appeared that they were not.

Different portions of the non-uniform gap are studied by rotating the eccentric stator with respect to the probe light beam. This is accomplished by means of the ring gear and tangential screw shown in Figure 9c. The ring gear has 80 teeth, so that one full revolution of the tangential screw rotates the entire gap through 4.5°. A 45 division scale on the periphery of the screw handle (not shown in Figure 9) permits accurate movement of the stator through angular increments as small as 0.10°.

Maintenance of the pressure gradient within the non-uniform gap is accomplished by means of a sliding "O" ring seal around the periphery of both end faces of the rotor. To compensate for thermal expansion or contraction of the enclosed liquid, two static head bellows communicate with gap (see Figure 9d). For operation at near-ambient temperatures a pair of rigid standpipes are used in place of the flexible bellows. Thus even at the no-flow condition, the upper end of the gap is subjected to a positive static pressure of about one inch of liquid.

Both stators and end plates are equipped with coils of stainless steel tubing which are silver-soldered to the external surfaces of these parts. Insulated from the atmosphere, these coils provide a means for maintaining a solution temperature significantly different from the ambient temperature as well as for controlling a constant temperature near the mean of the ambient over a period of days when the actual ambient temperature could vary considerably. The ability to thermostat at elevated temperatures will also be necessary should any future research on very viscous polymeric systems be undertaken.

All portions of the cell which are in direct contact with the test solution are made of stainless steel. When residing within the cell the test solution is also exposed to neoprene seals and possibly the brass bellows. The standpipes mentioned above, however, are of stainless steel. When working with chemically sensitive solutions it is essential to use the standpipes. Fairly concentrated (3%) solutions of TMV in Versene buffer, for example, were found to react rapidly with the walls of the brass bellows.

In operating position the internal cylinder rotates about a vertical axis. The bearing arrangement for the rotor is of the cantilever type. On the lower end of the bearing is a toothed pulley which is driven by a timing belt. As evidenced by Figure 8b, the timing belt encircles a supporting column, two idler pulleys, and a fourth pulley which is the actual driving pulley. Through a train of changeable gears this drive pulley is powered by a 1/75 hp synchronous motor having a constant 10 rpm output. Different gear ratios between the motor shaft and the take-off shaft are obtained by sliding the entire motor body closer to or farther away from this shaft and changing the two gears involved. For any particular value of this ratio, eight different rotor speeds are obtainable by changing and reversing four pairs of gears at the upper ends of the take-off shaft and the drive pulley shaft. By suitable permutations of the eleven gears displayed in Figure 8b, a fine grained series of steps of rotor speed is achievable in the range from 0 to 30 rpm, which was designated as the range of

interest. Many rotor speeds beyond 30 rpm, up to 200 rpm, are available. For a detailed tabulation of available speeds and the corresponding gear ratios, the reader is referred to Appendix A.

Each of the gears is secured to the shafts by a single set screw which permits very rapid changes of gears by hand. The slight inconvenience of manual gear changing is greatly outweighed by the fact that the use of gears obviates the need for speed measurement. Furthermore the constancy and reproducibility of a particular speed setting depends only upon the variation in frequency of the line voltage which supplies the synchronous motor. This variation is certainly less than ± 1/2 percent over a period of a few hours, the usual duration of an experimental run.

5. 1. 2 The Optical System

As depicted by Figure 10, the axis of the optical system is vertical. The lowermost element of the system is the high pressure mercury arc which is situated below the wooden top of the supporting framework (see Figure 8a). The arc is a water-cooled capillary type having a length of about 1 inch and a bore of about 1 mm. The arc is manufactured by PEK Labs of Palo Alto, California, and is designated as a Type A lamp. The rated power input is 2 kw, and according to the manufacturer the corresponding light output is 130,000 lumens.

Except on rare occasions the PEK arcs were never subjected to more than 50 percent of their rated voltage. One reason for this is that the intensity of the transmitted light received at the

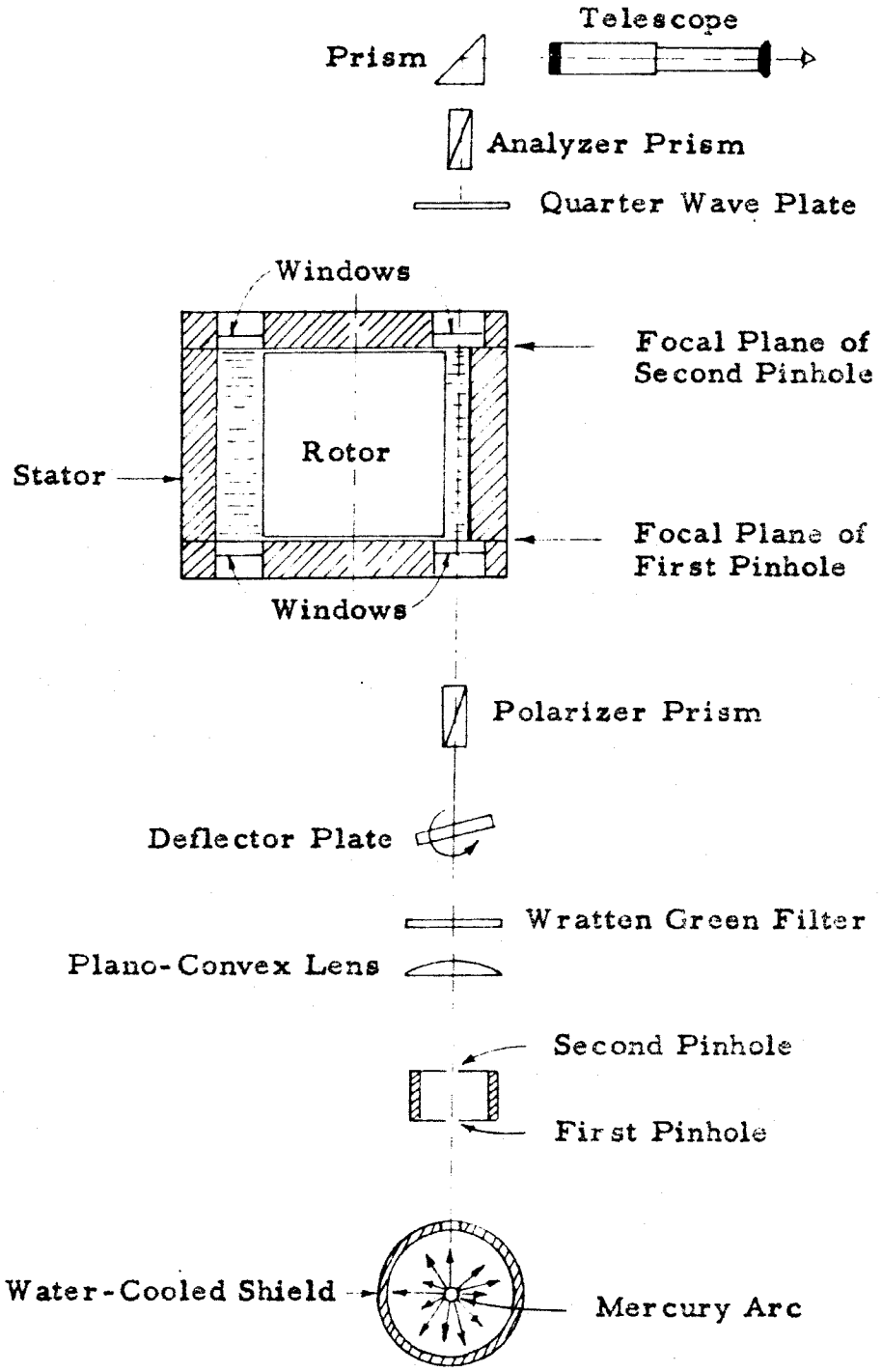

Figure 10. Schematic Diagram of the Optical System.

eyepiece seemed adequate even at the lower output. A more important reason, however, was to prolong the life of the arcs. According to the manufacturer, the average lifetime of this particular arc, operating at maximum output, is only five hours. Operating at 50 percent voltage or slightly less, one arc used in the experimental program lasted for about 50 hours. Another undesirable feature of the A lamp is its rather heavy cooling requirement. Even at the reduced power level a flow rate of approximately 1.5 to 2 gallons per minute of 60° tap water was needed to prevent boiling on the capillary exterior. Moreover the water seals in the arc housing proved to be unreliable for the pressures developed at flow rates much higher than 2 gpm.

Because of the erratic variations in the tap water supply in the laboratory, it eventually became necessary to install an independent cooling system for the arc. A motor-driven pump circulated distilled water through the arc from a reservoir. The reservoir was cooled by cold tap water circulating through a copper coil. Though this arrangement solved the problem of fluctuation in supply, the base temperature was still limited by the temperature of the tap water. During the summer months the latter would increase to almost 75°F.

The entire arc is enclosed in a water cooled copper shield. Through a rectangular opening in the shield the arc illuminates the lower face of a double pinhole collimation device. The actual diameters of the lower and upper pinholes are .008 inch and .006 inch respectively. A long focal length plano-convex lens is

positioned so as to focus an image of the lower pinhole at the bottom plane of the annular gap of the cell while an image of the upper pinhole is formed at the top of the gap. The vertical separation of the two pinhole discs was designed so that the diameters of both image circles in the appropriate planes are the same, about 0.2 mm measured across the first minimum circle of the circular diffraction pattern. In this way, the truncated cone of light rays defined by the unequal pinholes is focused approximately as a right circular cylinder of 0.2 mm diameter and extending from one end of the cell gap to the other. Because of the diffraction pattern, the image circle within the experimental cell becomes rather poorly defined when the polarizer and analyzer are near parallelism. Near extinction, however, the fringes disappear. Since the experimental measurements only involve location of positions of extinction, the presence of the fringe pattern is rarely perceived and thus does not effectively increase the beam dimension.

Translation of the beam is accomplished by rotating a glass plate with optically plane parallel faces about an axis perpendicular to the light beam. The thickness of the glass plate is such that a rotation of about 25° from normal incidence translates the beam through 1.0 mm with respect to its original direction. Rotations of the plate relative to its neutral position are very accurately indicated by a circular scale with vernier which can be read easily to one minute of arc. For rotations of 15° or less, the parallel deflection of the beam is for all practical purposes a

linear function of the angle of rotation. For rotations in excess of 15^{o}, the relation becomes noticeably non-linear. The calculation relating the beam deflection to the shaft rotation for a single ray is outlined in Appendix A. Also included is a graphical representation of the relationship. The shaft which holds the deflecting glass plate is visible in Figure 9a.

During birefringence measurements, a Wratten green filter (No. 77) is placed between the lens and the deflector plate. The principal wavelength transmitted by this filter is 5460 A.

The polarimeter is an integral separate unit. Mounted on rails (Figure 8), it can be conveniently moved out of the optical path during installation or removal of the experimental cell. Glan-Thompson prisms are used as polarizer and analyzer. The prisms are mounted in separate planes perpendicular to the optical path. The bearings of the optical heads of the two prisms are linked by a rigid arm. The upper or analyzer prism, however, is installed in a double bearing, and by means of a clamping arrangement the rotation of this prism can be uncoupled from that of the lower polarizer prism. When clamped together in any desired attitude, the polarizer-analyzer stage can be rotated through 180^{o}. Unclamped, the independent rotation of the analyzer is unlimited. The analyzer head is equipped with two circular scales, one for the motion of the complete stage and one for the independent analyzer motion. There is also a friction clutch-micrometer screw attachment available for very fine rotation of either whole stage or analyzer.

Just below the analyzer head is situated the quarter-wave plate holder. The holder is oriented in such a way that the principal optical axis of the plate is alligned with the principal axis of the polarizer prism. During measurement of the angle of extinction the quarter-wave plate is not needed; it then may be very easily removed from a slot in the holder and later replaced with its exact original orientation.

A 45^{o} prism turns the beam into a horizontal plane. A telescope with horizontal axis is employed for visual observation. The telescope is focused near the middle of the experimental cell.

5.2 The Colloidal Systems Used in the Experiments

In the early stages of the experimental program a considerable number of measurements were collected using solutions of white hector bentonite in distilled water, stabilized with sodium pyrophosphate, $Na_4P_2O_7 \cdot 10H_2O$. Bentonite has been used extensively in streaming birefringence work. It is a substance which occurs naturally in this country and is very low in price. Relatively easy to handle and stable for reasonable periods of time, its solutions boast a considerably stronger optical effect than most naturally occurring colloids. For these reasons, bentonite was the logical system to use during the necessary period required for familiarization with the apparatus and development of the measurement technique.

Bentonite crystals are geometrically anisotropic, and are made up of very thin laminae ranging from 1000 to 3000 Angstrom

units in length and about 10 A thick. Equivalent spherical diameters (based on sedimentation velocity) of from 50 to 2000 A have been measured for the bentonite crystals themselves. For use in birefringence work, bentonite is usually fractionated by centrifugation. (36)

Throughout the preliminary work done with bentonite, solution concentrations of approximately .3 percent by weight were used.

The major portion of the experimental program was effected using tobacco mosaic virus, in pure water and in water-glycerine solutions. TMV is a virus which is found infecting the tobacco plant and which was first isolated about 25 years ago. Recently there has developed a renewed interest in TMV among the biologists, and Boedtker and Simmons (37) reported a reproducible method for preparing highly monodisperse populations of TMV. They also verified that TMV is a rigid rod-shaped particle which has a length of 3000 A and an effective diameter of 149 A. Latest electron microscope information indicates, however, that its diameter may be 180 A.

As received from the Biology Division the TMV is dissolved in a .001M aqueous solution of Versene*, in relatively high concentrations of 1 to 3 percent by weight of TMV. It is in this form that TMV is kept in cold storage over long periods of time without noticeable change in its physical properties. The purpose of the

---

* Disodium Ethylenediamine Tetraacetate, Dihydrate: $(NaOOCCH_2)_2 NCH_2CH_2N(CH_2COOH)_2 \cdot 2H_2O$.

Versene is to inhibit aggregation of TMV particles and consequent increase of polydispersity. It accomplishes this by holding down the concentration of divalent ions which tend to favor dimerization of the TMV. Under suitable conditions TMV is noticed to dimerize (end-to-end combination of two single particles or monomers to form a particle of double length) rather readily.

All of the aqueous solutions of TMV used in the research were actually solutions in .001M (one-thousandth molar) Versene. In the final phase of the measurements solutions of TMV in water-glycerol solvents were employed. No information was available on the stability of TMV in a glycerine environment; and in these solutions no attempt was made to control the pH, the factor which inhibits the aggregation tendency of TMV, except to keep it constant during any one set of experiments. It was hoped that, if aggregation were to occur, it would proceed slowly enough so as not to affect significantly the birefringence measurements, which, for any one filling, could be gathered in a few days. In any event, an examination of the birefringence measurements for anomalies due to polydispersity was expected to reveal whether or not the glycerine environment was satisfactory for TMV.

Boedtker and Simmons recorded two other observations which were considered significant to the TMV experiments. Firstly, they made birefringence measurements at different concentrations and found that the extinction angle was independent of concentration for the range .05 to .5 grams TMV per 100 cc of solution. This is taken to mean that, within this concentration range, interaction

Figure 11

effects are not apparent. In this range the amount of birefringence should be linearly dependent on the concentration, but Boedtker and Simmons did not report a check on this point. The concentrations employed in the present experiments with TMV were well within the range given above.

Secondly, they observed that flow birefringence measurements were very sensitive to small amounts of aggregated particles. Their data showed that the presence of small amounts of long particles caused the isoclinic axes to make smaller angles with the streamline direction as the shear gradient approaches zero, than would be expected for a perfectly monodisperse population.

Near the final stages of the experimental program an electron microphotograph was obtained of the TMV strain which was actually used in the experiments. This photograph is included here as Figure 11. The total magnification as seen in Figure 11 is approximately 100,000 times. Evident in Figure 11 are a few dimers as well as a considerable number of shorter molecules.

5.3 The Experimental Technique

All of the measurements performed can be classed into two groups: calibration measurements and traverse measurements. In the first group, the position of the light beam is held fixed and the speed of the moving wall is varied. For each speed, one of the two orthogonal principal optical axes is located and the amount of birefringence is measured. In the second group, the speed of the moving wall is kept constant, and the light beam is translated through the flow. At discrete positions within the flow the optical

axes are located and the amount of birefringence is determined. The calibration runs are normally performed in the gap between concentric cylinders, one of which rotates relative to the other (Couette flow), although in this research program some were also carried out in the minimum gap between the eccentric cylinders. The traverses were almost exclusively performed in the eccentric gap, at four different stations: the minimum and maximum width positions, one station where the streamlines diverge, and one where they converge. One traverse was also effected in the Couette cell.

From a calibration experiment two pieces of information are obtained for each rotor speed: the angle between the principal optical axis closest to the streamline and the streamline, and the amount of birefringence Δn. The first quantity is called the angle of extinction and denoted by χ in the literature [3]. In the present work the notation χ will be consistently applied to the acute angle between the two orthogonal optical axes and the two orthogonal principal strain-rate axes. It was demonstrated in Section 4.0 that in Couette flow the principal rate-of-strain axes are rotated by 45° from the streamline direction. Hence the two conventions concerning the extinction angle differ by exactly 45°, and confusion on the issue is avoided with no difficulty.

Actually χ and Δn are not measured directly. Three angles, θ_1, θ_2, and a are measured, each of which locates an extinction orientation, with respect to some reference, for either the entire polarizer-analyzer stage or the analyzer prism alone. θ_1 and θ_2

together provide the angle χ while Δn is derived from a. For a detailed description of the theory underlying the optical measurements, the reader is referred to Appendix B. In this section only a qualitative explanation will be given of what is involved in measuring θ_1, θ_2, and a. Two schematic diagrams of the optical transformations undergone by the light as it progresses through the essential elements of the optical system will be extremely helpful in these explanations.

In measuring θ_1 and θ_2 one is concerned only with locating one or the other of the optical axes of the birefringent system. To do this, the polarizer and analyzer are locked in a crossed position and rotated together until the intensity of the transmitted light vanishes or goes through a minimum. In Figure 12a the plane polarized light is seen entering the birefringent medium with its plane of polarization making some arbitrary angle with the optical axes x, y. The light leaves the medium elliptically polarized, and consequently some light gets through the analyzer prism whose principal plane makes 90° with that of the polarizer prism. Figure 12b shows what happens when the polarizer-analyzer stage has been rotated so that the plane of polarization is parallel to one of the optical axes of the birefringent medium. The light leaving the medium is still plane polarized, and hence none of it is transmitted by the analyzer. The angle θ_1 or θ_2 is the angle through which the polarizer-analyzer stage was rotated from some reference position to the extinction position shown in Figure 12b.

The purpose of making two measurements, θ_1 and θ_2, is just to establish the streamline as the reference direction for the optical

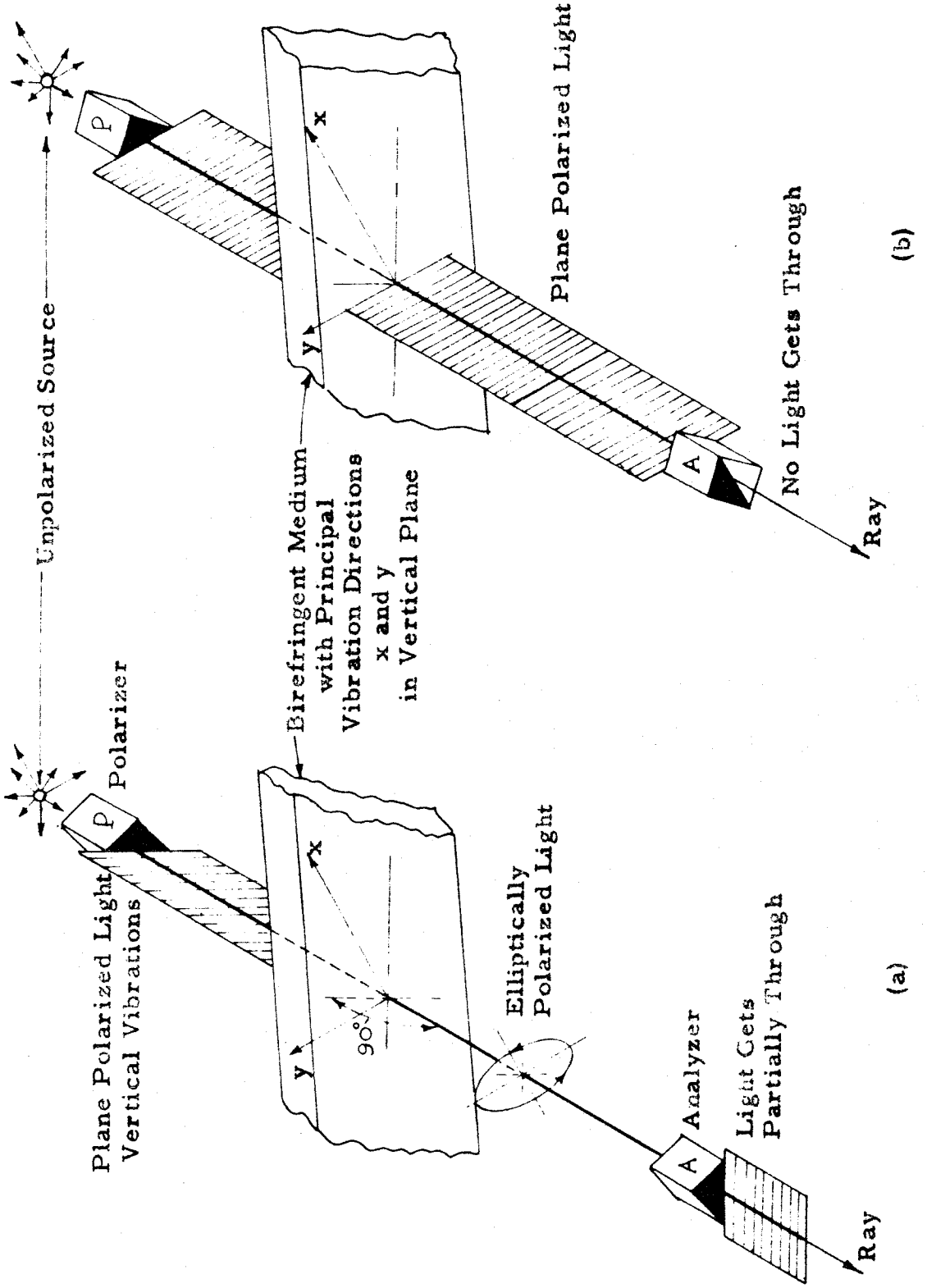

Figure 12. Location of Principal Vibration Directions.

axes. In Couette flow the principal strain-rate axes are always inclined at 45° to the streamline. Hence the principal optical axes of the fluid will be inclined at $45^{\circ} - \chi$ to the streamline.

The original reference direction for the plane of polarization was determined by nothing more than some fiducial mark, say zero, on the graduated circular scale of the optical head in which the polarizing prism is mounted. When the polarizer has its "zero" orientation, the plane of polarization makes some angle, say θ_o, with the streamline direction. θ_o is usually not known with precision. In the case of Couette flow, this can be found by making an additional measurement with the streamline direction reversed. In Figure 13 the streamlines are heading to the right and are denoted by S. The plane of polarization P is shown in its zero orientation. "x" is the optical axis closest to the streamline. A counter clockwise rotation of P through an angle θ_1 locates the x axis. When the streamlines are heading to the left (Figure 14), however, P must be rotated clockwise through an angle θ_2 in order to coincide with x. Then since

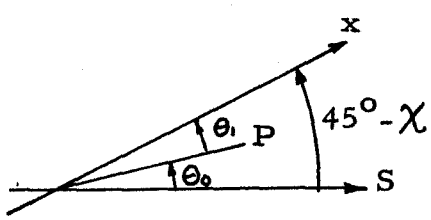

Figure 13

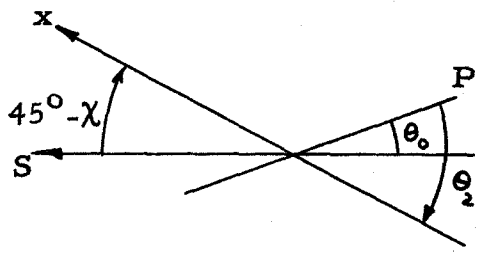

Figure 14

$$\theta_1 = (45^{\circ} - \chi) - \theta_o \quad \text{and} \quad \theta_2 = (45^{\circ} - \chi) + \theta_o$$

it is seen that

$$\chi = 45^{o} - \frac{\theta_1 + \theta_2}{2} \tag{38}$$

and

$$\theta_o = \frac{\theta_2 - \theta_1}{2} \tag{39}$$

Should the zero orientation of P lie in some other quadrant, with respect to the "x" axis, than that depicted in the above illustration, χ and θ_o can still be determined by a forward and reverse measurement if it is kept in mind that $0 < \chi < 45^{o}$ always. The fact that χ is so bounded is predicted by the orientation theory and is well established by experiments in Couette flow. As the principal strain-rate E becomes infinitely great ($\sigma \rightarrow \infty$) the particles tend to complete allignment along the axis of maximum shear rate, which, in Couette flow, is just the streamline.

It was convenient to use this same procedure in the eccentric cylinder flow. In the minimum gap position the flow is parallel, so that a reversal of the rotor's sense of rotation simply reverses the direction of the streamlines without altering the character of the flow. Furthermore, by symmetry considerations it was deduced that the principal strain-rate axes are inclined at 45^{o} to the streamlines there. Such being the case, the forward and reverse measurements provided the angle θ_o between the polarizer zero direction and the streamline direction. In other sections of the eccentric cylinder flow, where the streamlines are not parallel,

the rotor streamline, i.e., the local tangent to the rotor, was used as the reference. This was the logical reference to use since the rotation of the eccentric gap takes place about the rotor axis. Thus the θ_o calculated in the minimum gap is the angle between the polarizer zero direction and the rotor tangent for any other portion of the eccentric gap as well.

If one were concerned with a test flow which lacked the peculiar symmetries of the circular flows studied in this research program, the forward and reverse flow technique for establishing a streamline or boundary reference might not be at all feasible. Then it would be necessary to establish directly the orientation of some convenient portion of the boundary in terms of a scale reading on the optical head of the polarizing prism. There are at least two or three ways in which this could be done with good precision. The direct determination could have a real advantage over the two measurement technique from the point of view of overall accuracy. In the latter technique, the accuracy with which χ is known is limited by the accuracy with which either θ_1 or θ_2 is known. It is quite possible that the boundary orientation can be determined directly with a much greater accuracy than that associated with the extinction measurements. If such be the case, the final accuracy in the knowledge of χ could be improved.

Figure 15 shows the optical transformations associated with the measurement of the angle α. This measurement also results from location of a position of extinction. The plane of polarization of the incident light is set at 45^o to the local optical axes. These

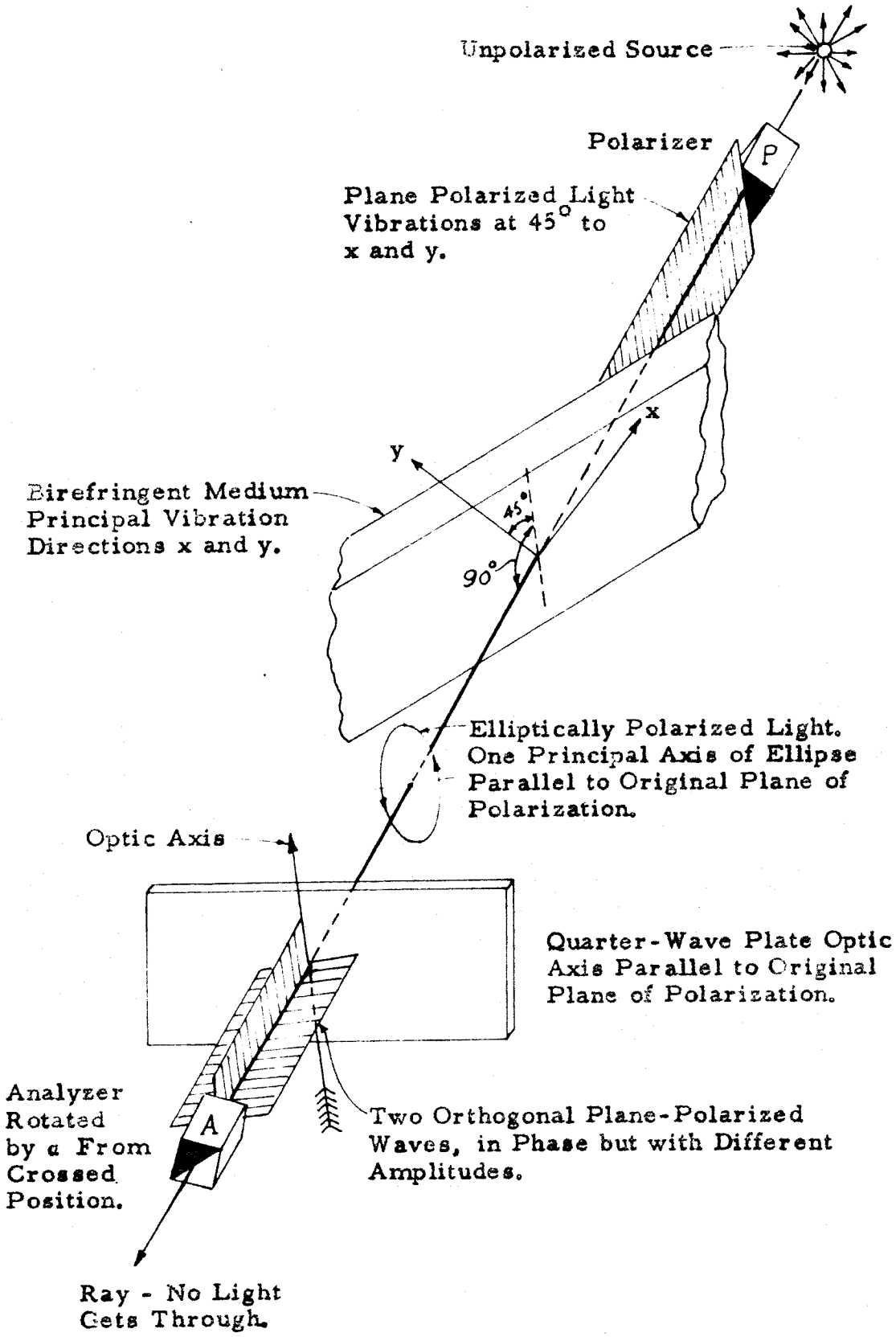

Figure 15. Measurement of Birefringence.

axes, it will be recalled, were located in the previous step. This gives equal intensities to the two components of the polarized electric vector along the two local optical axes, both of which lie in a plane perpendicular to the incident light ray. Upon emergence from the fluid, one of these components is retarded relative to the other, and the resultant light wave is elliptically polarized. The principal axes of the ellipse traced by the electric vector are parallel and perpendicular to the original plane of polarization. Next, a quarter-wave plate with its optic axis also alligned with the original polarization plane converts the elliptically polarized light into two orthogonal plane polarized waves which are in phase. The resultant of the two plane polarized waves is just a single plane polarized wave. The new plane of polarization is, however, no longer parallel to the original plane of polarization. The angle a between these two planes is proportional to the retardation of one of the electric vector components relative to the other which is, after all, a measure of the amount of birefringence. By rotating the analyzer independently to the position of extinction or minimum intensity, this angle is determined directly.

The angle a differs only by a multiplicative constant from the amount of birefringence in units of Angstroms retardation per centimeter of path traveled in the birefringent medium.

$$\Delta n = n_x - n_y = \frac{\lambda}{\ell} \cdot \frac{a}{\pi} \qquad (40)$$

where n_x and n_y are the indices of refraction associated with the optical axes x and y, λ is the wavelength of the incident light,

ℓ is the length of path in the medium, and a is in radians. The derivation of this equation is given in Appendix B.

At this point a few general remarks on certain practical aspects of the experimental method are appropriate. In order to gain the benefit of the greater intensity, the unfiltered emission of the mercury arc was used in the determination of the angle of extinction. Where the birefringence was feeble, and the intensity minimum corresponding to parallelism of the incident electric vector and the local optical axis correspondingly broad, several readings of extinction angle were taken. Invariably an equal number of readings was taken approaching the minimum from either side. These were then averaged and the average value recorded as the local angle of extinction. Birefringence measurements were made using the 5460 A principal line of the mercury arc spectrum.

It is difficult to make a blanket statement on the accuracy of measurement since this depends on the level of birefringence. Total spread in the extinction angle data was greatest where the amount of birefringence was least. In these instances a larger number of readings, usually six or more, was taken. It was hoped that the distribution of data about the true intensity minimum could be kept fairly normal by taking the readings on both sides of the minimum. In both the dilute aqueous solutions and the water-glycerol solutions standard deviations for the θ_1 and θ_2 data ranged from 0.1° in a region of large Δn, to 2.5° in a region of relatively small Δn. The average standard deviation was approximately 0.5°.

The scatter in the a measurements was consistently less than that for the θ_1 and θ_2 measurements. Standard deviations for the a data ranged from $.03^\circ$ to 0.5° with an average between 0.1° and 0.2°. It is to be expected that the scatter in the a readings will always be less than that in the θ_1 and θ_2 measurements. In both cases the intensity of light transmitted by the analyzer varies quadratically with the analyzer angle when extinction is near. In the θ_1 and θ_2 measurements, however, the flux is proportional to the square of the birefringence as well. Hence, the smaller the birefringence, the flatter the intensity minimum for the θ_1 and θ_2 measurements, and the greater the difficulty in measuring θ_1 and θ_2 precisely. The sharpness of the intensity minimum in the a measurement does not depend on the amount of birefringence. To a small extent the accuracy of the a measurement depends indirectly on the birefringence. For if the location of the principal optical axes is known with uncertainty, then the positioning of the plane of polarization at 45° to these directions is liable to error. An error of a degree or so in this positioning turns out, however, to have a very small effect on the final reading of a.

There was no detectable residual birefringence in the windows when the fluid was at rest. Tests were conducted with inactive aqueous solutions to determine whether pressure gradients developed in the eccentric flow could induce measurable strain birefringence in the windows, and none was observed.

In executing a traverse the positions of the two walls are first determined by recording the rotations of the deflector plate

from its neutral or normal incidence attitude to those orientations for which half the beam cross section appears to be vignetted by first one wall, then the other. The location of these extremes is judged by eye, and consequently there is an expected error in the recorded wall positions. It is estimated that this error, which is the distance between the wall and the beam center-line when the beam is judged to be split by the wall, is never greater than half the radius of the beam cross section, i.e., .05 mm. The dimensionless coordinates of the interior points are necessarily referred to the recorded wall positions. Thus it can be reasoned that a position coordinate, listed as .10 mm for a wall coordinate, which is itself a possible .05 mm away from the true wall position, is only accurate to within 50 percent; whereas the location of a point listed as 1.0 mm from a wall is known with an accuracy of 95 percent.

This apparently serious error in the location of the beam centerline near the walls should not, however, be regarded as a direct indication of the reliability of the spatial distribution of the experimental traverse points. The reason for this is that the exploring light beam is not an infinitely slender ray, but a bundle of rays of significant cross section. What is actually observed when this bundle interacts with the oriented medium is some sort of space-averaged optical behavior for a circular region approximately .20 mm in diameter. These average local properties are then attributed to the supposed location of the center of the bundle. Thus the extent of the region over which the optical properties are averaged is always greater than "the circle of error" drawn about

the recorded position of the beam center-line. Although it is difficult to make a quantitative statement on the matter, it is suspected that this averaging process mitigates the inaccuracy of placement of the experimental points due to uncertainty in the knowledge of the beam center-line location.

At or very near the walls, the disturbing presence of glancing reflections makes complete extinction impossible. Consequently measurements are difficult in these neighborhoods, and in many cases the distribution of data is noticeably irregular there.

5.4 Presentation and Discussion of the Experimental Results

Birefringence data were collected at four positions in the non-uniform gap: the minimum width position, the maximum width position, a position 60° away from the minimum gap where the streamlines are converging, and a diverging flow position, also 60° away from the minimum gap. At each position measurements were taken at a minimum of ten nearly equally spaced points between the stator and rotor. The full set of data taken across any particular gap position will be referred to as a "traverse". A calibration experiment was performed before and after each group of traverses.

The actual data consisted of angle measurements, which located the principal optical axes with respect to a suitable reference, and measurements of the amount of birefringence. In the four regions of the eccentric cylinder flow which were explored, the angle Λ_o never differs by more than 2° from 45°. In the minimum and maximum gaps Λ_o is exactly 45°. Consequently the factor $\sin 2\Lambda_o$ which enters into the expression for χ is equal to unity with less than one percent error in the regions explored. Thus a Couette flow calibration could be used to translate the optical data into principal strain rates (E) and other angles which permit location of the principal strain rate axes with negligible approximation. This information concerning the strain rate tensor was then compared with similar information calculated from Jeffery's theoretical solution [35]. (See Appendix C for details of these calculations.)

Three main data collection programs were carried out. In the first a very dilute solution of TMV, designated as Solution A,

was used. The approximate concentration of Solution A was .085 gram of TMV per 100 cc of .001 M (one-thousandth molar) Versene with pH 7.5. Satisfactory angle of extinction measurements were very difficult to make in these dilute solutions. In these experiments the birefringences were generally small; the highest recorded was of the order of 20 A/cm. Extinction angle measurements are always more difficult to perform than birefringence measurements, and in this case the combination of a small birefringence with an extremely small pencil of light makes for considerable scatter. Six or more readings were usually taken of the extinction angle, and in regions of low birefringence the standard deviation of these readings about the average ranged as large as 2.5^{o}. This is comparable to the total variation of the angle of extinction over the range of strain rates imposed in the experiments.

This condition led to the initiation of the second phase of data collection. The primary purpose of this was the repetition of the angle measurements with aqueous TMV solutions of much higher concentration. The approximate concentration of the solution used in these runs, called Solution B, was .26 gram of TMV per 100 cc of .001 M Versene, pH 7.5. This was about three times as great as the concentration of Solution A.

Although the scatter in the angle measurements was generally reduced in the more concentrated solution, it still was annoyingly high in particular regions of very low birefringence. One such region is in the neighborhood of the rotor wall in the minimum gap. This is a region of relatively small velocity gradient and hence low birefringence. The lack of agreement between the interpreted

orientation of the principal strain rates and that predicted by the theoretical solution in that neighborhood made it expedient to push for still greater accuracy in the angle measurements. It was not feasible to go to greater concentrations since much larger quantities of TMV could not be had at one time, and because of the imminent possibility of interaction effects. Nor were higher running speeds deemed advisable because of the possibility of separation in the diverging flow.

The idea was conceived to increase the viscosity of the solvent liquid, thereby decreasing the rotational diffusion proportionately. This would have the effect of producing sharper particle orientations for the same amount of hydrodynamic distortion. It was decided to suspend TMV in solutions of glycerine and water. Since glycerine and water are miscible in any porportions, a wide range of viscosity, covering three orders of magnitude, was easily obtainable. An 85 percent glycerine solution, having a viscosity roughly 100 times that of water at 20°C, was used throughout the third and final phase of experiments. The approximate concentration of TMV in Solution C was .1 gram per 100 cc of the glycerine-water solution. The rate of strain optical coefficient, defined as the amount of birefringence produced by a unit rate of strain, was higher by a factor of 10 over that exhibited by Solution A.

In the final phase of experiments the minimum gap was the only portion of the non-uniform gap in which a traverse was performed. In addition to this traverse, the solution was calibrated in a 1 mm gap between concentric cylinders.

From the very start, the handling of the solutions and the filling of the cells proved to be difficult problems. Having of necessity been stored at near freezing temperatures, the aqueous TMV solutions tended to release dissolved air when allowed to warm up to room temperature. The possibility of heating to drive off dissolved air was prohibited because of the harm which might be suffered by the virus. Weakening of optical activity due to chemical or physical change was also observed in solutions which were allowed to remain in contact with metallic surfaces at room temperature for several days. Filling the cells had to be done slowly to prevent the entrainment of air which, once trapped in the narrow passages, was almost impossible to remove. A single filling was observed to result in the inclusion of a considerable amount of dust and lint into the solutions. In most instances the amounts of foreign particles present were not great enough to obstruct the birefringence measurements, but it seemed probable that a second filling with any particular sample could introduce a prohibitive concentration of such particles.

Because of the apparent impracticability of three or even two transfers of the solution between the eccentric and the concentric cells under the existent laboratory conditions, it was decided to attempt to calibrate in the minimum gap of the eccentric cell. The streamlines are parallel there, the principal strain rate axes are inclined at 45° to the streamlines, and the Jeffery solution was deemed capable of providing a fairly reliable knowledge of the principal strain rate as a function of position within the gap. If

possible, such calibrations, it was realized, would not be absolute in the sense that they depended upon the accuracy of the Jeffery solution. However, it was anticipated that all measurements would be effected at low rates of strain well within the linear range of birefringence, so that an error due to an inaccurate knowledge of E at the calibration position would show up as a constant multiplicative discrepancy, the same for all traverses.

The minimum gap calibrations appeared to give very satisfactory results for the aqueous TMV runs and were used in all of the experiments performed with Solutions A and B. In the light of the aging characteristic of the aqueous solutions, the time saved by avoiding transfer of the solution from cell to cell was also very significant, since the better part of one day is needed to properly prepare a cell for filling, then to fill it, then to install and align it in the optical system.

Figures 16 through 22 represent the results of the runs made with Solution A. Figure 16 shows the calibration curves. In the angle of isocline calibration only those points were plotted for which the standard deviation of the readings about the average was less than one degree. The vertical segments attached to the experimental points in this plot represent one standard deviation in each direction. On the basis of the six points plotted, a smooth curve was constructed, but it is clear that the shape of this curve near the origin is open to discussion. Note that while the birefringence curve shows no sign of becoming non-linear in the range of strain rates covered, the angle of isocline curve is definitely non-linear

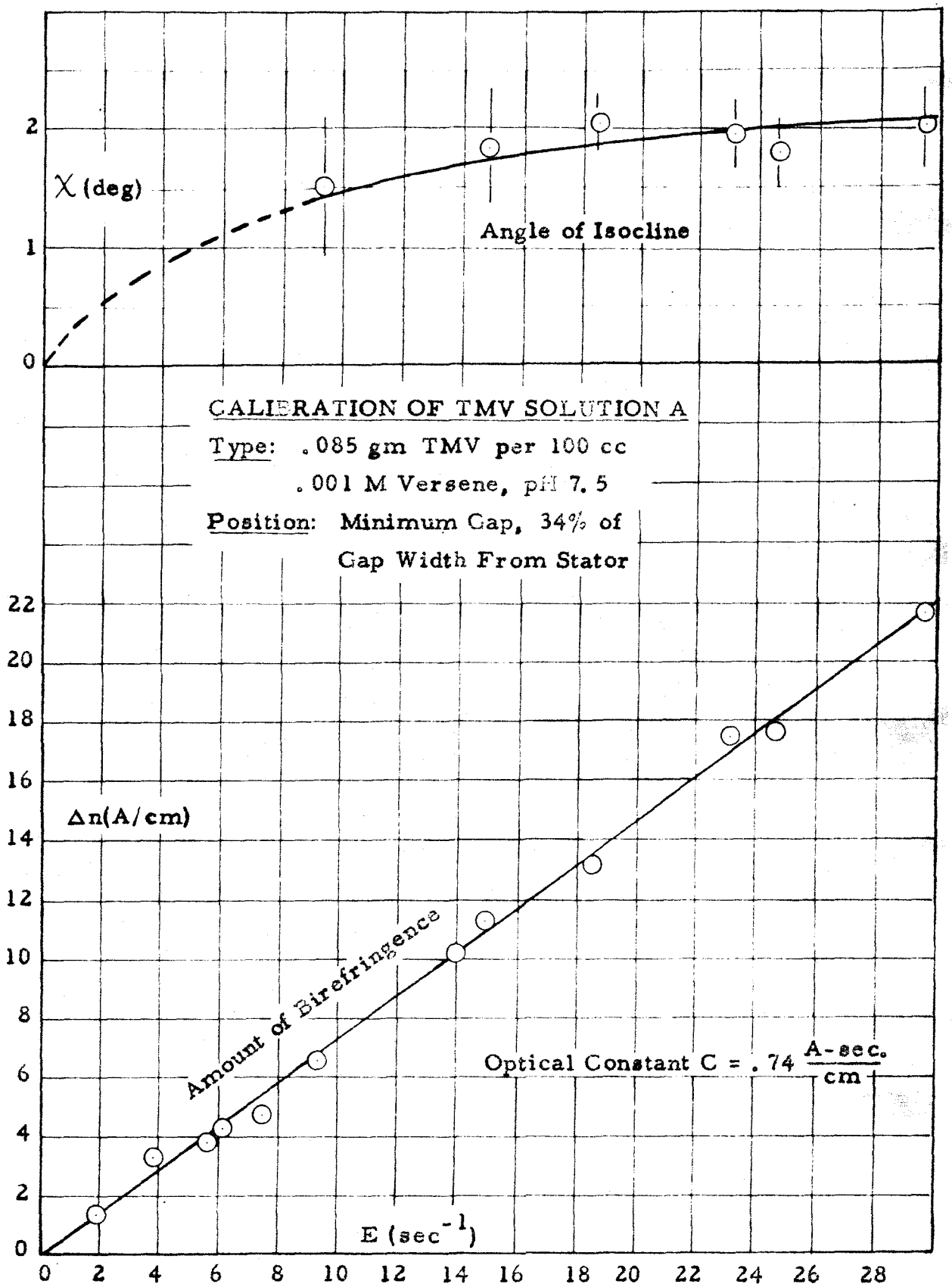
χ (deg)
Angle of Isocline
CALIBRATION OF TMV SOLUTION A
Type: .085 gm TMV per 100 cc
.001 M Versene, pH 7.5
Position: Minimum Gap, 34% of
Gap Width From Stator
Δn(A/cm)
Amount of Birefringence
Optical Constant C = .74 A-sec./cm
E (sec⁻¹)
0
1
2
0
2
4
6
8
10
12
14
16
18
20
22
24
26
28

Figure 16

and will be for any reasonable fit of the data. The general orientation theory predicts that the linear ranges of Δn and χ should be nearly equal for a monodisperse population. It also predicts that the initial slope of the angle of isocline curve is remarkably sensitive to the presence of even small concentrations of the TMV dimer, the effect of this type of polydispersity being to increase the initial slope of the χ curve. This is in accord with the observations of Boedtker and Simmons [37] mentioned previously in Section 5.2. This non-linearity in the behavior of χ was prevalent in all of the calibrations performed on the dilute aqueous solutions. Later on in the program an electron microphotograph of the particular TMV strain was acquired from the CRM (Centre de Recherches sur les Macromolécules) Laboratory in Strasbourg, France, where some work was being done with the Caltech TMV. This photograph has been included as Figure 11 in Section 5.2, and the presence of dimers as well as some shorter molecules is apparent. More attention will be directed to this polydispersity in the discussions to follow.

Incidentally, the range of the parameter σ covered in the Solution A calibration extends from approximately 0 to .15. This is based on an estimated rotary diffusion constant for TMV particles in an aqueous solution of 200 sec^{-1}.

Figure 17 shows the change with time of the optical constant of Solution A. This information was taken from three calibrations performed over a seven day span. It should be brought out that the brass static head bellows were installed on the cell during the

AGING CHARACTERISTIC FOR
TMV SOLUTION A.

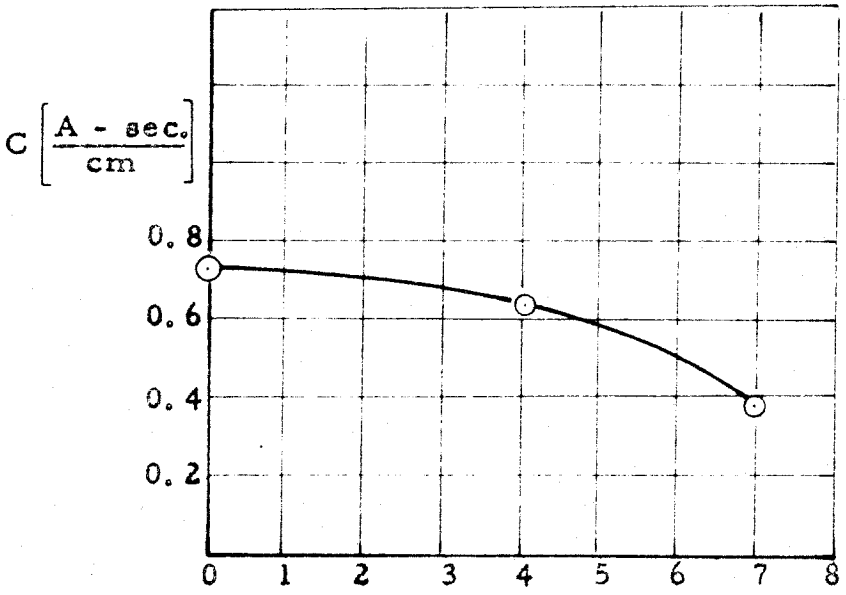

Figure 17

period, and that this contact with brass might be a factor in the aging. In later work the brass was observed to react very rapidly with Versene solutions of higher molarity than that used in Solution A. The four traverses effected with Solution A were completed within the first three days after filling.

The results of these traverses are depicted by Figures 18 through 22 inclusive. The first three of these show how the principal strain rate (E), as interpreted from the birefringence measurements, compares with that calculated from the Jeffery solution. The comparisons for the converging and diverging flow measurements are both given in the same graph, Figure 19, since the theoretical curve is the same for both of these positions.

Special attention is called to Figure 20 wherein E/ω_2 takes on negative values. This is expected theoretically since, for the particular geometry chosen, Jeffery's solution predicts a region of reversed flow having its maximum thickness in the maximum gap. On this basis then, it would be anticipated that a traverse of the maximum gap reveal a zero in the distribution of Δn and hence the quantity E. This point of vanishing E corresponds to the minimum in the velocity profile that lies within the region of reverse flow. The optical data recorded in the maximum gap definitely gave evidence to the presence of this region. A reversal in the sign of Δn in this case is first perceived as a reversal in sign of the extinction angle measured with respect to the streamline direction. In addition to this, the rotation of the analyzer prism necessary to achieve extinction in the birefringence measurement also changes direction.

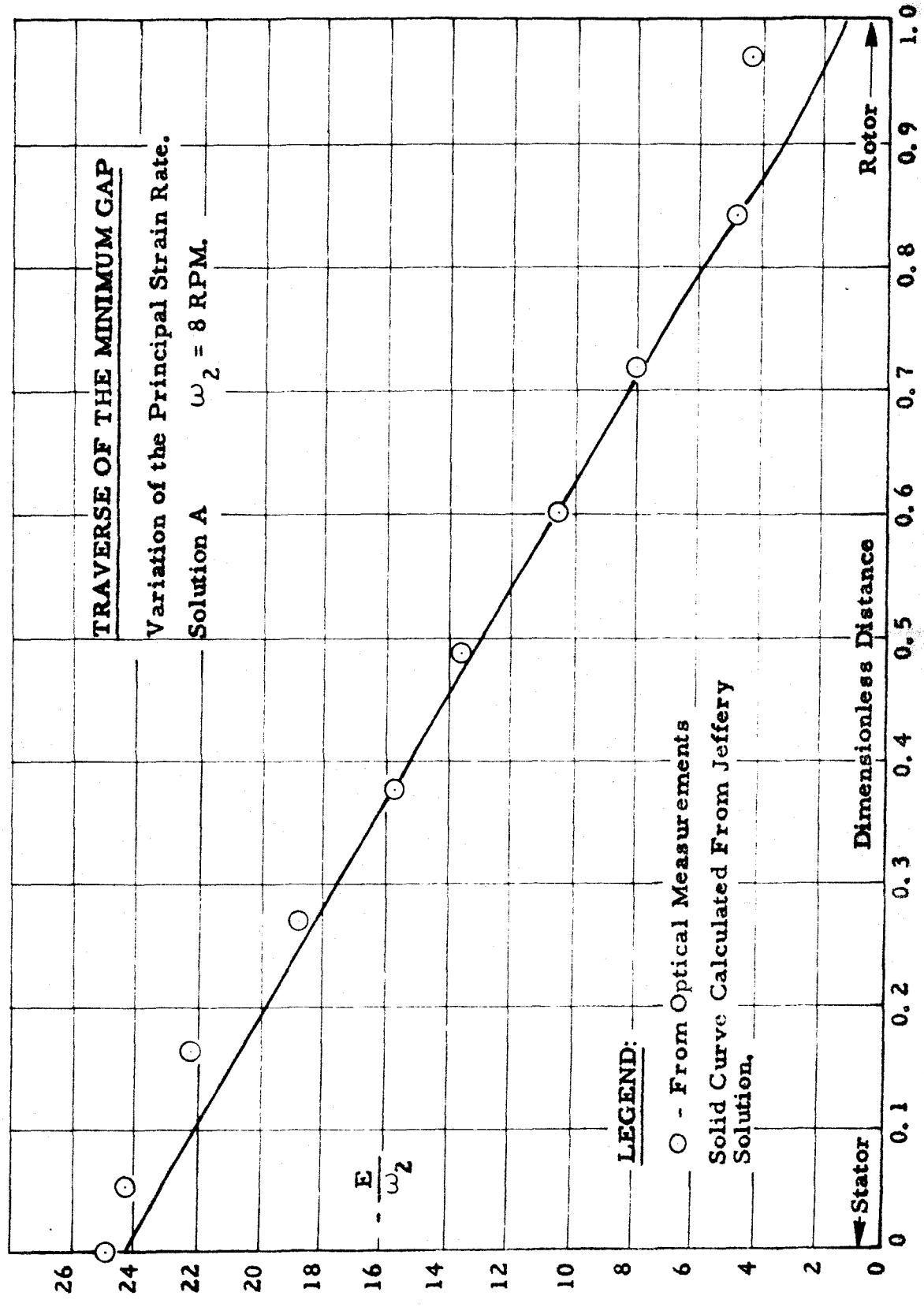
TRAVERSE OF THE MINIMUM GAP
Variation of the Principal Strain Rate.
Solution A
ω_2 = 8 RPM.
$-\frac{E}{\omega_2}$
LEGEND:
○ - From Optical Measurements
Solid Curve Calculated From Jeffery Solution.
Dimensionless Distance
Stator
Rotor
0
0.1
0.2
0.3
0.4
0.5
0.6
0.7
0.8
0.9
1.0
2
4
6
8
10
12
14
16
18
20
22
24
26

Figure 18

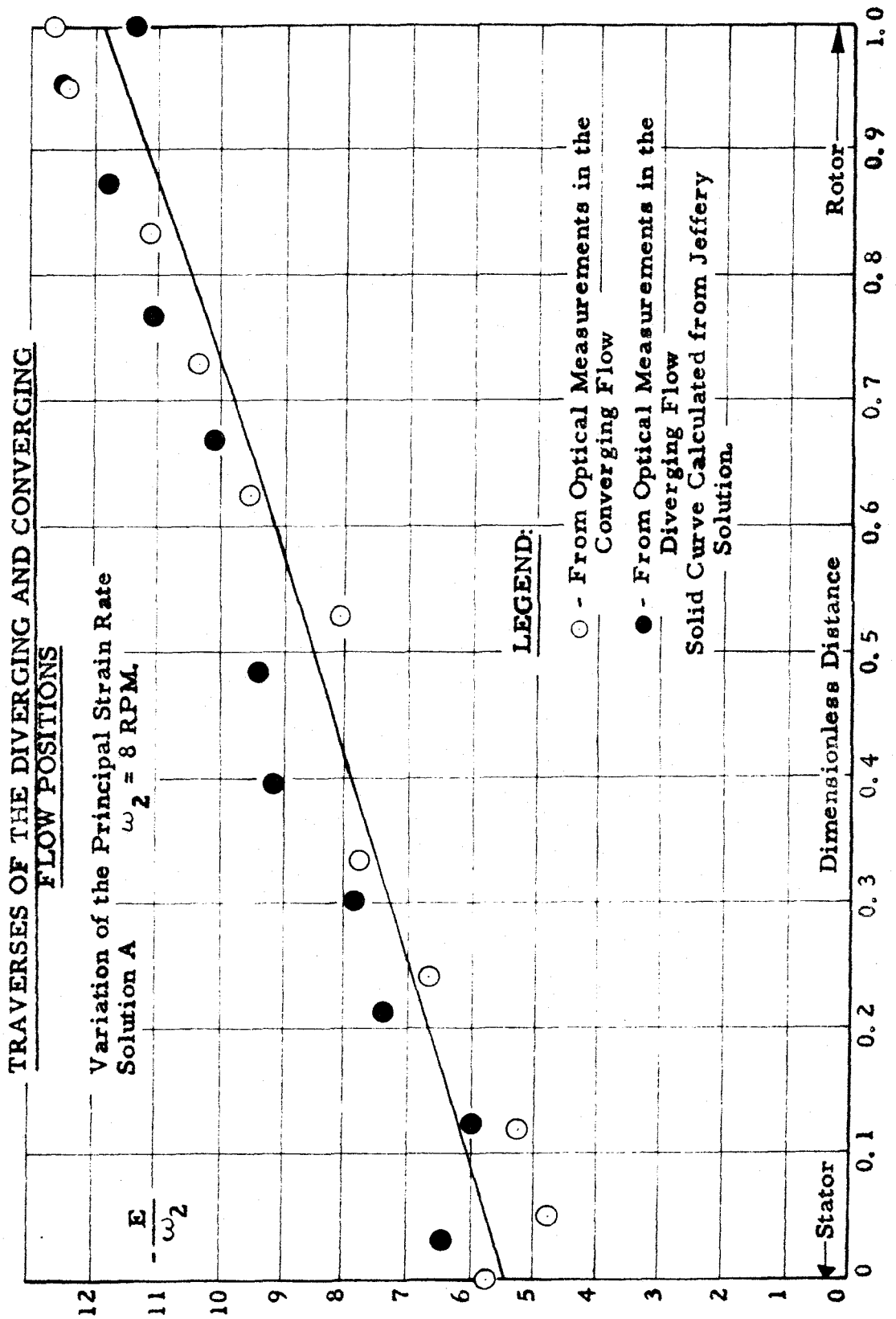
TRAVERSES OF THE DIVERGING AND CONVERGING FLOW POSITIONS
Variation of the Principal Strain Rate
Solution A
ω_2 = 8 RPM.
$-\frac{E}{\omega_2}$
LEGEND:
○ - From Optical Measurements in the Converging Flow
● - From Optical Measurements in the Diverging Flow
Solid Curve Calculated from Jeffery Solution.
Stator
Rotor
Dimensionless Distance
0
0.1
0.2
0.3
0.4
0.5
0.6
0.7
0.8
0.9
1.0
1
2
3
4
5
6
7
8
9
10
11
12

Figure 19

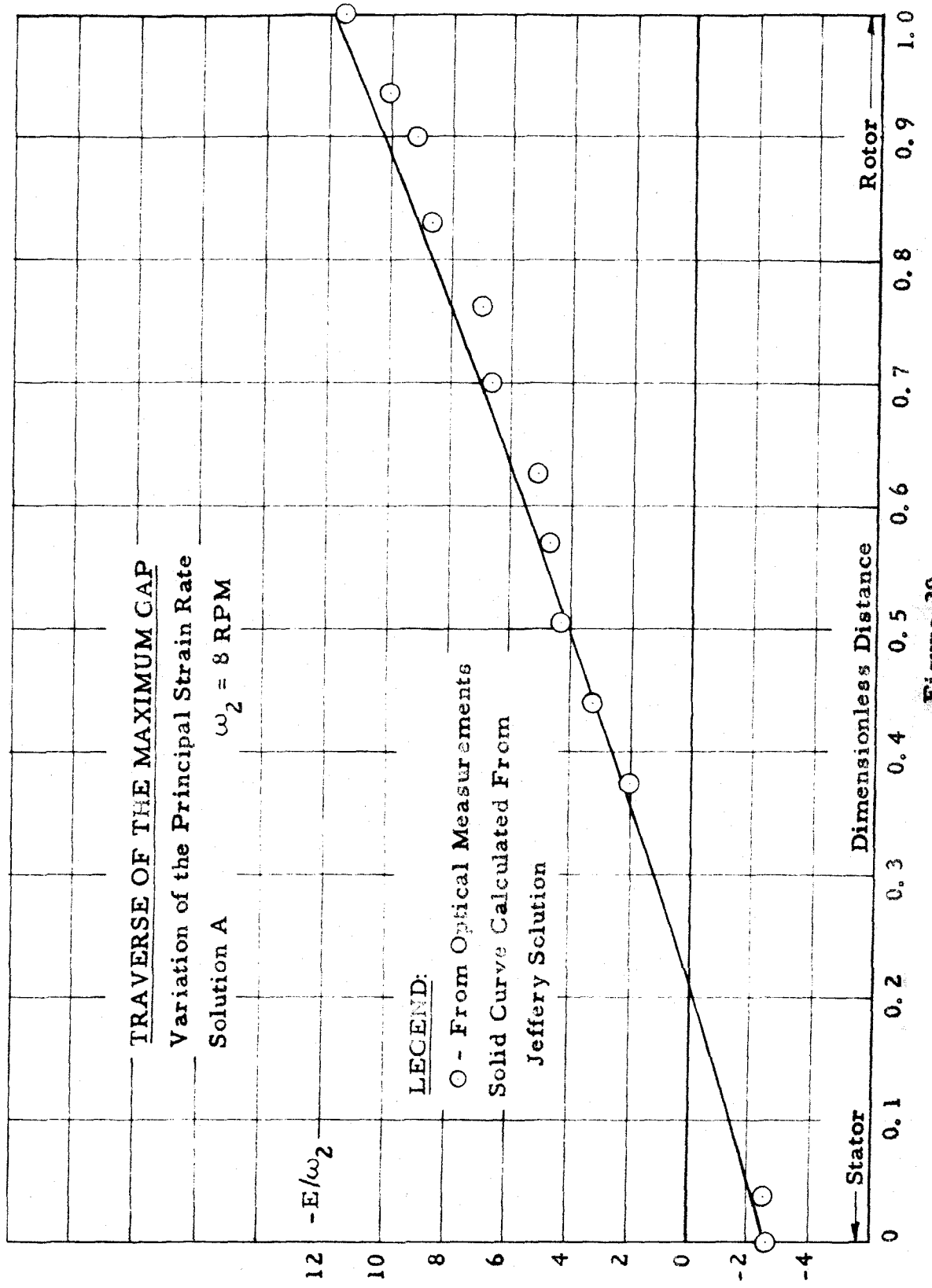
TRAVERSE OF THE MAXIMUM GAP
Variation of the Principal Strain Rate
Solution A
ω_2 = 8 RPM
LEGEND:
O - From Optical Measurements
Solid Curve Calculated From
Jeffery Solution
$-E/\omega_2$
12
10
8
6
4
2
0
-2
-4
0
0.1
0.2
0.3
0.4
0.5
0.6
0.7
0.8
0.9
1.0
Stator
Rotor
Dimensionless Distance

Figure 20

Figures 21 and 22 show how the orientation of the principal strain rates as deduced from the optical data compare with those predicted by the Jeffery solution. The location of an experimental point on these plots involves the calibration curve in the following way: At a particular station the birefringence is measured and the principal optical axes are located with respect to the rotor streamline. For the particular birefringence, the calibration gives a definite angle of isocline, χ, which, it will be recalled, is the angular separation between the principal optical axes and the principal axes of rate of strain. Having already located the principal optical axes, one then knows the location of the principal strain rate axes, at least with respect to the reference streamline. Hence it is difficult to attach a meaningful confidence interval to the points plotted in these figures because the reliability of the χ calibration is also involved. The ranges indicated for the points signify one standard deviation in each direction for the extinction angle data. In regions where E is relatively large, these ranges are probably quite realistic as 95 percent confidence intervals. For some of these points 95 percent confidence intervals were calculated on the basis of Student's "t" distribution for small sample analysis. Because of the small number of readings involved and the size of the sample variance in these curves, the 95 percent confidence interval was quite close to the interval determined by marking off one standard deviation on each side of the sample mean.

The reader will note that in the maximum gap the constant 45° orientation is verified quite well within the limits of the

TRAVERSES OF THE MAXIMUM AND MINIMUM GAP

Orientation of the Principal Strain Rate Axes

Referred to the Rotor Streamline

Solution A ω_2 = 8 RPM

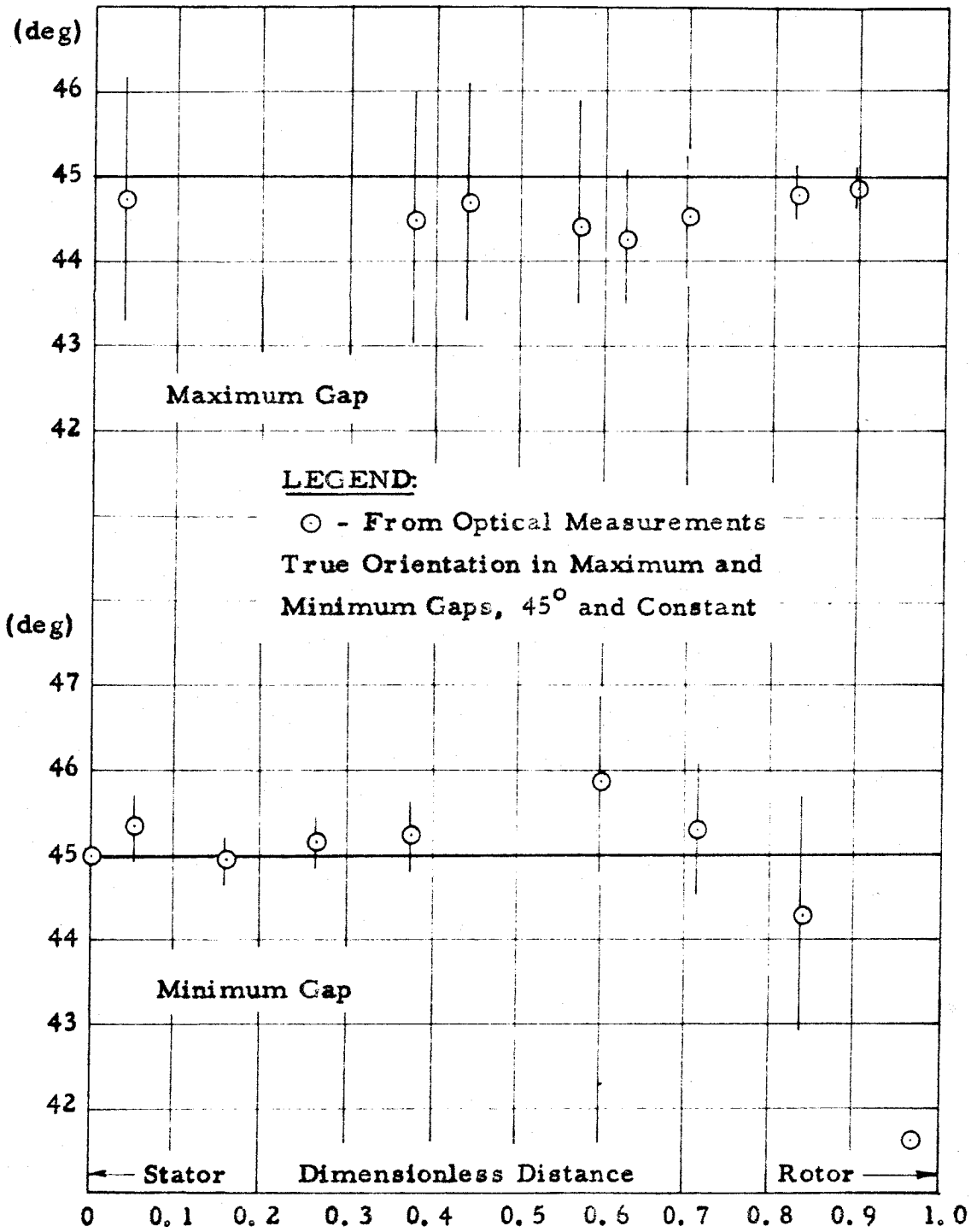

Figure 21

TRAVERSE OF THE DIVERGING FLOW POSITION

Orientation of the Principal Strain Rate Axes

Referred to the Rotor Streamline

Solution A ω_2 = 8 RPM

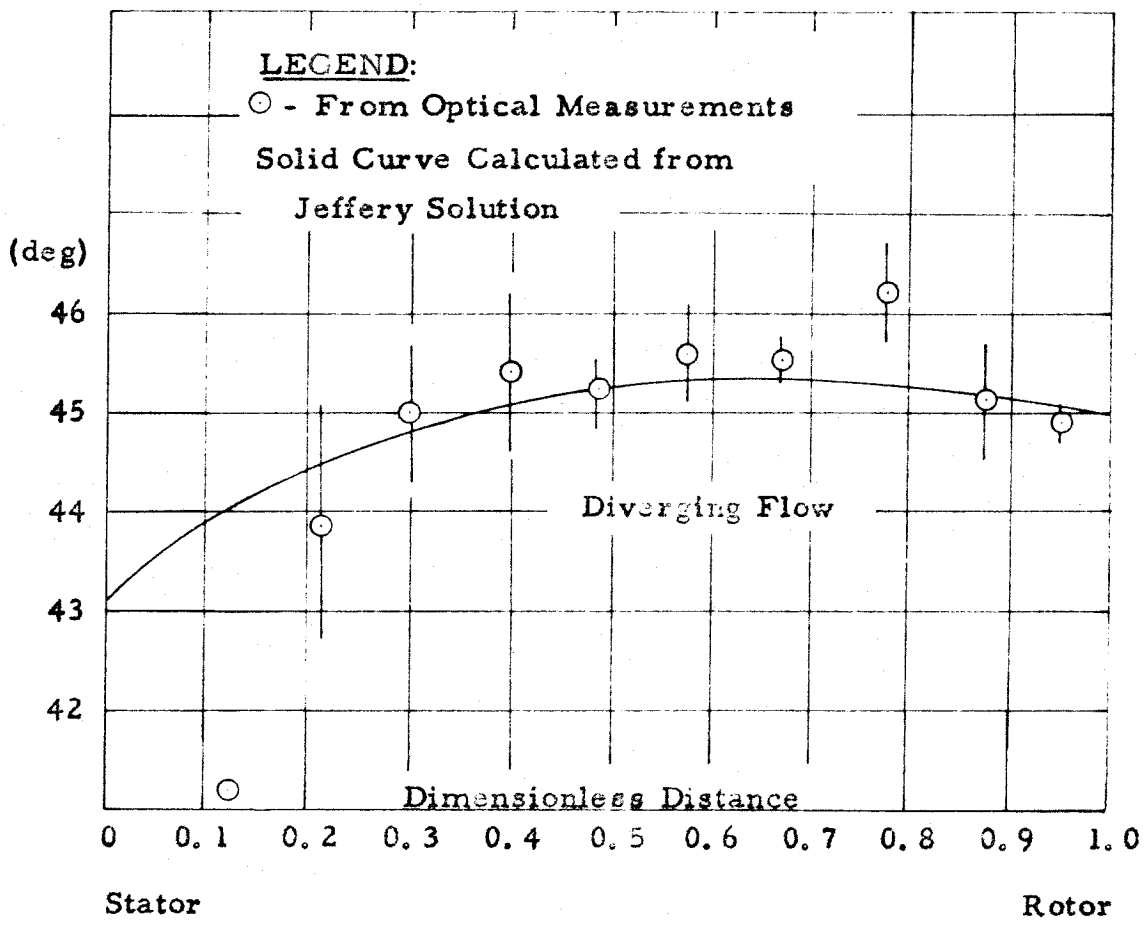

Figure 22

experimental accuracy. The absence of points between the 5 and 35 percent positions (of the gap width from the stator wall) is due to the vanishing birefringence in the neighborhood of the stagnation zone and velocity minimum in the reversed flow. Agreement is also satisfactory in that half of the minimum gap adjacent to the stator. This is the region where the principal strain rate is the highest for the entire non-uniform gap. As evidenced by Figure 18, however, E decreases steadily to a very low value as one approaches the rotor in the minimum gap. Between the gap mid-point and the rotor the angle data seems to exhibit a definite curved nature contrary to the expected constant 45° orientation. The scatter in the data is admittedly higher there, due to the small strain rates, but the downward trend is prominent nevertheless.

This lack of accord on the orientation of the principal strain rates in the minimum gap near the rotor persisted in all of the traverses of the minimum gap flow. It is believed significant that this neighborhood is also one of very small E values, such that interpretation of the extinction angle data there depends upon the extrapolated portion of the χ calibration (Figure 16). It is unfortunate that the sensitivity of the angle of isocline measurements in the present work was not sufficient to provide reliable values of χ in the range of very small E. One can conjecture that if the χ curve were higher than the extrapolated curve in the range of E less than 10 sec^{-1}, the discrepancy would not be so great. Such a χ curve would have a steeper slope at the origin and break off more sharply than that constructed in Figure 16. It has already

been stated that the steeper slope is predicted by the general orientation theory for a population containing some dimers. The author considers extremely noteworthy a private communication which reported that Dr. Joseph Leray of the CRM in Strasbourg, working with a more sensitive instrument, found just such a behavior for the angle of isocline in the Caltech TMV strain. He even observed a slight increasing trend in χ as the breaking-off point was approached from the high strain rate side.

Except for two isolated points the angle data taken within the diverging flow (Figure 22) lies within one-half a standard deviation from the curve calculated from the Jeffery solution. The vertical segments attached to the experimental points in Figure 22 represent one-half the standard deviation of the readings for the particular points. A curve showing the similar comparison for the converging flow position is not included because of a nearly uniform 5^{o} discrepancy exhibited by the angle data taken in that position. This was believed due to a zero shift error possibly brought on by the disturbance of the polarimeter and/or the cell before the traverse of the converging flow position could be performed. The converging flow traverse was the last taken, three days after the first one in the minimum gap. It is very possible that the polarimeter could have been jarred inadvertently between the third and last traverses, thereby upsetting the zero orientation for the polarimeter scale which was determined just once during the first traverse in the minimum gap. An even more plausible explanation might be a disturbance of the cell position during

rotation of the gap position. It will be recalled that this rotation is accomplished by manipulating a worm gear which drives a ring gear built onto the eccentric stator. Occasionally binding would occur somewhere along the ring gear, and when it did, considerable force was required to override the bound tooth or teeth. The exertion of this force could conceivably have moved the cell which is held in place by only four bolts passing through holes with clearance fits.

Figures 23 through 27 display the results of the survey conducted with Solution B. The concentration of Solution B was estimated to be about three times that of Solution A, but this estimate may be unreliable since the calculated concentrations were always based on the stated concentrations of the solutions received from the Biology Division. These statements were admitted to be approximate only. For sufficiently small concentrations, the optical coefficient should be directly proportional to the concentration. On this basis, the concentration of Solution B appears to be about two and one-half times that of Solution A.

Despite the greater optical activity the scatter in the extinction angle data in regions of low birefringence was still discouraging. For this reason, the remarks made above concerning the angle of isocline calibration of Solution A pertain equally strongly to that of Solution B. The number of points considered sufficiently reliable to include in the angle of isocline calibration is really too small to permit the attachment of much

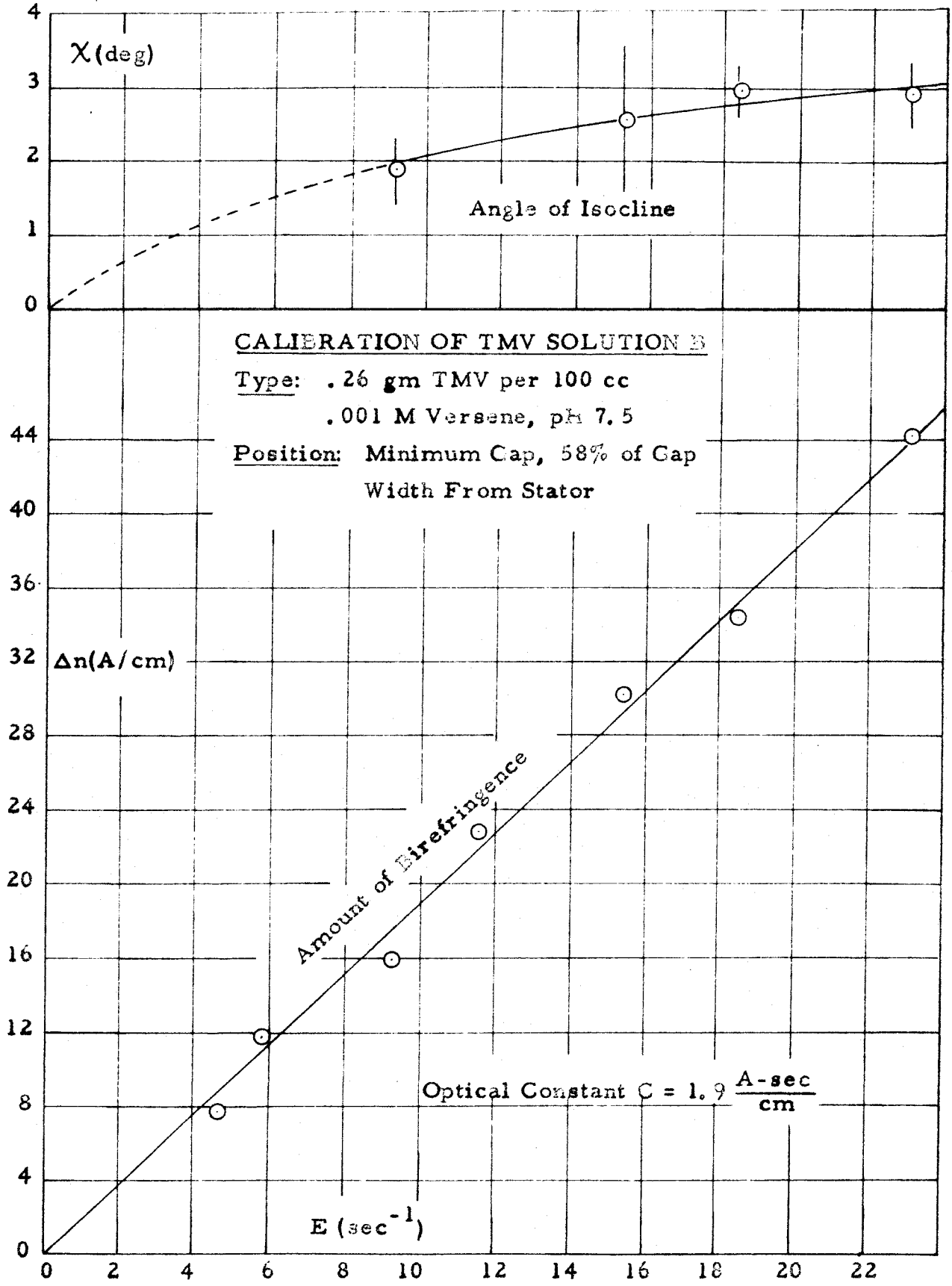
χ(deg)
Angle of Isocline
CALIBRATION OF TMV SOLUTION B
Type: .26 gm TMV per 100 cc
.001 M Versene, pH 7.5
Position: Minimum Cap, 58% of Gap
Width From Stator
Δn(A/cm)
Amount of Birefringence
Optical Constant C = 1.9 A-sec/cm
E (sec⁻¹)
0
2
4
6
8
10
12
14
16
18
20
22
1
3
44
40
36
32
28
24

Figure 23

weight to the validity of the detailed character of the χ curve in Figure 23. The overall increase of 3^{o} for the particular range of strain rates is reasonable enough, but the shape of the curve for low E values could be, and quite probably is, markedly different from the extrapolated one in Figure 23. Strong evidence to support this probability is again available in the angle data taken during the minimum gap traverse. Figure 24 shows how the interpreted orientations of the principal strain rates stray even more gravely away from the expected 45^{o} orientation as the rotor is approached.

Except for what appears to be a zero shift error of one degree in the results of the diverging flow traverse, the comparisons shown in Figure 25 can be said to constitute agreement within the limits of experimental error. In this set of runs, the diverging flow traverse was the last one of the three performed. This means that the non-uniform gap had to be rotated through 300^{o} between the first (minimum-gap) traverse and the diverging flow traverse. The suggestion is again made that the apparent zero shift in the latter traverse might be due to a slight displacement of the cell during the rotation.

It will be noticed from Figures 26 and 27 that agreement on the principal strain rate variation in the three traversed positions is not as good as that obtained with Solution A. The runs made with the two aqueous solutions were alike in all respects save for the concentrations. Since the discrepancies are not such as could be corrected by a simple multiplying factor, the possibility

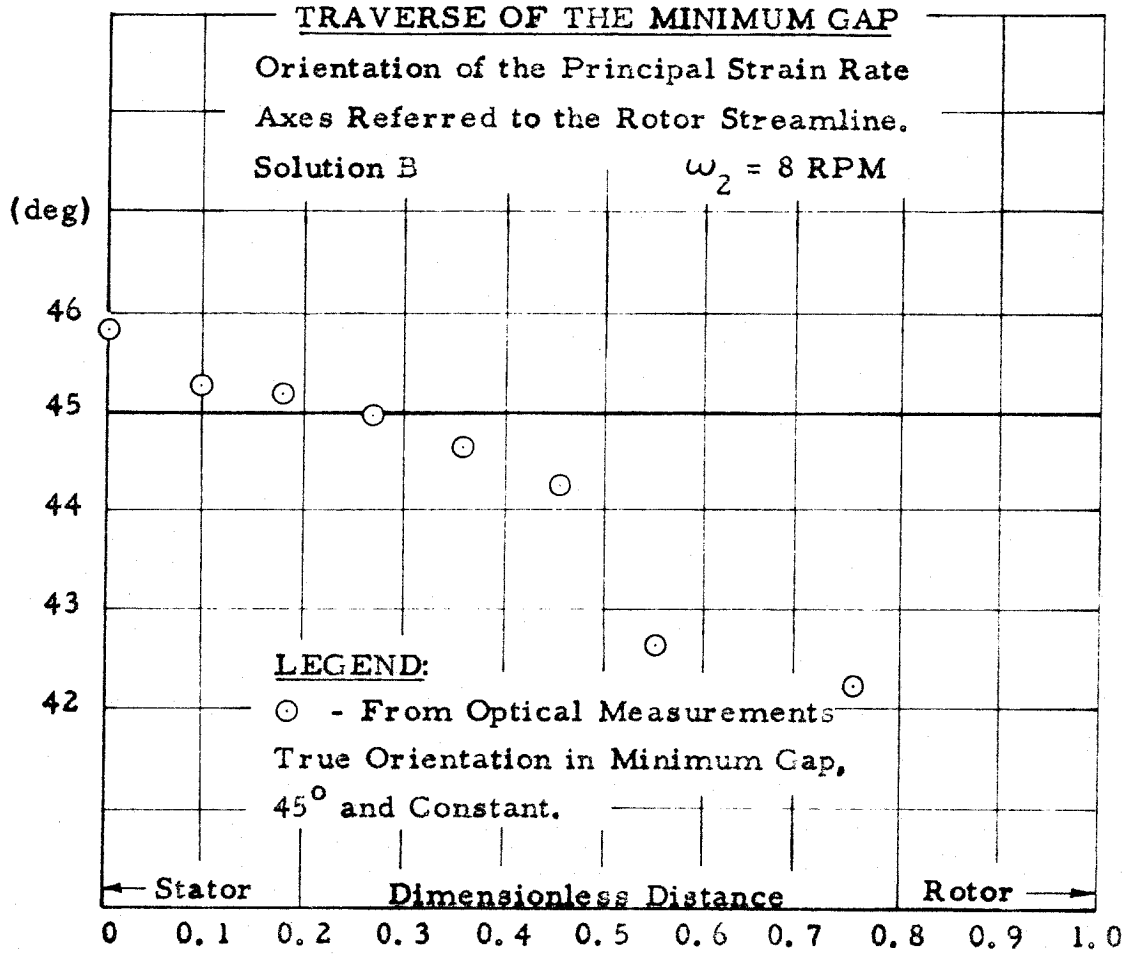
TRAVERSE OF THE MINIMUM GAP
Orientation of the Principal Strain Rate Axes Referred to the Rotor Streamline.
Solution B
ω_2 = 8 RPM
(deg)
46
45
44
43
42
LEGEND:
⊙ - From Optical Measurements
True Orientation in Minimum Gap, 45° and Constant.
← Stator
Dimensionless Distance
Rotor →
0
0.1
0.2
0.3
0.4
0.5
0.6
0.7
0.8
0.9
1.0

Figure 24

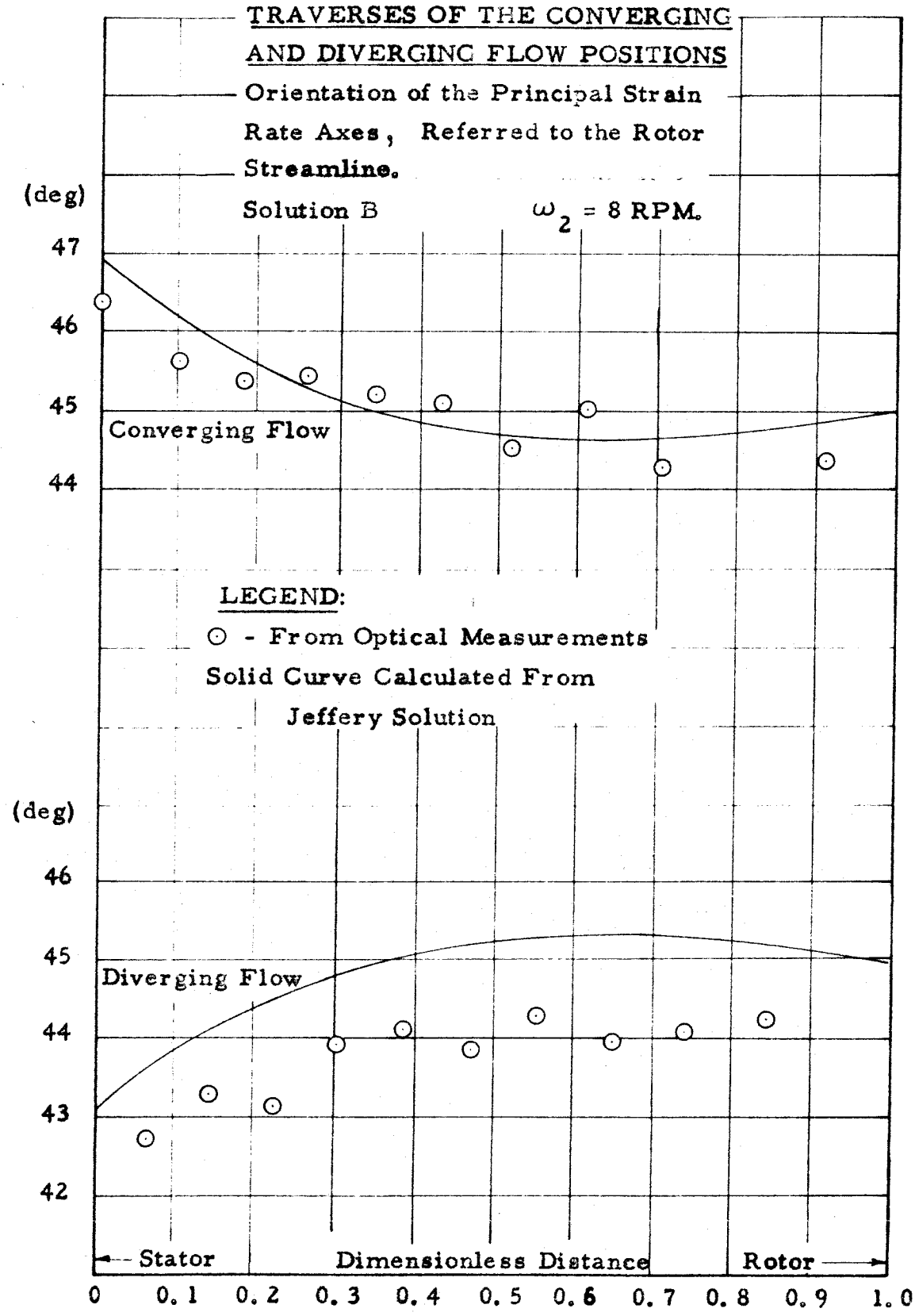
TRAVERSES OF THE CONVERGING AND DIVERGING FLOW POSITIONS
Orientation of the Principal Strain Rate Axes, Referred to the Rotor Streamline.
Solution B
ω_2 = 8 RPM.
(deg)
47
46
45
44
Converging Flow
LEGEND:
⊙ - From Optical Measurements
Solid Curve Calculated From Jeffery Solution
(deg)
46
45
44
43
42
Diverging Flow
Stator
Dimensionless Distance
Rotor
0
0.1
0.2
0.3
0.4
0.5
0.6
0.7
0.8
0.9
1.0

Figure 25

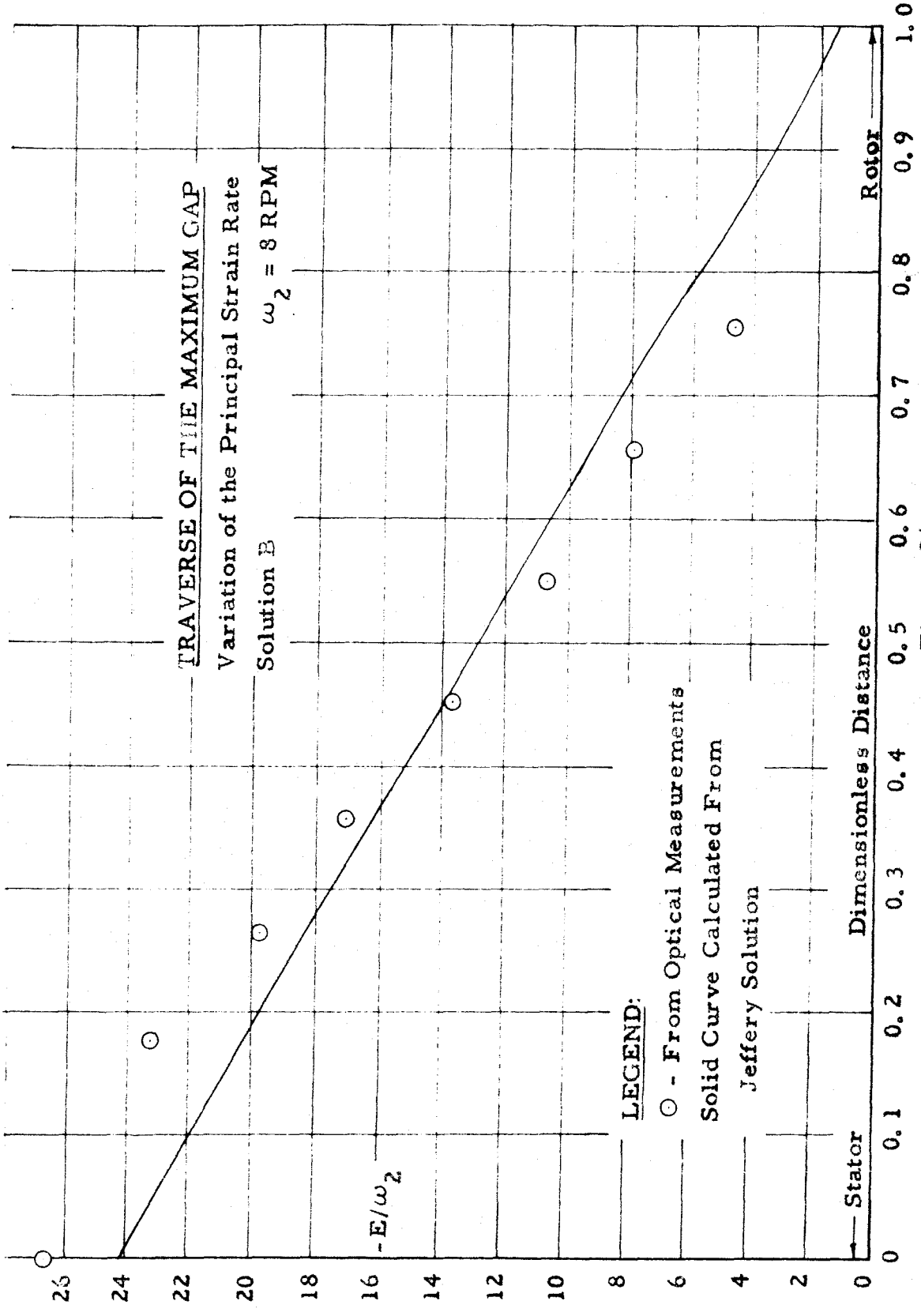
TRAVERSE OF THE MAXIMUM GAP
Variation of the Principal Strain Rate
Solution B
ω_2 = 8 RPM
$-E/\omega_2$
LEGEND:
⊙ - From Optical Measurements
Solid Curve Calculated From
Jeffery Solution
Stator
Rotor
Dimensionless Distance
0
2
4
6
8
10
12
14
16
18
20
22
24
25
0.1
0.2
0.3
0.4
0.5
0.6
0.7
0.8
0.9
1.0

Figure 26

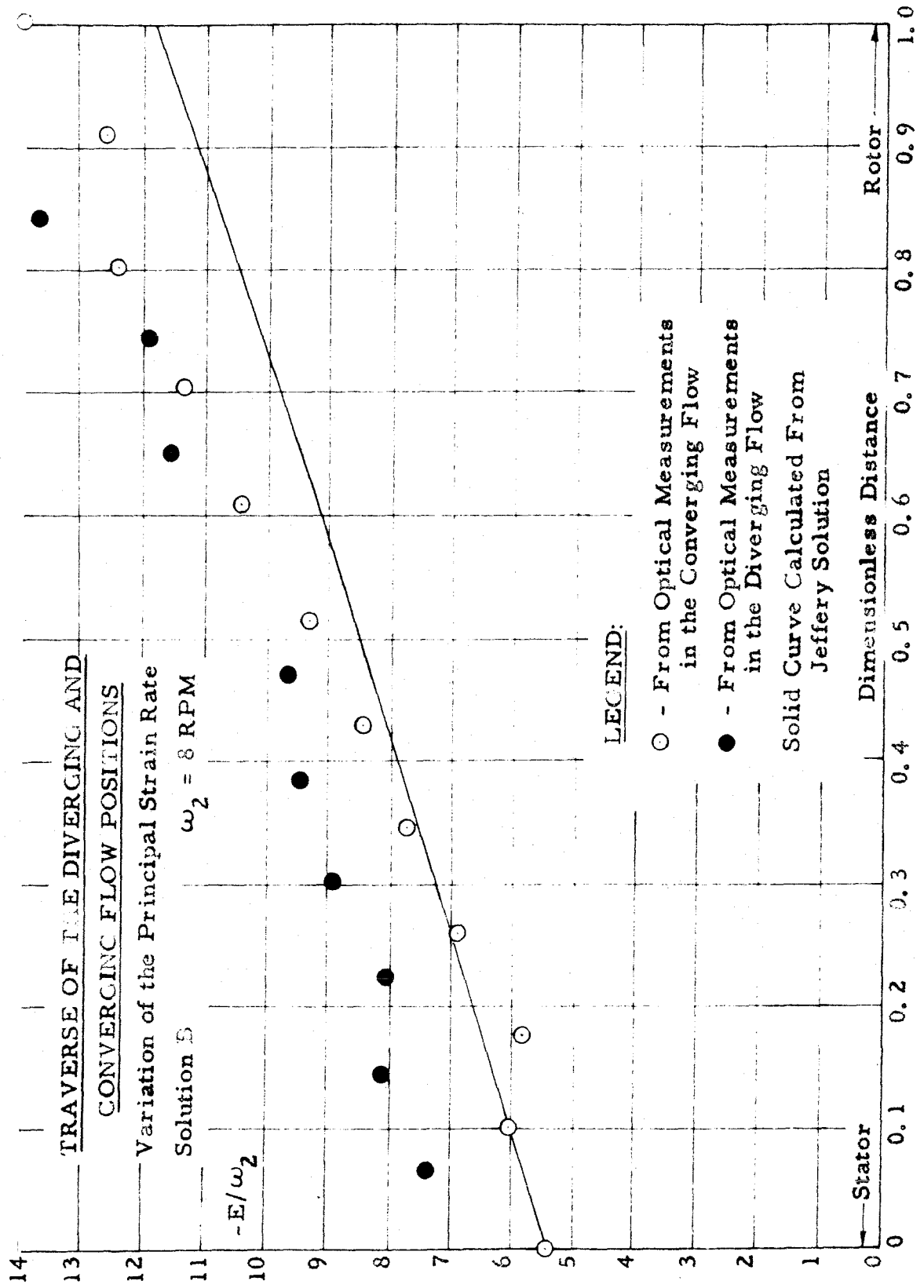
TRAVERSE OF THE DIVERGING AND
CONVERGING FLOW POSITIONS
Variation of the Principal Strain Rate
Solution 5
ω_2 = 8 RPM
$-E/\omega_2$
LEGEND:
○ - From Optical Measurements in the Converging Flow
● - From Optical Measurements in the Diverging Flow
Solid Curve Calculated From Jeffery Solution
Stator
Rotor
Dimensionless Distance
0
0.1
0.2
0.3
0.4
0.5
0.6
0.7
0.8
0.9
1.0
1
2
3
4
5
6
7
8
9
10
11
12
13
14

Figure 27

of their being due to a calibration error is discounted. The question of whether or not the large particle concentration might be producing some observable distortion of the flow, so that the Jeffery solution no longer gives a true description of the flow, is a legitimate one. It is interesting that the distribution of experimental points in the minimum gap (Figure 26) is just what one would expect to observe if the pressure gradient in the minimum gap were greater than that predicted by Jeffery's solution. The minimum gap velocity profile predicted by the theoretical solution is almost the exact resultant of a pure shear or linear profile and a pressure flow or parabolic profile. Let x be a normalized coordinate for the minimum gap with origin at the stator. The velocity profile can then be approximated by

$$u_\beta = Cx + 4B\,(x - x^2)$$

where C is the rotor wall velocity and B is the velocity maximum of the pressure flow part of the profile. B is proportional to the pressure gradient producing the pressure flow. Since the transverse variation of u_β makes up the major portion of the principal strain rate in the minimum gap, then to the same order of approximation

$$E = \frac{du_\beta}{dx} = C + 4B - 8Bx$$

whence

$$\frac{dE}{dx} = -8B$$

The slope of the principal strain rate distribution in the minimum gap is constant and proportional to the pressure gradient. If the

pressure gradient is higher than that theoretically predicted, the slope of the E curve will be proportionately greater. The value of E at the midpoint ($x = 1/2$) will still be C, however. The line E(x) will just be rotated about this value C at $x = 1/2$. (This is logical since the area under the curve must remain constant if the boundary condition $u_\beta = C$ at $x = 1$ is to hold.) The experimental points in Figure 26 do seem to fall along a line of steeper slope rotated about a point close to the mid-section of the theoretical curve.

Figures 28, 29 and 30 illustrate the results of the work done with Solution C. Although the TMV concentration in Solution C is only 18 percent greater than that in Solution A, comparison of the two calibrations, Figures 16 and 28 gives evidence to a tenfold increase in the optical activity of C over that of A. Note also that the overall change in the angle of isocline over the range $0 < E < 30$ sec^{-1} has increased by nearly the same factor of ten. Another interesting observation that can be made from the calibration of Solution C concerns the extent of the linear birefringence range. The break in linearity occurs around $E = 4$ sec^{-1} for the angle of isocline and around $E = 6$ sec^{-1} for the birefringence. The general orientation theory predicts that the second order term in σ should be perceived for a value of σ slightly greater than unity. This would indicate that the rotary diffusion constant for the glycerol solution is of the order of 4 sec^{-1}. If the rotary diffusion constant is simply inversely proportional to the solvent viscosity, and if D for the aqueous solutions is really 200 sec^{-1},

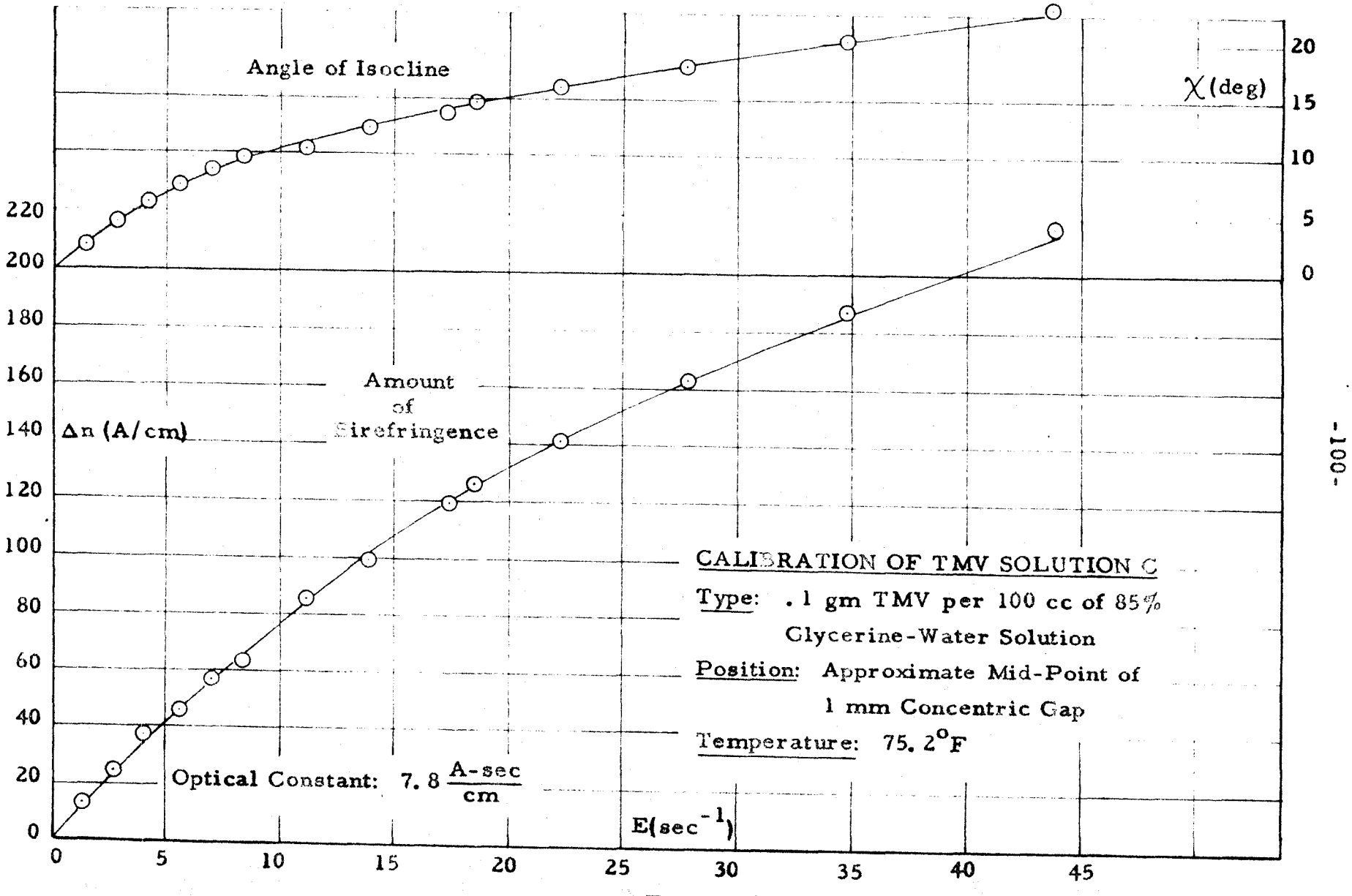
Angle of Isocline
χ (deg)
20
15
10
5
0
220
200
180
160
140
120
100
80
60
40
20
0
Amount
of
Birefringence
Δn (A/cm)
CALIBRATION OF TMV SOLUTION C
Type: .1 gm TMV per 100 cc of 85% Glycerine-Water Solution
Position: Approximate Mid-Point of 1 mm Concentric Gap
Temperature: 75.2°F
Optical Constant: 7.8 A-sec/cm
E(sec⁻¹)
0
5
10
15
20
25
30
35
40
45

Figure 28

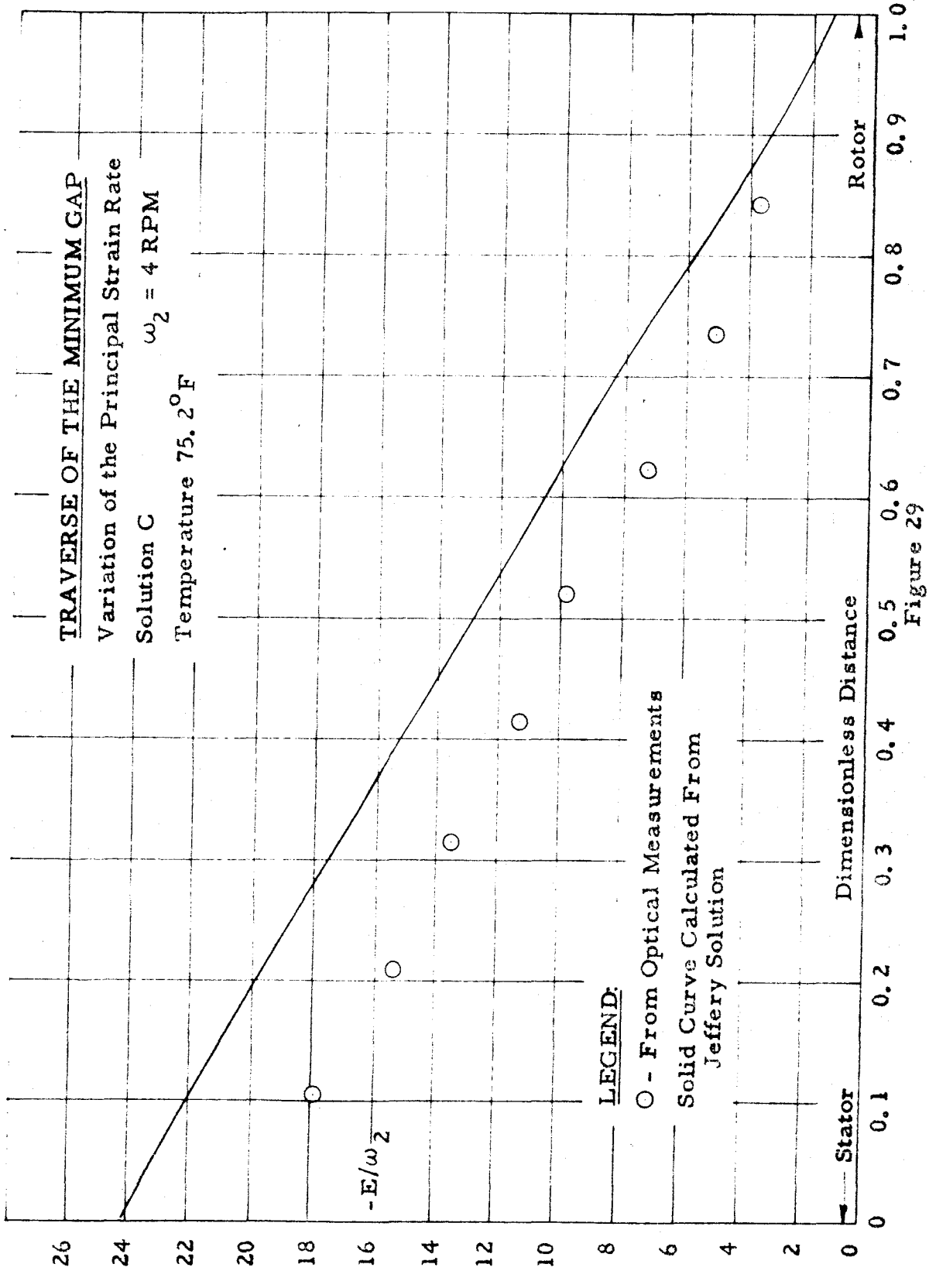
TRAVERSE OF THE MINIMUM GAP
Variation of the Principal Strain Rate
Solution C
ω_2 = 4 RPM
Temperature 75.2°F
$-E/\omega_2$
LEGEND:
O - From Optical Measurements
Solid Curve Calculated From
Jeffery Solution
Stator
Rotor
Dimensionless Distance
0
0.1
0.2
0.3
0.4
0.5
0.6
0.7
0.8
0.9
1.0
2
4
6
8
10
12
14
16
18
20
22
24
26

Figure 29

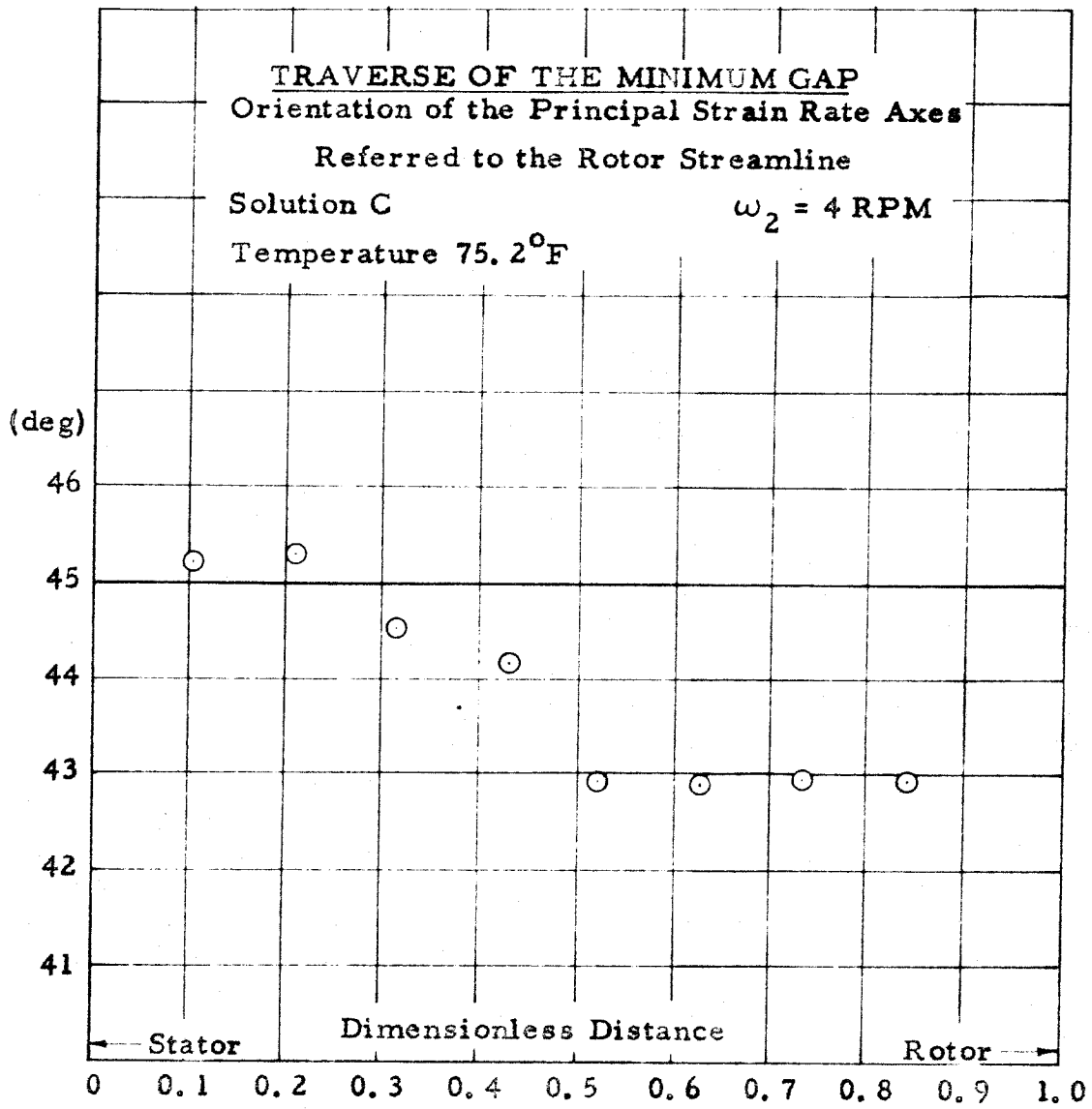
TRAVERSE OF THE MINIMUM GAP
Orientation of the Principal Strain Rate Axes
Referred to the Rotor Streamline
Solution C
ω_2 = 4 RPM
Temperature 75.2°F
(deg)
46
45
44
43
42
41
Stator
Dimensionless Distance
Rotor
0
0.1
0.2
0.3
0.4
0.5
0.6
0.7
0.8
0.9
1.0

Figure 30

then a viscosity increase of about 50 times seems apparent. Actually the glycerol solution was prepared to be more like 80 to 100 times more viscous than pure water. This rather hasty comparison shows definite order of magnitude correctness, but it seems to cast some doubt on the exactitude of the 200 sec^{-1} value of D for the aqueous solutions. A value one and a half to two times higher would be more compatible with the Solution C calibration and the orientation theory's results.

With Solution C only the minimum gap was explored. The solution was calibrated in the Couette cell with a 1 mm gap. At first these runs were performed on successive days at ambient temperature, without temperature control. The comparison between interpreted and calculated values of E/ω_2 revealed a uniform 20 percent discrepancy, such as could be caused by a calibration error. The possibility that the solution temperatures might have been significantly different during the calibration and traverse led to a study of the temperature dependence of the optical properties of Solution C. It was found that the birefringence and the angle of isocline corresponding to a particular value of E varied by about 2 percent per degree Fahrenheit. It therefore seemed unlikely that temperature differences could account for the entire discrepancy. The runs were nevertheless repeated with the temperature rigidly controlled at 75. $2^{o}F$. The results of the traverses, displayed in Figures 29 and 30, attest to the prevalence of the discrepancy in the interpreted distribution of the principal strain rate. The curious behavior of the angle data in the minimum gap also persisted.

No outstanding explanation was conceived for the discrepancies exhibited in the experiments conducted with Solution C. However, the author feels that the results of these last experiments should be considered suspect since no effort was given to the maintenance of a proper pH for the solution. Almost certainly the pH of the glycerol solutions was lower than the recommended level of 7.5. This condition leaves open the possibility that aggregation was progressing during the experiments. It seems quite certain now that the TMV strain used was polydisperse when received. Progressive aggregation would result in even greater polydispersity with even higher concentrations of the dimer.

The rotary diffusion constant for the TMV dimer is approximately six times smaller than that for the monomer. In the viscous glycerol solutions, where the monomer diffusion constant is already as low as 2 to 4 sec^{-1}, the dimer's diffusion constant would be about 0.5 sec^{-1}. The relaxation time, τ, of an orientable particle is a measure of the speed with which it can adjust to or come to equilibrium with a changing orienting field. According to a rule-of-thumb the relaxation time is of the order of $1/6D$. Whereas τ for the monomer suspended in the glycerol solution is of the order of 0.1 second, it becomes as large as 0.5 second, or thereabouts, for the dimer in the same solvent. Remembering that a stationary general flow appears unsteady to a particle traveling through it, one can reason that a dimer moving with an average velocity of 2 cm/sec may still be influenced by conditions 1 cm upstream of its instantaneous location. These remarks point out that relaxation effects due to significant concentrations of the TMV dimer might at

least have contributed to the anomalous results obtained with Solution C.

By way of summary, it seems permissible to conclude that, in the particular general flow investigated, the experimental results support the conclusions of the general orientation theory. The agreement between the principal strain rates interpreted from birefringence measurements and those predicted theoretically is especially encouraging. In most instances the interpreted orientations of the principal strain rates agreed with the theoretical orientations within the limits of the experimental accuracy. Certain anomalous results have been presented; these generally have to do with interpreted directions of the principal strain rates. The experimental accuracy is definitely poorest for the measurements which lead to the latter interpretations. There is very strong evidence that polydispersity has affected the results, especially those results which depend on extinction angle measurements in regions of low rate of strain.

6.0 The Problem of Calculating the Velocity Field from Information Supplied by Birefringence Measurements

It was stated in the Introduction that a second objective of the thesis was to study the mathematical problem of reconstructing a general two-dimensional velocity field from the information which, according to the orientation theory, is provided by the optical measurements. An answer to this problem is of basic importance to the question of whether or not streaming birefringence can be of use as a tool for hydrodynamic analysis.

6.1. Relation to Previous Work on the Problem

Rosenberg [18] has considered a related mathematical problem and proposed a method for deducing the flow pattern from photographed interference patterns. Prados [25] actually applied this method to bounded flow past a cylindrical obstacle. By pure coincidence, certain features of the problem considered by Rosenberg are closely related to the problem which is to be analyzed in this section of the thesis. As a prelude to this analysis, it will be worthwhile to review briefly the thinking behind the method proposed by Rosenberg, and then to criticize this method in the light of the conclusions reached by the author.

As discussed in Section 2.0 Rosenberg made certain hypotheses concerning a stress-optic law which governed the birefringence observed in pure liquids. On the basis of these hypotheses he reasoned that, in Newtonian liquids at least, birefringence measurements could be interpreted to give the maximum rate of shear strain and the orientation of the plane of maximum

rate of shear. He then was faced with the following problem: Given the maximum rate of shear and the orientation of the maximum shear rate planes throughout a two-dimensional laminar flow, can the complete velocity field be calculated? Rosenberg concluded that it could, and demonstrated how the calculation might be carried out for an open rectangular two-dimensional region through which passes a known quantity of fluid per unit time. His proposed method involves the stream function and results in a second order partial differential equation for this function. This method will now be briefly reviewed.

First of all envision a Cartesian frame x, y with its x axis along the semi-infinite boundary of the flow region. The flow enters across the line x = 0, and the width of the entrance is "a" $(0 < y < a)$. At any point in the flow the maximum rate of shear is $E(x, y)$, and the angle between the direction of maximum shear rate and the x axis is called $\eta(x, y)$. Then the local rate of shear acting in the x direction along the plane y = constant is just

$$e_{xy} = E \cos 2\eta \tag{41}$$

Now

$$e_{xy} = \frac{1}{2}\left(\frac{\partial u}{\partial y} + \frac{\partial v}{\partial x}\right) \tag{42}$$

where u and v are the local x and y velocity components. By definition of the stream function this last equation can be written

$$\frac{\partial^2 \Psi}{\partial x^2} - \frac{\partial^2 \Psi}{\partial y^2} = 2E \cos 2\eta = f(x, y) \tag{43}$$

In principle, if E cos 2η is known throughout the flow field, this partial differential equation can be solved for Ψ provided the boundary conditions are known and proper.

Rosenberg suggested a way to integrate numerically for Ψ in the previously mentioned open rectangular region. In the entrance cross section the flow is parallel (v = 0), and if the streamline curvature in the "x" direction also vanishes there ($\partial^2\Psi/\partial x^2 = 0$), the velocity distribution u(y) and the stream function distribution $\Psi(y)$ at the entrance can be computed directly from

$$\left(\frac{\partial^2\Psi}{\partial y^2}\right)_{0,y} = -f(0, y) \qquad (44)$$

Ψ may be arbitrarily set equal to zero on one boundary, say y = 0, and since the flow rate is known, the value of Ψ on the other boundary y = a is automatically determined. With a knowledge of Ψ on each of the three boundaries one can at least begin downstream-running computations of Ψ at the intersections of a rectangular grid superimposed on the flow region.

Prados [25] applied the procedure suggested by Rosenberg in his attempt to construct the streamlines in the flow normal to a cylindrical obstacle. The test section in which he obtained his photographs of interference patterns was an open two-dimensional rectangular channel containing a cylindrical obstacle, as depicted in Figure 31. Somewhere upstream of the test section the volumetric flow rate was measured. The stream function was set equal to zero along the centerline of the channel (y = a/2),

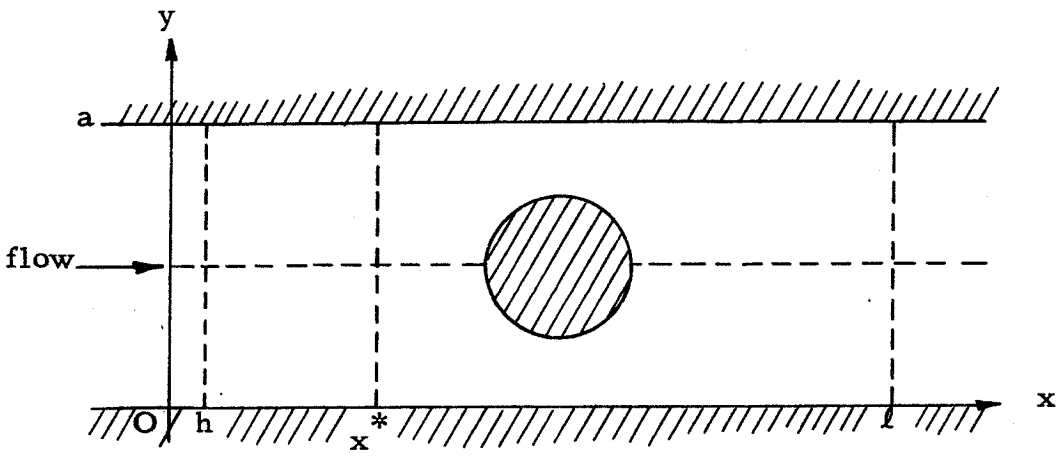

Figure 31

and the stream function distribution was then calculated at some cross section far upstream from the obstacle, say $x = 0$, by integration of Eq. 44. The values of Ψ calculated for the two boundaries ($y = 0$, $y = a$) at the entrance were then the specified values of Ψ all along those two boundaries. Prados resorted to symmetry considerations to reason that the cylinder boundary was part of the zero streamline. He then had Ψ specified along all the rigid boundaries.

In order to initiate his numerical integration and carry it downstream from the entrance he needed to know Ψ along two adjacent vertical grid lines upstream of the obstacle. He obtained this information at $x = 0$ and $x = h$, both sections wherein he assumed that $\partial\Psi/\partial x = \partial^2\Psi/\partial x^2 = 0$. To complete the integration over the entire region he also found it necessary to know $\Psi(y)$ along two adjacent vertical grid lines far downstream of the obstacle, say at $x = \ell - h$ and $x = \ell$. This he obtained by making

the same assumptions as before concerning the velocity component v and the streamline curvature. The computation process was therefore an iterative one starting along both upstream and downstream edges of the grid and working toward the middle.

There were no existent theoretical treatments corresponding to the actual bounded flow against which Prados could compare his derived flow pattern. Hence he was not able to assess the validity of his integration. Nor could he check his velocity profiles by calculating discharges since the flow through the channel was already determined by fixing the values of the stream function along the boundaries.

The general orientation theory, on which this thesis research is based, predicts that, at best, the optical measurements can be interpreted to give the principal strain rate (E) and the orientation of the principal strain rate axes. This will be so if the strain rates are sufficiently small, such that the birefringence is a linear function of E, and if the streamlines are inclined at 45^{o} to the principal strain rate axes. If the angle Λ_{o} is equal to 45^{o}, then within the bounds of the linearity restriction the orientation of the principal strain rates will be given exactly by the birefringence measurements. If Λ_{o} does not differ by very much from 45^{o}, so that $\sin 2\Lambda_{o}$ does not differ greatly from unity, the optical measurements can be interpreted to yield a good approximation to the principal strain rate directions.

The hypotheses of Rosenberg deal with the direction and magnitude of the maximum rate of shear. The rate of strain

tensor in an incompressible fluid always has zero trace and hence, principal values which are equal and opposite in sign. It follows that the magnitude of the maximum shear rate is identical with that of the principal strain rate, and the two orthogonal maximum shear rate directions are rotated by exactly 45° from the principal axes. Thus the information which Rosenberg hypothesized could be generally derived from birefringence measurements is also the information which the orientation theory allows under the very restricted circumstances stated above. To put it another way, in the light of the general orientation theory, the Rosenberg hypotheses are valid for colloidal systems only for flows in which E is sufficiently small and Λ_o is equal to 45°, or very nearly so. As long as one is concerned with a flow that is so restricted, the problem of constructing the flow pattern is the same as that considered by Rosenberg. For this reason some thought was given to the merits of his stream function proposal, its mathematical soundness, and particularly its applicability to more general boundary conditions than those possessed by the simple rectangular test section envisaged by Rosenberg and used by Prados.

The flow region between the eccentric cylinders is an approximately annular region with a periodic boundary condition in the direction of flow. The solid boundaries are both streamlines, but the difference in the Ψ values to be assigned to each is not known in advance because the flow rate is not known. The normal derivative of the stream function vanishes on one boundary (the stator) while it assumes a known value on the other (the rotor).

This combination of a Cauchy condition on one boundary, a Neumann condition on the other, and a periodicity condition in the flow direction, or time-like variable, would not, under normal circumstances, be viewed as constituting a properly-posed boundary value problem for the hyperbolic partial differential equation which Ψ appears to satisfy. The theory of partial differential equations says that unique and stable solutions to the hyperbolic differential equation are possible only in open regions with boundary conditions of Cauchy type. On this basis it seems that a solution for Ψ in the eccentric cylinder flow is not rigorously possible. A more obvious impediment in the way of carrying out such a numerical integration in the eccentric cylinder flow is the absence of an entrance section wherein the second derivative of Ψ with respect to one of the variables vanishes. In the eccentric cylinder flow there is no position where two fully specified boundaries intersect and from which the numerical integration can be initiated.

Another undesirable feature of the stream function calculation is the necessity of formulating a specified exit section and propagating the computations from both ends toward the middle. Furthermore, if one is studying the flow around a body which is not symmetrical like the circular cylinder, it does not appear feasible to assign a stream function value to the body boundary as Prados did.

6. 2. A Direct Integration Method

Aside from questions of mathematical correctness which one might be tempted to raise concerning certain aspects of the

stream function method, the amount and nature of the boundary information required by it are very restricting. Given further thought, however, it becomes very clear that a much simpler, more direct method exists for constructing the velocity field. This direct method deals directly with first derivatives of the velocity components themselves. It requires no boundary conditions other than the true no-slip condition which exists on every solid boundary in the flow region.

Given the principal values and the orientation of the principal axes of the rate of strain tensor at any point in an incompressible flow, then the components of the rate of strain tensor with respect to any set of orthogonal coordinates are known at the point. For if a pair of coordinate axes, say 1 and 2, are rotated by some angle β from the principal axes at the point in question, then the rate of strain matrix referred to the 1, 2 system is related to the matrix in the principal system by

$$S' = N^{-1} S N \tag{45}$$

where S' and S are the matrices of the strain rate tensor expressed in the 1, 2 coordinates and principal coordinates respectively,

$$S' = \begin{pmatrix} e_{11} & e_{12} \\ e_{21} & e_{22} \end{pmatrix} \qquad S = \begin{pmatrix} E & 0 \\ 0 & -E \end{pmatrix}$$

and N and N^{-1} represent the rotation matrix and its inverse,

$$N = \begin{pmatrix} \cos\beta & -\sin\beta \\ \sin\beta & \cos\beta \end{pmatrix} \qquad N^{-1} = \begin{pmatrix} \cos\beta & \sin\beta \\ -\sin\beta & \cos\beta \end{pmatrix}$$

Performing the multiplication indicated by Eq. 45, one finds that

$$\begin{aligned} e_{11} &= -e_{22} = \mathbf{E}\cos 2\beta \\ e_{12} &= e_{21} = \mathbf{E}\sin 2\beta \end{aligned} \tag{46}$$

A knowledge of the two independent components, e_{11} and e_{12}, and the velocity on all solid boundaries is more than sufficient to permit calculation of the velocity field within the most general region. The calculations can be initiated at any solid boundary.

Figure 32 shows a portion of a general flow region in which

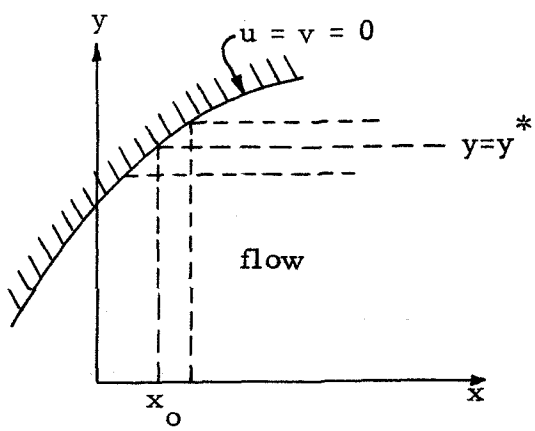

Figure 32

E cos 2β and E sin 2β are presumed known everywhere with respect to a Cartesian coordinate system. A portion of a static boundary is also present within the region. Let E cos 2β = f(x, y) and E sin 2β = g(x, y), then

$$\begin{aligned} e_{xx} &= \frac{\partial u}{\partial x} = -e_{yy} = -\frac{\partial v}{\partial y} = f(x, y) \\ e_{xy} &= \frac{1}{2}\left(\frac{\partial u}{\partial y} + \frac{\partial v}{\partial x}\right) = g(x, y) \end{aligned} \tag{47}$$

Since f(x, y) is known throughout, u can be determined along any line of constant y, say y^*, simply by integrating out from the boundary:

$$u(x, y^*) = u(x_o, y^*) + \int_{x_o}^{x} f(\xi, y^*)d\xi = \int_{x_o}^{x} f(\xi, y^*)d\xi \qquad (48)$$

By performing such integrations along lines of constant y, spaced arbitrarily closely, u(x, y) is determined everywhere. In a similar manner v(x, y) can be determined throughout by integrating from the boundary along lines of constant x. Note that in this example it was necessary to use only the function f in the integrations for u and v. This will be the case whenever the boundaries do not coincide with the coordinate directions.

An example of when it would be necessary to use both functions f and g is provided by the problem studied by Prados. Suppose that f and g were known throughout the flow shown in Figure 31, but that the velocity profile entering the region were <u>not</u> known. It is still possible to calculate u and v everywhere, and no boundary information is required other than the fact that u = v = 0 on y = 0, y = a, and on the obstacle. One could first determine v(x, y) by integrating into the flow from either the upper or lower boundary along lines of constant x. Thus

$$v(x^*, y) = -\int_{o}^{y} f(x^*, \zeta)d\zeta = \int_{a}^{y} f(x^*, \zeta)d\zeta \qquad (49)$$

Once $v(x, y)$ has been so calculated, its partial derivatives can be taken with the result that $\partial u/\partial y$ can be obtained from

$$\frac{\partial u}{\partial y} = 2g(x, y) - \frac{\partial v}{\partial x} \tag{50}$$

Now $u(x, y)$ can be calculated by integrating into the flow along lines of constant x starting from any of the boundaries where $u = 0$. Of course, if the entrance velocity profile is known, u can be determined by direct integration of $\partial u/\partial x = f(x, y)$, and recourse to the function g will not be necessary.

The need for both f and g in the last example can be avoided, however, by using a different Cartesian coordinate system for a reference, in particular, one which is not parallel to the boundaries. Such a frame is the $x'y'$ frame depicted in Figure 33. With respect to the $x'y'$ coordinates Eqs. 47 become

$$\begin{aligned} e_{x'x'} &= \frac{\partial u'}{\partial x'} = -e_{y'y'} = -\frac{\partial v'}{\partial y'} = f(x', y') \\ e_{x'y'} &= \frac{1}{2}\left(\frac{\partial u'}{\partial y'} + \frac{\partial v'}{\partial x'}\right) = g(x', y') \end{aligned} \tag{51}$$

where $f(x', y') = E \cos 2\beta'$ and $g(x', y') = E \sin 2\beta'$. β' is now the angle between the local principal strain rates and the $x'y'$ axes. This transformation accomplished, it is then possible to obtain both $u'(x', y')$ and $v'(x', y')$ by integration of the one function $f(x', y')$ away from the boundaries in the manner of Eqs. 48 and 49.

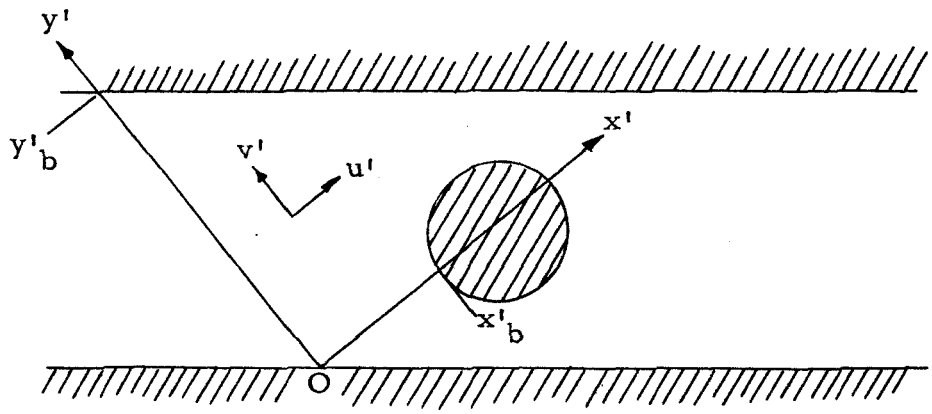

Figure 33

The fact that the integration problem is simplified by the use of a coordinate system which does not coincide with the boundaries is interesting enough to warrant further comment. It is the custom in boundary value problems to employ a coordinate system in which the boundaries may be represented as a curve or surface on which one of the coordinates is a constant. This permits the most convenient expression of the boundary conditions. However, the complexity of the differential equations to be integrated depends upon the particular coordinate system. For example, the rate of strain components in general orthogonal curvilinear coordinates (α, β) are

$$e_{\alpha\alpha} = \frac{1}{h_1}\frac{\partial u_\alpha}{\partial \alpha} + \frac{u_\beta}{h_1 h_2}\cdot\frac{\partial h_1}{\partial \beta}$$

$$e_{\beta\beta} = \frac{1}{h_2}\frac{\partial u_\beta}{\partial \beta} + \frac{u_\alpha}{h_1 h_2}\cdot\frac{\partial h_2}{\partial \alpha}$$

$$e_{\alpha\beta} = e_{\beta\alpha} = \frac{1}{2}\left[\frac{h_2}{h_1}\frac{\partial}{\partial \alpha}\left(\frac{u_\beta}{h_2}\right) + \frac{h_1}{h_2}\frac{\partial}{\partial \beta}\left(\frac{u_\alpha}{h_1}\right)\right]$$

The h factors, themselves known and continuous functions of α and β, may be considered as defined by the expression for the line element, i.e., the distance between the points α, β and $\alpha + d\alpha$, $\beta + d\beta$:

$$(ds)^2 = (h_1 d\alpha)^2 + (h_2 d\beta)^2$$

The calculation of u_α and u_β from the differential equations $e_{\alpha\alpha} = -e_{\beta\beta} = f(\alpha, \beta)$ and $e_{\alpha\beta} = g(\alpha, \beta)$ is now more complicated because of the extra terms present in the differential equations. These equations are still integrable, but the integrations are more involved, and manipulations with both f and g may be necessary.

Convenient expression of boundary conditions is not at all helpful, however, in the problem at hand, and the foregoing considerations make it clear that nothing is to be gained by the choice of a special boundary coordinate system except unnecessary complexity. A Cartesian frame, without a doubt, provides the simplest set of differential equations. Furthermore, it was demonstrated above that if the region's boundaries are rectilinear, a Cartesian frame which is not parallel to any of the boundaries will permit a more direct calculation of the velocity components than will a frame which is parallel to the boundaries.

The direct integration method makes evident an interesting property of the function $f(x, y) = E \cos 2\beta$. That property is the vanishing of its integral whenever this integral is taken over a line segment which is terminated at both ends by static boundaries.

Referring to Figure 33, one sees that since $u' = 0$ at the point O and at the point x'_b, 0 on the cylindrical body, then

$$\int_o^{x'_b} f(\xi, 0)d\xi = 0$$

necessarily. Similarly

$$\int_o^{y'_b} f(0, \zeta)d\zeta = 0$$

since v' vanishes at the points O and 0, y'_b. There are, in fact, an infinite number of such vanishing integrals for each possible choice of a coordinate system. If one of the boundaries terminating the integration interval is a moving boundary, then of course the integral must be equal to the magnitude of one of the velocity components of the boundary at its termination point.

Up to this point the functions f and g have been handled as though they were continuous functions. In principle they are, but in actuality f and g must be derived from pointwise optical measurements, and consequently they will be discrete in nature. The size of the intervals between the data points is, of course, something to be decided by the circumstances surrounding the individual experiment. The calculation of the velocities will also be performed in a stepwise numerical fashion, and the fineness of the intervals used in the computations may or may not be the same as that employed in the data collection. If ℓ be the interval length chosen

for the velocity computations, then the finite difference form of the basic differential equations, Eqs. 47, is just

$$u(x + \ell, y) - u(x, y) = \ell\, f(x, y)$$

$$v(x, y + \ell) - v(x, y) = -\ell\, f(x, y) \qquad (52)$$

$$u(x, y + \ell) - u(x, y) + v(x + \ell, y) - v(x, y) = 2\ell\, g(x, y)$$

The accuracy of the results obtained by the direct integration will depend first upon the accuracy with which f and g are yielded by the experimental data, and secondly, upon the accuracy of the numerical computations. It is easy to see that if the experimental errors contained in the measured values of f and g are truly random, i. e., if the errors will be positive or negative with equal probability, then these errors will not accumulate in the integration process. Suppose that the true velocity component u_c at a point x, y is given by

$$u_c(x, y) = u(0, y) + \int_0^x f(\xi, y)\, d\xi$$

where f is the true function, unadulterated by experimental defects. The computed velocity component is

$$u(x, y) = u(0, y) + \int_0^x \left[f(\xi, y) + \epsilon(\xi, y) \right] d\xi$$

where $\epsilon(x, y)$ is the experimental error associated with f(x, y). The discrepancy between the true and computed values is seen to be

$$u(x, y) - u_c(x, y) = \int_0^x \epsilon(\xi, y) d\xi$$

Thus, if $\epsilon(x, y)$ is truly random and alternating in sign, the discrepancy will not tend to grow.

Errors associated with the numerical integrations can be of two or three types, such as round-off and truncation errors. There are well documented standard techniques for minimizing these errors, and it seems reasonable to hope that the effect of these could be controlled to the point where they become less significant than the effect due to the experimental errors.

Before closing this section a few summarizing remarks are in order. It has been shown that it is a relatively simple matter to reconstruct an unknown two-dimensional velocity field, given the magnitude and direction of the principal strain rates throughout the flow. According to the general orientation theory, streaming birefringence measurements taken in flows of colloidal solutions will yield the necessary information exactly only for very specialized flows, viz. those in which the streamlines lie 45° away from the principal strain rate axis, i.e., in which $\Lambda_o = 45^\circ$. In such flows, fluid elements lying along or perpendicular to the streamlines do not undergo any extension or contraction. With respect to the streamlines then, these flows have the local appearance of pure shear flows. Couette flow and Poiseuille flow are examples of flows in which $\Lambda_o = 45^\circ$. If there is divergence or convergence of streamlines, the fluid elements along and perpendicular to the streamlines will

experience extension or contraction and Λ_o will differ from 45^o. Then birefringence measurements can no longer give an unequivocal indication of the orientation of the principal strain rates. It must be said, however, that in any flow where the rate of dilatational strain due to streamline divergence or convergence is predominated by the rate of shearing strain parallel to the streamline, Λ_o will be close to 45^o. This is the case in the eccentric cylinder flow studied in the experimental work. And if Λ_o is not less than 35^o, the error in the principal strain rate orientation given by birefringence measurements in conjunction with a Couette calibration will be less than six percent.

This fact, that streaming birefringence as exhibited by colloidal solutions can be a useful visualization tool only for a restricted class of flows, should not, however, detract too much from the value of the analytical procedure set forth in this section. There is good scientific evidence that in certain birefringent <u>pure liquids</u> the optical tensor remains aligned with the strain rate tensor over a very large range of strain rates. Ethyl cinnamate is one such liquid, and the data of Wayland [26] on ethyl cinnamate contributes to this evidence. In such a system the strain rate tensor might be obtained unequivocally from birefringence measurements, and then the direct integration method would have indisputable value.

7.0 Conclusions and Recommendations

The orientation theory predicts that the optical anisotropy exhibited by a colloidal system undergoing laminar two-dimensional flow depends locally upon the principal rate of strain, the orientation of the principal strain rate axes, and the angle made by the streamline with these axes. For sufficiently small rates of strain, the amount of birefringence is a linear function of the principal rate of strain even for polydisperse systems, but the orientation of the principal optical axes depends upon the streamline direction as well as the principal rate of strain, even in the linear range of birefringence. If the flow is such that the angle between the streamline and the principal strain rate axes is 45°, as in shear flows, then the birefringence measurements can be interpreted unequivocally to give the magnitude and direction of the principal strain rates. If the angle between the streamline and the principal strain rate axes is not less than 35°, the orientation of the principal strain rate axes can be deduced from birefringence measurements with less than 6 percent error.

Experiments were performed to test these conclusions in the laminar flow between eccentric rotating cylinders. The flows generated by the particular apparatus used in the experiments is one in which the angle of the streamline referred to the principal strain rates is always very close to 45°. Except in certain isolated cases the experimental results support the conclusions drawn from the orientation theory. Qualitative as well as quantitative disagreement between the principal strain rate directions interpreted from optical measurements and those actually existing in

a portion of the minimum gap flow was consistent. It seems reasonable to conclude that major responsibility for this disagreement is chargeable to the polydisperse nature of the colloidal system used in the experimental work. Concentration and relaxation effects might possibly have contributed as well.

With the optical system developed for the experimental work described in this thesis it is possible to make precise pointwise birefringence measurements as close as 0.1 mm to a bounding wall. The main feature of the system is a well-collimated beam of light having a circular cross section about 0.2 mm in diameter. Total retardations as small as 5 Angstroms were measured visually using only a quarter-wave plate compensator. Good angle of isocline measurements at such low birefringences cannot be performed satisfactorily, however, with the instrument as it stands.

As a first recommendation it is proposed that more sensitive instrumentation be used to review the angle of isocline calibrations of the aqueous solutions in the range of very low rates of strain. At this writing a photoelectric detection system is in construction which will be capable of locating the optical axes of a weakly birefringent medium with a precision far surpassing that of the visual system used in the present experimental program. The author feels confident that an accurate knowledge of the angle of isocline behavior for very small rates of strain and very small concentrations will help greatly in clarifying the anomalous extinction angle results in the minimum gap of the eccentric cylinder flow.

The experiment as designed was not capable of testing the orientation theory at the other extreme, i.e., in flows where the principal strain rate axes lie close to the streamlines. An investigation of this type would be a very worthwhile complement to the experimental work reported in this thesis. The flow through a plane symmetrical converging or diverging channel is one obvious example of a flow containing a region where one of the principal strain rate axes coincides with the streamline. This condition exists along the centerline of such a channel. As one departs from the center streamline the principal strain rates rotate away from the streamline.

There is still much to be learned about the handling of TMV. In addition to a study of the angle of isocline behavior at low rates of strain, periodic calibrations could supply valuable information on the stability of TMV in the metallic environment of the experimental cells where the virus is also exposed to various lubricants and the window sealing compound. It is known that wetting agents can be used to reduce the surface tension of the solutions and thereby facilitate both the filling operation and the elimination of air bubbles. The effect of these wetting agents on the rotational diffusion constant deserves to be investigated. Accurate birefringence measurements could reveal an effect, if one exists. Also warranted is a critical look at the concentration dependence of birefringence in TMV solutions.

If the magnitude and direction of the principal strain rates can be everywhere deduced from measurements of birefringence,

then the velocity field can be reconstructed by the straight forward integration technique developed in this thesis. The only additional information required by the method is the velocity on all boundaries. Only in a restricted class of flows, however, can the streaming birefringence of colloidal solutions provide the necessary description of the local strain rate tensor. Thus the usefulness of such birefringent fluids as agents for flow visualization is limited.

For this reason primarily the author believes that the future of streaming birefringence as a truly useful tool for hydrodynamic research lies with the birefringent pure liquids. There is good experimental evidence that in certain of these liquids the optical tensor remains proportional to and coaxial with the rate of strain tensor over a very large range of strain rates. If such were truly the case, a Couette flow calibration could be used to determine the factor of proportionality, and birefringence measurements could then yield a complete and unambiguous description of the rate of strain tensor. It is strongly recommended that fundamental studies of streaming birefringence in such pure liquid systems be undertaken. The comparatively weak optical activity which is characteristic of such systems need be no deterrent to such research once the development of the photoelectric detector is complete.

REFERENCES

1. Wayland, H., "Streaming Birefringence of Rigid Macromolecules in General Two-Dimensional Laminar Flow", J. Chem. Phys., (in press).
2. Cerf, R. and Scheraga, H. A., Chem. Rev., 51, (1952), 185-261.
3. Jerrard, H. G., Chem. Rev., 59, (1959), 345-428.
4. Humphry, R. H., Proc. Phys. Soc. (London), 35, (1923), 217-218.
5. Alcock, E. D. and Sadron, C. L., Physics, 6, (1935), 92-95.
6. Hauser, E. A. and Dewey, D. R., Ind. Eng. Chem., 31, (1939), 786.
7. Hauser, E. A. and Dewey, D. R., J. Phys. Chem., 46, (1942), 212-213.
8. Dewey, D. R., "Visual Studies of Fluid Flow Patterns Resulting From Streaming Double Refraction", Doctoral Dissertation, Massachusetts Institute of Technology, (1941).
9. Weller, R., J. Appl. Mech., 14, (1947), 103-107.
10. Weller, R., Middlehurst, D. J., and Steiner, R., NACA Tech. Note No. 841, (1942).
11. Ullyott, P., Trans. ASME, 69, (1947), 245-251.
12. Leaf, W., Mech. Engr., 67, (1945), 586-590.
13. Binnie, A. M., Proc. Phys. Soc. (London), 57, (1945), 390-402.
14. Binnie, A. M., and Fowler, J. S., Proc. Roy. Soc. (London), A192, (1947), 32-44.

15. Lindgren, E. R., Arkiv Fysik, 7, (1954), 293-308.

16. Lindgren, E. R., Appl. Sci. Res., A4, (1953), 313.

17. Lindgren. E. R., Arkiv Fysik, 12, (1957), 1-169.

18. Rosenberg, B., "The Use of Doubly Refracting Solutions in the Investigation of Fluid Flow Phenomena", Navy Dept., David W. Taylor Model Basin Report No. 617, (1952).

19. Tolstoi, N. A., Doklady Akad. Nauk. S.S.S.R., 59, (1948), 1563-1566.

20. Young, D. F., "Determination of Streamlines Using a Photo-viscous Fluid", Doctoral Dissertation, Iowa State College, (1956).

21. Peebles, F. N., Garber, H. J., and Jury, S. H., "Preliminary Studies of Flow Phenomena Utilizing a Doubly Refracting Liquid", Proc. Third Midwestern Converence on Fluid Mechanics, University of Minnesota Press, (1953).

22. Peebles, F. N., Prados, J. W. and Honeycutt, E. H., Jr., "A Study of Laminar Flow Phenomena Utilizing a Doubly Refracting Liquid", Progress Report 1, University of Tennessee, Eng. Exp. Station and Dept. Chem. Engr., (1954).

23. Prados, J. W. and Peebles, F. N., "Determination of Flow Double Refraction Properties of Aqueous Milling Yellow Dye Solutions", Progress Report 2, University of Tennessee, Eng. Exp. Station and Dept. Chem. Engr., (1955).

24. Honeycutt, E. H., Jr. and Peebles, F. N., "A Study of Laminar Flow Phenomena Utilizing a Doubly Refracting Liquid", Progress Report 3, University of Tennessee, Eng. Exp. Station and Dept. Chem. Engr., (1955).

25. Prados, J. W., "The Analysis of Two-Dimensional Laminar Flow Utilizing a Doubly Refracting Liquid", Doctoral Dissertation, University of Tennessee, (1957).

26. Wayland, H., J. App. Phys., 26, No. 10, (1955), 1197-1205.

27. Jeffery, G. B., Proc. Roy. Soc. (London), A102, (1922-23), 161-179.

28. Peterlin, A., Z. Physik, 111, (1938), 232-263.

29. Peterlin, A. and Stuart, H. A., Z. Physik, 112, 1, (1939), 129-147.

30. Demetriades, S. T., J. Chem. Phys., 29, (1958), 1054-1063.

31. Snellman, O. and Bjornstahl, Y., Kolloid-Beih., 52, (1941), 403.

32. Sadron, C., J. phys. radium, 8, (1937), 481-488.

33. Sadron, C., J. phys. radium, 9, (1938), 381-383.

34. Perrin, F., J. phys. radium, 5, (1934), 497-511.

35. Jeffery, G. B., Proc. Roy. Soc. (London), A101, (1922), 169-174.

36. Hauser, E. A. and Lynn, J. E., Ind. and Eng. Chem., 32, No. 5, (1940), 659-662.

37. Boedtker, H. and Simmons, N., J. Am. Chem. Soc., 80, (1958), 2550-2555.

38. Bateman, H., in "Hydrodynamics" by Dryden, Murnaghan and Bateman, Dover Reprint, (1956).

39. Wayland, H. and Sutera, S. P., "Streaming Birefringence as a Hydrodynamic Research Tool", a report conducted under Research Grant NSF G-2400 from the Engineering Science Division of the National Science Foundation, (1959).

Appendix A

The Rotor Drive System and the Beam Deflector

1. The Rotor Drive

Figure a-1 below is a schematic drawing of the rotor drive gear train.

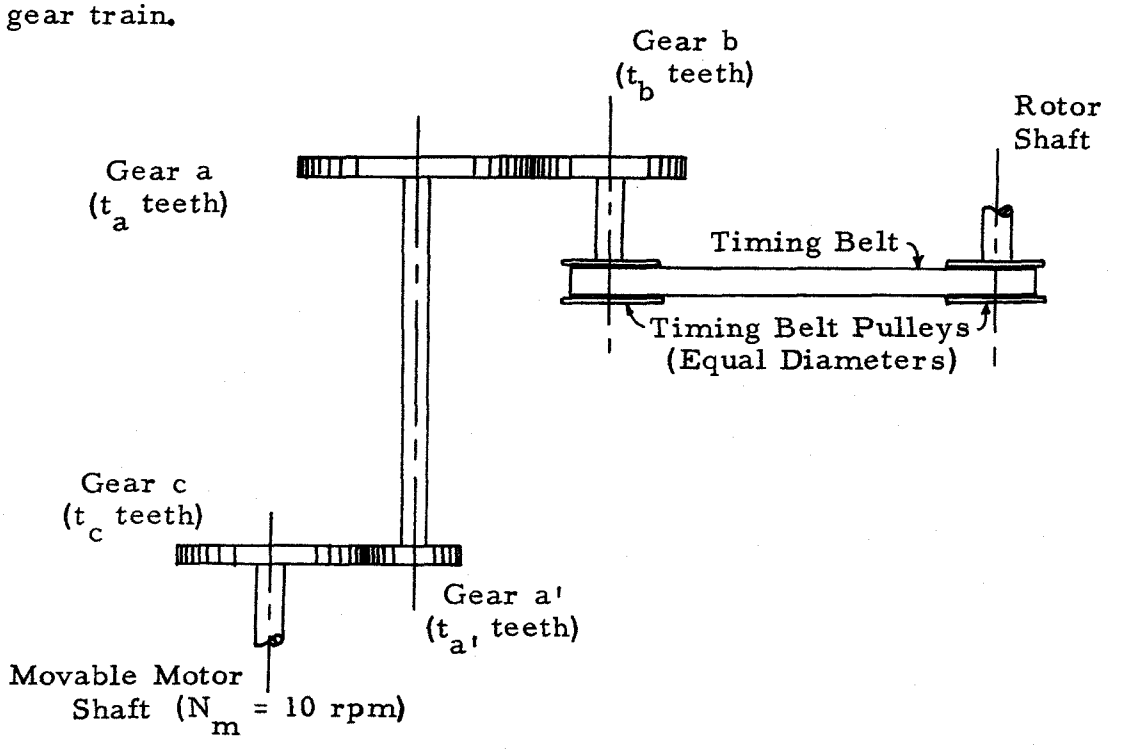

Figure a-1

The relation between the rotor speed N_r and the motor speed N_m is

$$N_r = N_m \times \left(\frac{t_c}{t_{a'}} \cdot \frac{t_a}{t_b}\right) \qquad (a\text{-}1)$$

Table Ia shows some of the available rotor speeds and the corresponding gear combinations.

2. The Beam Deflector

Consider the refraction of a single ray of light making an angle "i" with the normal of a glass plate of index of refraction

"n" and thickness "t". According to Snell's law, the angle of refraction "r" is given by

$$\frac{\sin i}{\sin r} = n$$

from which

$$\tan r = \frac{\sin i}{\sqrt{n^2 - \sin^2 i}} \qquad (a\text{-}2)$$

From Figure a-2 it is easily seen that

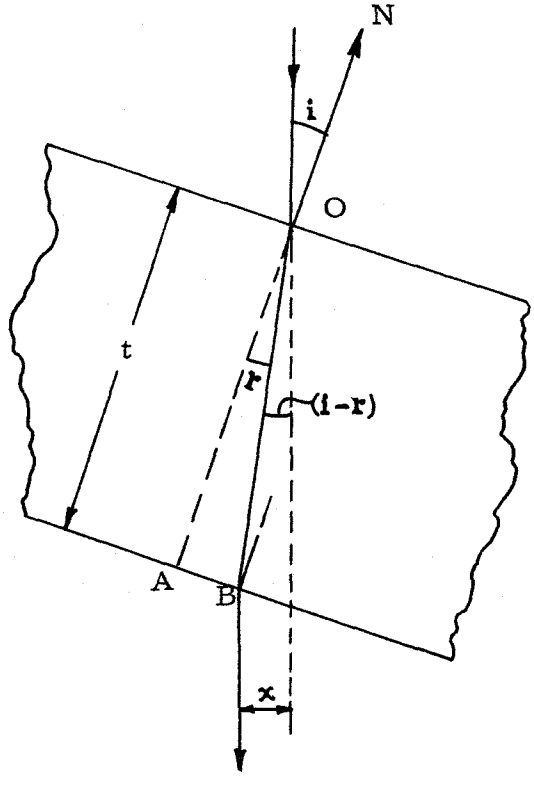

Figure a-2

$$\overline{OB} = t/\cos r$$

and that

$$x = \overline{OB} \sin (i - r)$$

$$= t \frac{\sin (i - r)}{\cos r}$$

$$= t (\sin i - \cos i \tan r)$$

Substitution for tan r from Eq. a-2 yields

$$x = t \sin i \left[1 - \sqrt{\frac{1 - \sin^2 i}{n^2 - \sin^2 i}} \right] \qquad (a\text{-}3)$$

For an ordinary crown glass n = 1.52. Figure a-3 is a plot of x/t as a function of i for n = 1.52.

TABLE IA

N_r	t_c	$t_{a'}$	t_a	t_b
0.5 rpm	24	120	24	96
1.0 "	24	120	40	80
2.0 "	24	120	60	60
3.0 "	24	120	72	48
4.0 "	24	120	80	40
5.0 "	60	120	60	60
6.0 "	24	60	72	48
8.0 "	24	120	96	24
10.0 "	60	120	80	40
12.5 "	120	24	24	96
15.0 "	60	60	72	48
20.0 "	120	60	60	60
25.0 "	120	24	40	80
33.33"	120	24	48	72

CHARACTERISTIC OF THE BEAM DEFLECTOR

For n = 1.52

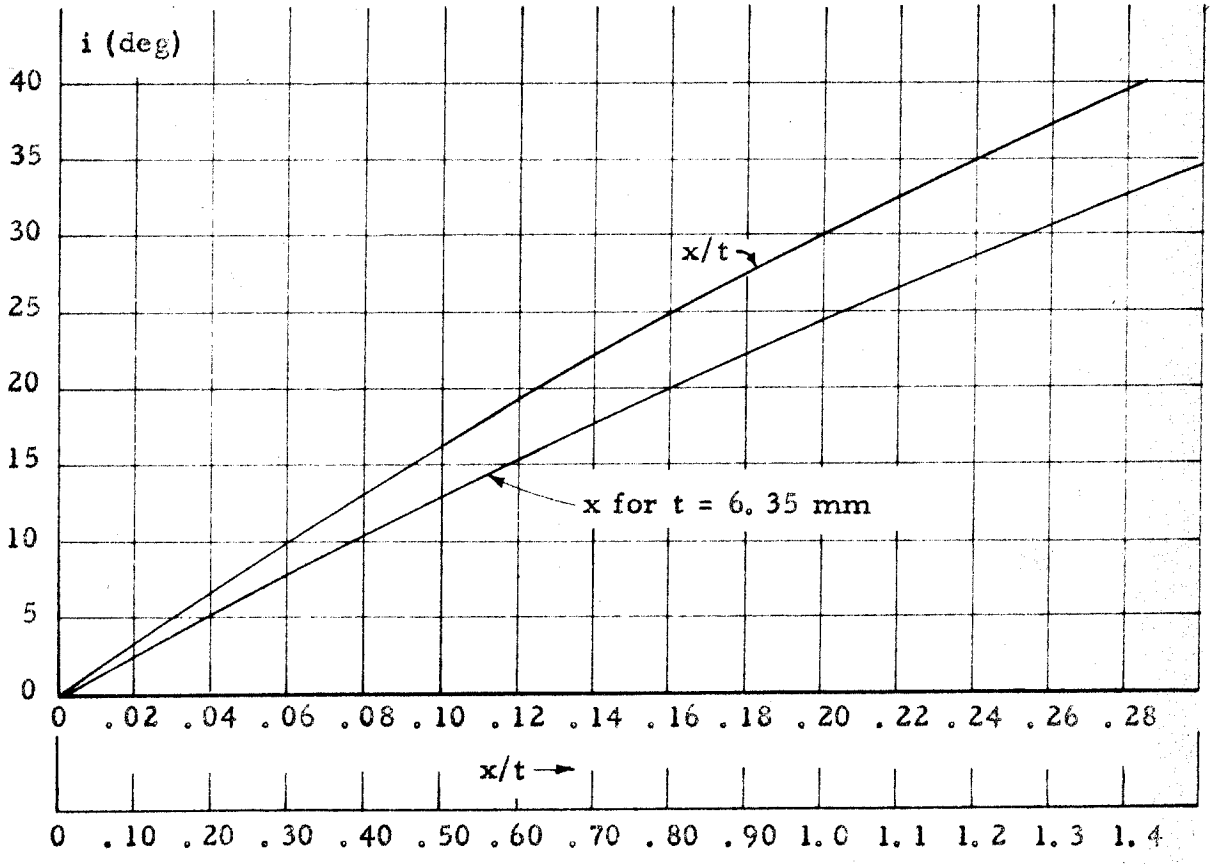

Figure a-3

Appendix B

Theory of Optical Measurements in a Flowing Birefringent System

The measurements of angle of isocline and degree of birefringence in a simple two-dimensional flow are performed with a polarimeter, an instrument consisting of two polarizing prisms mounted on a common axis. The optically anisotropic medium to be studied is positioned between the prisms. The prism separating the medium from the light source is called the polarizer; the other, which is mounted on a graduated circle, is called the analyzer.

The linearly polarized light beam enters the flowing medium perpendicularly to the plane of flow. The birefringent system is characterized by an index of refraction ellipsoid which possesses three distinct principal axes x, y, z with principal indices of refraction, n_x, n_y, n_z. The system is similar, in this respect, to a biaxial crystal. Consider the x and y directions to lie in the plane of flow. Then the light beam coincides in direction with the z axis. This axis is therefore not observable, and only the difference between the optical properties of axes x and y can be studied.

The birefringence is $\Delta n = n_x - n_y$, the difference in the indices of refraction with electric vectors vibrating parallel to the principal directions x and y. Δn may be positive or negative. In this thesis the notation χ is applied to the acute angle between the orthogonal principal vibration directions and the principal rate-of-strain axes.

Consider the exploring light ray as it travels along the z coordinate. If the light wave associated with this ray is mono-

chromatic, with period T, then it may be represented by the following equation for a simple harmonic plane wave:

$$D(t, z) = D \sin \frac{2\pi}{T} (t - \frac{z}{V}) \qquad (b-1)$$

where D is the amplitude of the vibration and V is the velocity of propagation. V is related to the wave length λ and the period T according to

$$\lambda = VT \qquad (b-2)$$

The amplitude D, usually taken as the dielectric displacement, is actually a vector which vibrates in a plane perpendicular to the direction of propagation, in this case the plane z = constant. If the vector D always remains in one plane, the light is said to be plane polarized, and the plane containing D is called the plane of polarization.

When the polarized light enters the anisotropic medium its two component vibrations parallel to the x and y axes are propagated with different velocities V_x and V_y. Let the plane of polarization P make an angle φ with the x direction as shown in Figure b-1. Furthermore let the principal plane of the analyzer prism (A) be set at 90° to P. Ignoring the effect of absorption, the two orthogonally polarized component waves which emerge from the birefringent medium are given by

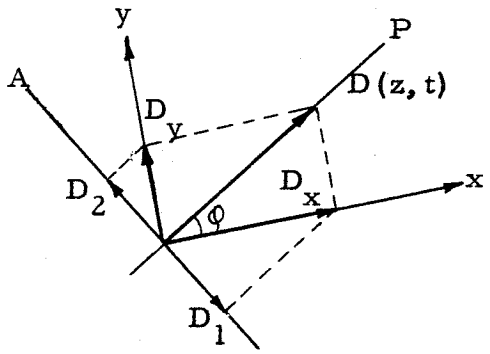

Figure b-1

$$D_x = (D \cos \varphi) \sin \frac{2\pi}{T} (t - \frac{z}{V_x}) \qquad (b-3)$$

$$D_y = (D \sin \varphi) \sin \frac{2\pi}{T} (t - \frac{z}{V_y}) \qquad (b-4)$$

Because of the difference in V_x and V_y, a phase difference Δ develops which remains constant after the two component waves leave the medium. At any point z after emergence, the resultant vibration can be thought of as a superposition of two simple harmonic vibrations of the form

$$D_x = (D \cos \varphi) \sin \omega t \qquad (b-5)$$

$$D_y = (D \sin \varphi) \sin (\omega t + \Delta) \qquad (b-6)$$

By eliminating the time t between Eqs. b-5 and b-6, the relation between D_x and D_y in the resultant vibration is obtained:

$$\frac{D_x^2}{\cos^2 \varphi} - \frac{2 D_x D_y \cos \Delta}{\cos \varphi \sin \varphi} + \frac{D_y^2}{\sin^2 \varphi} = D^2 \sin^2 \Delta \qquad (b-7)$$

The end of the resultant light vector (D_x, D_y) describes an ellipse in time and the emerging light is said to be elliptically polarized.

1.0 Measurement of Angle of Extinction

The technique used in locating extinction in the flowing medium may be readily explained by considering the amplitude of the resultant wave transmitted by the analyzer. The analyzer transmits only those components of D_x and D_y that are parallel to A, i.e.,

$$D_1 = (D \cos\varphi \sin\varphi) \sin\frac{2\pi}{T}\left(t - \frac{z}{V_x}\right) \qquad \text{(b-8)}$$

$$D_2 = -(D \sin\varphi \cos\varphi) \sin\frac{2\pi}{T}\left(t - \frac{z}{V_y}\right) \qquad \text{(b-9)}$$

The resultant of these two waves is a plane wave whose amplitude is given by

$$D_A^2 = D^2 \sin^2 2\varphi \sin^2\frac{\Delta}{2} \qquad \text{(b-10)}$$

According to Eq. b-10 the intensity of the transmitted light depends on the orientation of the polarizer-analyzer combination and the phase difference produced by the flowing medium. Regardless of the phase difference, however, D_A vanishes if $\varphi = 0$, $\pi/2$, π, $3\pi/2$. Hence no light is transmitted if the principal plane of the polarizer coincides with either the x or y axis.

As explained in the section on experimental technique (5. 3), the principal vibration directions or optical axes of the flowing medium are located by locking the polarizer and analyzer in a crossed position and rotating them together until the intensity of the transmitted light vanishes or goes through a minimum. Then the inclination of the x and y axes to the reference direction is known.

2. 0 Measurement of Birefringence

If P is set at 45° to the optical axes of the flowing medium (x, y axes), then according to Eqs. b-5 and b-6, the two component vibrations which emerge from the fluid have equal amplitudes

$$D_x = .707\, D \sin \omega t \qquad \text{(b-11)}$$

$$D_y = .707\, D \sin (\omega t + \Delta) \qquad \text{(b-12)}$$

The resultant vibration is one of elliptically polarized light; and the ellipse described by the resultant displacement vector (D_x, D_y),

$$D_x^2 - 2 D_x D_y \cos \Delta + D_y^2 = \frac{D^2}{2} \sin^2 \Delta \qquad \text{(b-13)}$$

has principal axes inclined at 45° to the x, y axes.

If new coordinate axes x', y' are introduced parallel to the principal axes of the ellipse, Eq. b-13, which are also coincident with the principal planes of the polarizing prisms P and A, (see Figure b-2), then the equation of the ellipse in terms of these coordinates is just

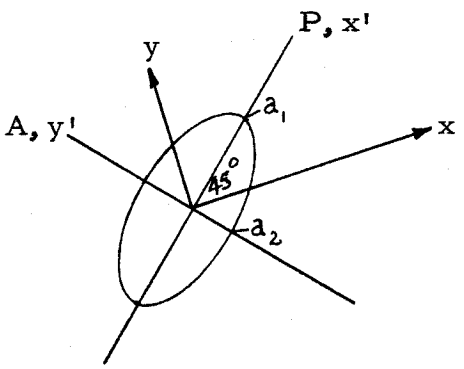

Figure b-2

$$\frac{D_{x'}^2}{a_1^2} + \frac{D_{y'}^2}{a_2^2} = 1 \qquad \text{(b-14)}$$

where

$$a_1 = \frac{D \sin \Delta}{\sqrt{2\,(1 - \cos \Delta)}}, \qquad a_2 = \frac{D \sin \Delta}{\sqrt{2\,(1 + \cos \Delta)}} \qquad \text{(b-15)}$$

are the major and minor radii respectively of the ellipse. With respect to the principal planes of polarizer and analyzer then,

the elliptically polarized light can be resolved into two orthogonally polarized waves with a phase difference which is an integral multiple of $\pi/2$, i.e.,

$$D_{x'} = a_1 \sin \omega t \tag{b-16}$$

$$D_{y'} = a_2 \sin (\omega t + \Delta') \tag{b-17}$$

$$\Delta' = \frac{\pi}{2}, \frac{3\pi}{2}, \ldots (n + \frac{1}{2})\pi$$

By inserting a quarter wave plate with its optic axis alligned with P or A, between the birefringent medium and the analyzer prism, an additional phase difference of $\pi/2$ is introduced. This brings the two component vibrations, Eqs. b-16 and b-17, into phase and the resultant light is once again plane polarized. Depending upon whether the "fast" axis of the $\lambda/4$ plate coincides with the x' or the y' axis, the equation of the line parallel to the resultant displacement vector $(D_{x'}, D_{y'})$ is

$$\frac{x'}{y'} = \frac{a_1}{a_2} \quad \text{or} \quad \frac{x'}{y'} = -\frac{a_1}{a_2} \tag{b-18}$$

From the definitions of a_1 and a_2, Eq. b-15, it follows that these equations may also be written as

$$\frac{y'}{x'} = \pm \tan \frac{\Delta}{2} \tag{b-19}$$

Thus the new plane of polarization is inclined at an angle of 45° $\pm \Delta/2$ to the optical axes of the medium (x, y).

By unlocking the analyzer prism and rotating its principal plane through $\pm \Delta/2^{o}$, extinction is once again achieved. The angle $\Delta/2$ is read from the graduated circle on which the analyzer prism is mounted. Δ is related to the difference $n_x - n_y$ in a simple way. Consider the two continuous component wave trains, $D_x(z,t)$ and $D_y(z,t)$, Eqs. b-3 and b-4, in their passage through the test medium. Before entering the medium, the two waves are exactly in phase, and their velocities of propagation are both equal to C, the velocity of light in air. Once in the medium, the two component wave fronts advance at different rates, $V_x \neq V_y$. If the length of path traveled in the medium is 'ℓ', then any wave front of the D_x wave will require a time ℓ/V_x to traverse the medium, while a wave front of the D_y wave will do so in ℓ/V_y units of time. The difference between these two intervals of time represents the phase lead or lag of one component with respect to the other upon emergence of the two from the anisotropic medium, if they were exactly in phase upon entrance thereto.

Assume that $n_x > n_y$, then $V_y > V_x$, and the time lag of the D_x wave front with respect to a formerly coincident D_y wave front is just

$$\delta t = \frac{\ell}{V_x} - \frac{\ell}{V_y} = \frac{\ell}{C}(n_x - n_y) \qquad \text{(b-20)}$$

After emergence from the medium the resultant light wave, and hence its components, again propagate with velocity C. Thus, at any position z, the angular phase difference between the two components is

$$\Delta = 2\pi \cdot \frac{\delta t}{T} = 2\pi \cdot \frac{C}{\lambda} \cdot \frac{\ell}{C} (n_x - n_y)$$

$$= \frac{2\pi\ell}{\lambda} (n_x - n_y) \qquad \text{(b-21)}$$

Finally then, the birefringence is given by

$$(n_x - n_y) = \frac{\lambda}{\ell} \frac{\Delta}{2\pi}$$

where Δ is the previously introduced phase angle, Eq. b-6, in radians.

It should be remembered that the analyzer rotation described above gives $\Delta/2$ directly in degrees. If the actual angular rotation of the analyzer is referred to as a $(= \Delta/2)$, then the birefringence is calculated from

$$n_x - n_y = \frac{\lambda}{\ell} \cdot \frac{a}{180} \quad (a \text{ in degrees}) \qquad \text{(b-22)}$$

Sometimes it is convenient to speak of the birefringence in terms of relative retardation, i.e., the retardation in fractions of a wave length. Suppose the component waves are examined at a particular instant after emergence rather than at a particular spatial position. Then the actual separation δz between two formerly coincident wave fronts is

$$\delta z = C\,\delta t = \ell (n_x - n_y) \qquad \text{(b-23)}$$

δz is called the retardation. The relative retardation is just

$$r = \frac{\delta z}{\lambda} = \frac{\ell (n_x - n_y)}{\lambda}$$

so that

$$(n_x - n_y) = \frac{\lambda r}{\ell} \qquad \text{(b-24)}$$

A practical remark can now be made concerning the relative ease of the two types of measurement discussed above. Since the intensity of light is proportional to the square of the amplitude of the electromagnetic wave, Eq. b-10 shows that the intensity of light transmitted by the analyzer in the extinction angle measurement depends upon both the angle φ and the phase Δ:

$$I_A \sim D^2 \sin^2 2\varphi \sin^2 \frac{\Delta}{2}$$

Δ is directly proportional to the birefringence $\Delta n = n_x - n_y$. If the birefringence is small, then near extinction ($\varphi \to 0$)

$$I_A \sim D^2 \cdot \varphi^2 \cdot (\Delta n)^2$$

The intensity varies quadratically with φ as extinction is approached, but the sharpness of the minimum is attenuated by the factor $(\Delta n)^2$.

In the birefringence measurement, Eqs. b-16, b-17, and b-15 show that the intensity of the plane polarized wave entering the analyzer is given by

$$I \sim D_{x'}^2 + D_{y'}^2 = a_1^2 + a_2^2 = D^2$$

The intensity of the light transmitted by the analyzer is governed by the law of Malus,

$$I_A = I \sin^2 \alpha$$

so that near extinction ($\alpha \longrightarrow 0$)

$$I_A \sim D^2 \alpha^2$$

In this case the intensity is quadratic in α, but the amount of birefringence does not enter. The sharpness of the minimum depends only on the original intensity of the light entering the analyzer. It is for this reason that the extinction measurements are always the more difficult to perform in media of small birefringence.

Appendix C

Calculation of the Viscous Flow Pattern Between Rotating Eccentric Cylinders

The viscous flow between rotating eccentric cylinders was solved by Jeffery [35] and is also given by Bateman [38], but the results are not expressed in a convenient form for calculation. In a previous report by Wayland and Sutera [39], full details were given of a rearrangement of the analytical solution which proves to be more suitable for the numerical computation of particular solutions. A solution was computed and tabulated for the particular eccentric cylinder apparatus employed in the present research program. In this appendix the salient features of this computation will be given, along with certain tables of functions which are very useful for the calculation of velocities, strain rates, and vorticities anywhere in the flow field.

Jeffery assumes that the acceleration terms are negligible in the slow viscous flow and hence seeks a solution to

$$\nabla^4 \Psi = 0 \qquad \text{(c-1)}$$

for the stream function. He uses bipolar coordinates, α and β, shown in Figure c-1. The relationship between these coordinates and the Cartesian coordinates (x, y) is defined by

$$\alpha + i\,\beta = \ell n\, \frac{x + i\,(y + a)}{x + i\,(y - a)} \qquad \text{(c-2)}$$

from which

$$x = \frac{a \sin \beta}{\cosh \alpha - \cos \beta} \qquad y = \frac{a \sinh \alpha}{\cosh \alpha - \cos \beta} \tag{c-3}$$

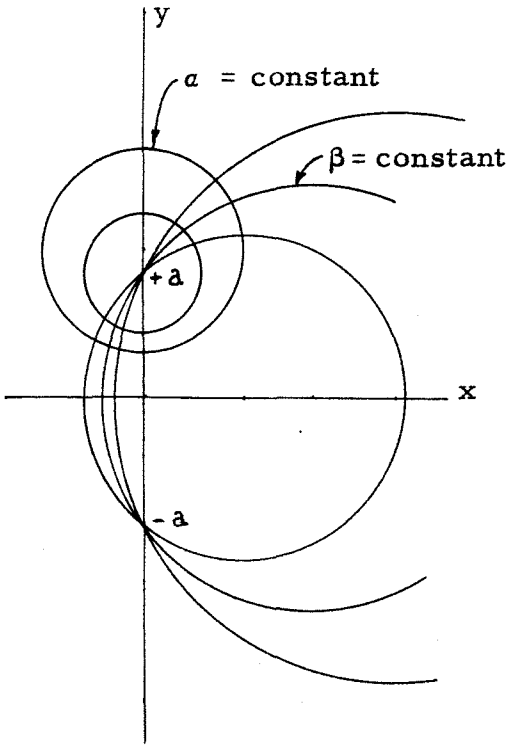

Figure c-1

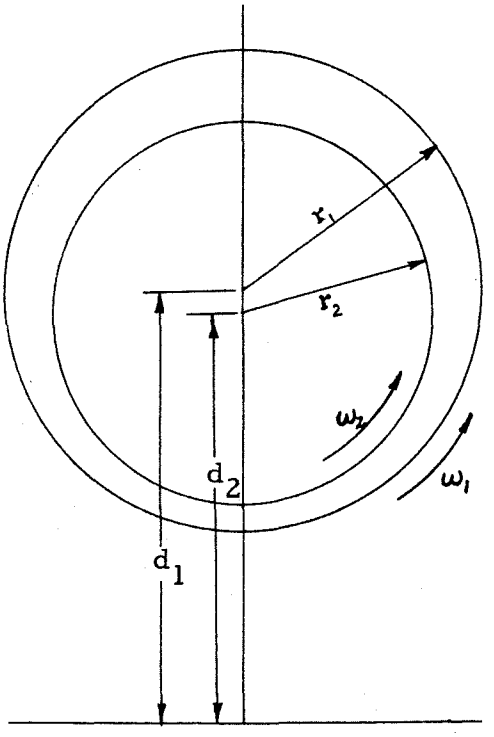

Figure c-2

For any pair of circles $\alpha = \alpha_1$, $\alpha = \alpha_2$, having radii r_1 and r_2, and situated as shown in Figure c-2.

$$\begin{aligned} r_1 &= a \operatorname{cosech} \alpha_1 \\ d_1 &= a \coth \alpha_1 \\ r_2 &= a \operatorname{cosech} \alpha_2 \\ d_2 &= a \coth \alpha_2 \end{aligned} \tag{c-4}$$

Given a particular apparatus, r_1, r_2, and $d_2 - d_1$ are known. α_1, α_2 and a can then be determined through the equations

$$\cosh \alpha_1 = \frac{(r_1^2 - r_2^2) + (d_1 - d_2)^2}{2 r_1 (d_1 - d_2)}$$

$$\cosh \alpha_2 = \frac{(r_1^2 - r_2^2) - (d_1 - d_2)^2}{2 r_2 (d_1 - d_2)} \qquad \text{(c-5)}$$

$$a = r_1 \sinh \alpha_1 = r_2 \sinh \alpha_2$$

The general solution for Ψ obtained by Jeffery is

$$\Psi = \frac{a}{\cosh \alpha - \cos \beta} \left[A_o \cosh \alpha + B_o \alpha \cosh \alpha + C_o \sinh \alpha \right.$$

$$\left. + D_o \alpha \sinh \alpha + (A_1 \cosh 2\alpha + B_1 + C_1 \sinh 2\alpha + D_1 \alpha) \cos \beta \right]$$

$$= \frac{a}{\cosh \alpha - \cos \beta} \left[\varphi_1(\alpha) + \varphi_2(\alpha) \cos \beta \right] \qquad \text{(c-6)}$$

where

$$\varphi_1(\alpha) = (A_o + B_o \alpha) \cosh \alpha + (C_o + D_o \alpha) \sinh \alpha$$

$$\varphi_2(\alpha) = A_1 \cosh 2\alpha + B_1 + C_1 \sinh 2\alpha + D_1 \alpha \qquad \text{(c-7)}$$

The boundary conditions to be satisfied in the case of internal cylinder rotating ($\omega_2 \neq 0$) and external cylinder stationary ($\omega_1 = 0$) are

$$\Psi = \Psi_1, \; u_\beta = 0 \qquad \text{on } \alpha = \alpha_1$$

and (c-8)

$$\Psi = \Psi_2, \; u_\beta = r_2 \omega_2 \qquad \text{on } \alpha = \alpha_2$$

In bipolar coordinates, the velocity components in the direction of α and β increasing (u_α and u_β) are given by

$$u_\alpha = - \frac{\cosh \alpha - \cos \beta}{a} \cdot \frac{\partial \Psi}{\partial \beta}$$
$$u_\beta = \frac{\cosh \alpha - \cos \beta}{a} \cdot \frac{\partial \Psi}{\partial \alpha} \qquad \text{(c-9)}$$

Another implicit condition to be satisfied by the solution is that of single-valuedness in the coordinate β. Furthermore, Ψ_2 can be arbitrarily set equal to zero. Along with the boundary conditions, Eq. c-8, these last two conditions provide enough equations to determine the eight constants of integration in Eq. c-7.

Computational simplication is accomplished by introducing a new variable ξ, where

$$\xi = \alpha_2 - \alpha \qquad \text{(c-10)}$$

By imposing the boundary conditions at $\alpha = \alpha_2$ on the functions $\varphi_1(\alpha)$ and $\varphi_2(\alpha)$, defined by Eq. c-7, these functions can be written very neatly in terms of the variable ξ and four new constants:

$$\varphi_1(\xi) = (r_2 \omega_2 + K_1 \xi) \sinh \xi + K_2 (\sinh \xi - \xi \cosh \xi)$$
$$\varphi_2(\xi) = K_3 (\cosh 2\xi - 1) - K_4 (\sinh 2\xi - 2\xi) \qquad \text{(c-11)}$$

The new constants are related to the old set in the following way:

$$\begin{aligned} K_1 &= B_o \sinh \alpha_2 + D_o \cosh \alpha_2 \\ K_2 &= B_o \cosh \alpha_2 + D_o \sinh \alpha_2 \\ K_3 &= A_1 \cosh 2\alpha_2 + C_1 \sinh 2\alpha_2 \\ K_4 &= A_1 \sinh 2\alpha_2 + C_1 \cosh 2\alpha_2 \end{aligned} \qquad \text{(c-12)}$$

The K's can be determined from the remaining boundary conditions at $\alpha = \alpha_1$, i.e., at

$$\xi = \alpha_2 - \alpha_1 \equiv \Delta$$

In terms of Ψ_1, they are

$$K_1 = \frac{\frac{\Psi_1}{a}(\Delta \sinh \alpha_2 - \sinh \Delta \sinh \alpha_1) + r_2 \omega_2 (\Delta - \frac{1}{2} \sinh 2\Delta)}{\sinh^2 \Delta - \Delta^2}$$

$$K_2 = \frac{\frac{\Psi_1}{a}(\Delta \cosh \alpha_2 + \sinh \Delta \cosh \alpha_1) - r_2 \omega_2 \sinh^2 \Delta}{\sinh^2 \Delta - \Delta^2}$$

$$K_3 = \frac{\Psi_1}{2a} \cdot \frac{\sinh \Delta}{\sinh \Delta - \Delta \cosh \Delta}$$

$$K_4 = \frac{\Psi_1}{2a} \cdot \frac{\cosh \Delta}{\sinh \Delta - \Delta \cosh \Delta} \qquad \text{(c-13)}$$

Ψ_1 is determined by the condition of single-valuedness which requires that

$$K_2 \cosh \alpha_2 - K_1 \sinh \alpha_2 - 2 K_4 = 0 \qquad \text{(c-14)}$$

Substituting in Eq. c-14 for K_1, K_2 and K_4 from Eqs. c-13, a single equation for Ψ_1 is obtained.

$$\Psi_1 = a r_2 \omega_2 \frac{\sinh a_2 - \frac{\sinh \Delta}{\Delta} \cdot \sinh a_1}{1 + \frac{\sinh \Delta}{\Delta} \cosh(a_1 + a_2) - \frac{\sinh^2 \Delta - \Delta^2}{\Delta \sinh \Delta - \Delta^2 \cosh \Delta} \cosh \Delta} \qquad (c\text{-}15)$$

Ψ_1 and the K's were computed for an apparatus having the following dimensions

$$r_1 = 27.000 \text{ mm}$$

$$r_2 = 25.009 \text{ mm}$$

$$d_1 - d_2 = .991 \text{ mm}$$

$$a = 45.305 \text{ mm}$$

These dimensions are within two percent of the actual dimensions of the apparatus used. Based on these dimensions

$a_1 = 1.289601$ $\qquad$ $a_2 = 1.356043$

$\cosh a_1 = 1.953358$ $\qquad$ $\cosh a_2 = 2.069242$

$\sinh a_1 = 1.677977$ $\qquad$ $\sinh a_2 = 1.811563$

$$a_2 - a_1 = \Delta = 0.066442$$

$$\Psi_1 = 16.49844\, \omega_2$$

$K_1 = -260.35656\, \omega_2$ $\qquad$ $K_3 = -123.77333\, \omega_2$

$K_2 = -2031.10080\, \omega_2$ $\qquad$ $K_4 = -1865.6183\, \omega_2$

The stream function, the velocity and rate of strain components may be expressed in terms of the φ functions and their derivatives:

$$\Psi = \frac{a}{\cosh \alpha - \cos \beta} \left[\varphi_1(\xi) + \varphi_2(\xi) \cos \beta \right]$$

$$u_\alpha = \left[\frac{\varphi_1(\xi) + \varphi_2(\xi) \cosh \alpha}{\cosh \alpha - \cos \beta} \right] \sin \beta$$

$$u_\beta = - \left[\varphi_1'(\xi) + \varphi_2'(\xi) \cos \beta \right] - \frac{\sinh \alpha}{a} \Psi(\xi, \beta) \qquad \text{(c-16)}$$

$$e_{\alpha\alpha} = - e_{\beta\beta} = - \frac{\cosh \alpha - \cos \beta}{a} \varphi_2' \sin \beta$$

$$e_{\alpha\beta} = e_{\beta\alpha} = \frac{1}{2} \cdot \frac{\cosh \alpha - \cos \beta}{a} \left[\varphi_1'' + \varphi_2'' \cos \beta - \varphi_1 \right]$$

The primes denote differentiation with respect to ξ.

The φ's and their derivatives are the following:

$$\varphi_1 = K_2 (\sinh \xi - \xi \cosh \xi) + (r_2 \omega_2 + K_1 \xi) \sinh \xi$$

$$\varphi_1' = (K_1 - K_2 \xi) \sinh \xi + (r_2 \omega_2 + K_1 \xi) \cosh \xi$$

$$\varphi_1'' = \varphi_1 + 2K_1 \cosh \xi - 2K_2 \sinh \xi$$

$$\varphi_2 = K_1 (\cosh 2\xi - 1) - K_4 (\sinh 2\xi - 2\xi) \qquad \text{(c-17)}$$

$$\varphi_2' = 2K_3 \sinh 2\xi - 2K_4 (\cosh 2\xi - 1)$$

$$\varphi_2'' = 4K_3 \cosh 2\xi - 4K_4 \sinh 2\xi$$

The space between α_1 and α_2 $(0<\xi<\Delta)$ was divided into ten intervals, and values for the functions φ_1 and φ_2 and their derivatives were

computed for the eleven interval boundaries. These are given in Tables I and II. Note from Eq. c-16 that the φ's and their derivatives with respect to ξ (or α) have the dimension of velocity.

Tables III, IV and V present the computed values of the stream function, velocities, and strain rates as functions of α for four values of β: $\beta = 0$ (maximum gap), $\beta = \pi$ (minimum gap), $\beta = \frac{\pi}{2}$, and $\beta = \frac{3\pi}{2}$. The latter two values of β correspond to the converging and diverging flow positions 60° from the minimum gap.

Figure c-3 shows qualitatively the streamline pattern calculated for the particular apparatus in question. All dimensions are greatly exaggerated. It is interesting to note that a region of reverse flow is predicted.

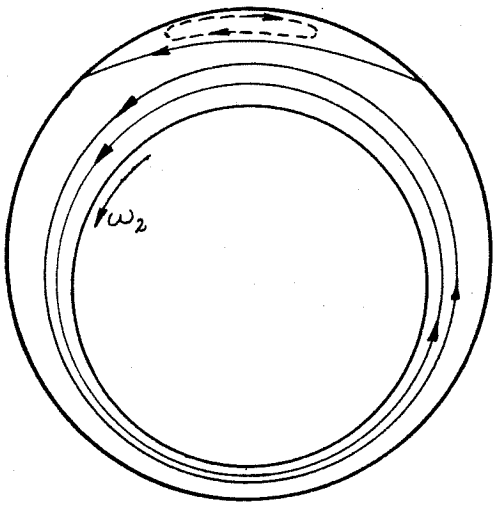

Figure c-3

The vorticity for the two-dimensional flow can also be computed from the numerical data in Tables I and II. In the plane curvilinear coordinates, the vorticity is given by

$$\zeta = \frac{1}{2} \cdot \frac{1}{h^2} \left[\frac{\partial}{\partial \alpha} (h\, u_\beta) - \frac{\partial}{\partial \beta} (h\, u_\alpha) \right] \qquad \text{(c-18)}$$

where

$$h = \frac{a}{\cosh \alpha - \cos \beta}$$

ζ was computed as a function of ξ for the four values of β, and the results of these computations are also included in Tables III, IV, and V.

The principal rates of strain at any point in the flow are

$$E = \pm \sqrt{e_{\alpha\alpha}^{\,2} + e_{\alpha\beta}^{\,2}} \qquad (c\text{-}19)$$

In the maximum and minimum gaps, where $e_{\alpha\alpha} = e_{\beta\beta} = 0$, E is just equal to $e_{\alpha\beta}$ which is tabulated in Tables III, IV, and V. Furthermore, the angle between the first eigen-direction, or principal axis of the rate of strain matrix, and the tangent to the α coordinate direction (which, it must be remembered, is perpendicular to the constant α curve) is

$$\theta = \arctan\left(\frac{e_{\alpha\alpha} - E}{-e_{\alpha\beta}}\right) \qquad (c\text{-}20)$$

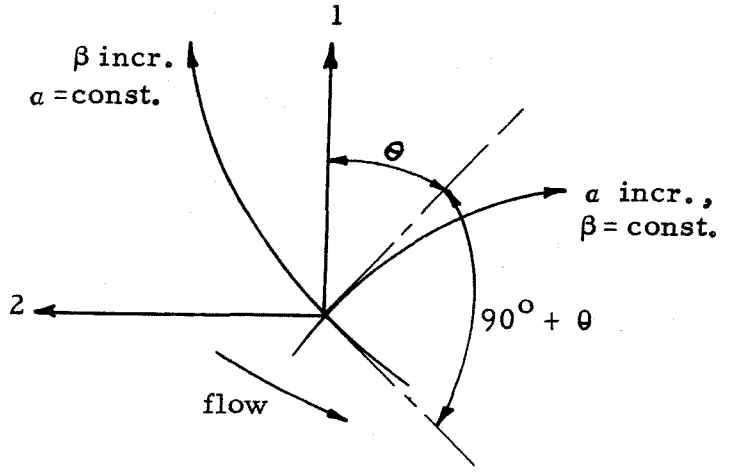

Figure c-4

In the experimental work, the flow was generally in the direction of β decreasing. This being the case, it was more convenient to deal with the angle between the first principal strain rate and the

negative β axis. This is just the clockwise angle of rotation from the principal axis 1 shown in Figure c-4 to the curve of constant α passing through the particular point, i.e., $90^{o} + \theta$.

In the eccentric cylinder apparatus the most convenient reference direction to use at any particular traverse position is that of the local tangent to the rotor or inner cylinder wall. From the relationship between the bipolar coordinates and the Cartesian coordinates, Eqs. c-3, it is possible to calculate the slope of any circle of constant α, say $\alpha = \alpha^{*}$, at its intersection with a circle of constant β. This is

$$\left(\frac{dy}{dx}\right)_{\alpha^{*},\beta} = - \frac{\sinh \alpha^{*} \sin \beta}{(\cosh \alpha^{*} - \cos \beta) \cos \beta - \sin^{2} \beta} \qquad \text{(c-21)}$$

At $\beta = 0$ and π, the slope vanishes, i.e., the tangents in these two gaps are parallel to the x axis. Along $\beta = \pi/2$

$$\left(\frac{dy}{dx}\right)_{\alpha^{*},\pi/2} = + \sinh \alpha^{*} \qquad \text{(c-22)}$$

while along $\beta = 3\pi/2$

$$\left(\frac{dy}{dx}\right)_{\alpha^{*},3\pi/2} = - \sinh \alpha^{*} \qquad \text{(c-23)}$$

By means of the last two equations, one can calculate the angle between the tangent to the particular circle α^{*} at $\beta = \pi/2, 3\pi/2$ and the tangent to the rotor ($\alpha = \alpha_{2}$) at the same β. If the angle between the tangent to α^{*} and the x axis be denoted by ν^{*}, where

$$\nu^* = \arctan\left(\frac{dy}{dx}\right)_{a^*,\beta} ,$$

then the slope of a^* at β referred to the slope of the rotor tangent at β is simply

$$\nu^* - \nu_2 = \arctan\left(\frac{dy}{dx}\right)_{a^*,\beta} - \arctan\left(\frac{dy}{dx}\right)_{a_2,\beta} \qquad \text{(c-24)}$$

The angle $(\nu^* - \nu_2)$ is zero in the minimum gap and maximum gaps, negative at $\beta = \pi/2$ (diverging flow) and positive at $\beta = 3\pi/2$ (converging flow).

Finally then, the total angle between the first principal axis and the rotor tangent at the same β is the sum of $90^\circ + \theta$ and $\nu - \nu_2$. Denote this angle by η ; then

$$\eta = (90^\circ + \theta) + (\nu - \nu_2) \qquad \text{(c-25)}$$

The variation of η with a at $\beta = 0$, $\pi/2$, π, and $3\pi/2$ is presented in Table VI. Tabulated along with η in this table is E, the magnitude of the principal strain rate.

Finally, Table VII gives the dimensionless distances, referred to the stator wall, which correspond to the eleven values of ξ used in the computations.

TABLE I $\phi_1(\xi)$

	ξ	$\phi_1(\xi)/\omega_2$	$\phi_1'(\xi)/\omega_2$	$\phi_1''(\xi)/\omega_2$
ξ_0	0.0000000	0.00000	25.0090	-520.7131
ξ_1	0.0066442	0.15487	21.6394	-493.5796
ξ_2	0.0132884	0.28795	18.4500	-466.4894
ξ_3	0.0199326	0.40044	15.4405	-439.4405
ξ_4	0.0265768	0.49353	12.6105	-412.4305
ξ_5	0.0332210	0.56841	9.9598	-385.4569
ξ_6	0.0398652	0.62628	7.4883	-358.5172
ξ_7	0.0465094	0.66831	5.1956	-331.6094
ξ_8	0.0531536	0.69571	3.0817	-304.7309
ξ_9	0.0597978	0.70966	1.1462	-277.8792
ξ_{10}	0.0664420	0.71134	-0.61095	-251.0522

TABLE II $\phi_2(\xi)$

	ξ	$\phi_2(\xi)/\omega_2$	$\phi_2'(\xi)/\omega_2$	$\phi_2''(\xi)/\omega_2$
ξ_0	0.0000000	0.00000	0.0000	-495.093
ξ_1	0.0066442	-0.01020	-2.9620	-395.970
ξ_2	0.0132884	-0.03788	-5.2654	-296.918
ξ_3	0.0199326	-0.07866	-6.9104	-197.917
ξ_4	0.0265768	-0.12819	-7.8972	-98.950
ξ_5	0.0332210	-0.18208	-8.2260	-0.003
ξ_6	0.0398652	-0.23597	-7.8972	+98.947
ξ_7	0.0465094	-0.28550	-6.9104	+197.910
ξ_8	0.0531536	-0.32628	-5.2654	+296.911
ξ_9	0.0597978	-0.35396	-2.9620	+395.967
ξ_{10}	0.0664420	-0.36416	0.0000	+495.091

TABLE III

Stream Function, Velocities, Strain Rates and Vorticity for $\beta = 0$ (maximum gap)

ξ	Ψ/ω_2	u_α/ω_2	u_β/ω_2	$e_{\alpha\alpha}/\omega_2$	$e_{\alpha\beta}/\omega_2$	ζ/ω_2
ξ_0	0.0000	$0.\overline{0}$	-25.0090	$0.\overline{0}$	-11.9869	-12.8366
ξ_1	6.1994	$0.\overline{0}$	-18.9253	$0.\overline{0}$	-10.3812	-11.1151
ξ_2	10.8380	$0.\overline{0}$	-13.6114	$0.\overline{0}$	-8.8106	-9.3181
ξ_3	14.1053	$0.\overline{0}$	-9.0813	$0.\overline{0}$	-7.2745	-7.5917
ξ_4	16.1984	$0.\overline{0}$	-5.3416	$0.\overline{0}$	-5.7725	-5.9358
ξ_5	17.3262	$0.\overline{0}$	-2.4007	$0.\overline{0}$	-4.3037	-4.3493
ξ_6	17.7071	$0.\overline{0}$	-0.2674	$0.\overline{0}$	-2.8673	-2.8297
ξ_7	17.5683	$0.\overline{0}$	+1.0489	$0.\overline{0}$	-1.4640	-1.3760
ξ_8	17.1517	$0.\overline{0}$	+1.5386	$0.\overline{0}$	-0.0917	+0.0136
ξ_9	16.7087	$0.\overline{0}$	+1.1922	$0.\overline{0}$	+1.2494	+1.3525
ξ_{10}	16.4986	$0.\overline{0}$	-0.001	$0.\overline{0}$	+2.5707	+2.6054

TABLE IV

Stream Function, Velocities, Strain Rates and Vorticity for $\beta = \pi$ (minimum gap)

ξ	ψ/ω_2	u_α/ω_2	u_β/ω_2	$e_{\alpha\alpha}/\omega_2$	$e_{\alpha\beta}/\omega_2$	ζ/ω_2
ξ_0	0.0000	$0.\overline{0}$	-25.0090	$0.\overline{0}$	-1.3678	-1.8679
ξ_1	2.4462	$0.\overline{0}$	-24.6983	$0.\overline{0}$	-3.2987	-4.2550
ξ_2	4.8473	$0.\overline{0}$	-23.9059	$0.\overline{0}$	-5.7089	-6.6309
ξ_3	7.1553	$0.\overline{0}$	-22.6300	$0.\overline{0}$	-8.0994	-8.9563
ξ_4	9.3213	$0.\overline{0}$	-20.8684	$0.\overline{0}$	-10.4709	-11.2468
ξ_5	11.2954	$0.\overline{0}$	-18.6195	$0.\overline{0}$	-12.8241	-13.5025
ξ_6	13.0274	$0.\overline{0}$	-15.8818	$0.\overline{0}$	-15.1585	-15.7255
ξ_7	14.4660	$0.\overline{0}$	-12.6543	$0.\overline{0}$	-17.4789	-17.9142
ξ_8	15.5593	$0.\overline{0}$	-8.9321	$0.\overline{0}$	-19.7819	-20.0727
ξ_9	16.2547	$0.\overline{0}$	-4.7145	$0.\overline{0}$	-22.0697	-22.1999
ξ_{10}	16.4985	$0.\overline{0}$	-0.0000	$0.\overline{0}$	-24.3429	-24.2966

TABLE V

Stream Function, Velocities, Strain Rates and Vorticity for $\beta = \frac{\pi}{2}$ (60° C. C. W. from minimum gap)

ξ	ψ/ω_2	u_α/ω_2	u_β/ω_2	$e_{\alpha\alpha}/\omega_2$	$e_{\alpha\beta}/\omega_2$	ζ/ω_2
ξ_0	0.0000	0.0000	25.0090	0.0000	-11.8913	-12.8914
ξ_1	3.4106	0.0651	21.5041	0.1345	-11.2099	-12.0616
ξ_2	6.3782	0.1029	18.1988	0.2377	-10.5366	-11.2507
ξ_3	8.9214	0.1182	15.0918	0.3102	-9.8712	-10.4588
ξ_4	11.0591	0.1159	12.1816	0.3524	-9.2137	-9.6833
ξ_5	12.8107	0.1007	9.4667	0.3650	-8.5640	-8.9258
ξ_6	14.1965	0.0774	6.9460	0.3484	-7.9209	-8.1855
ξ_7	15.2366	0.0508	4.6181	0.3031	-7.2872	-7.4613
ξ_8	15.9525	0.0258	2.4816	0.2296	-6.6601	-6.7527
ξ_9	16.3658	0.0072	0.5354	0.1284	-6.0404	-6.0603
ξ_{10}	16.4985	0.0000	0.0000	0.0000	-5.4274	-5.4421

At $\beta = 3\pi/2$: $x(\frac{3\pi}{2}) = -x(\frac{\pi}{2})$; $y(\frac{3\pi}{2}) = y(\frac{\pi}{2})$; $\Psi(a, \frac{3\pi}{2}) = \Psi(a, \frac{\pi}{2})$; $u_a(a, \frac{3\pi}{2}) = -u_a(a, \frac{\pi}{2})$

$u_\beta(a, \frac{3\pi}{2}) = u_\beta(a, \frac{\pi}{2})$; $e_{a\,a}(a, \frac{3\pi}{2}) = e_{a\,a}(a, \frac{\pi}{2})$; $e_{a\,\beta}(a, \frac{3\pi}{2}) = e_{a\,\beta}(a, \frac{\pi}{2})$; $\zeta(a, \frac{3\pi}{2}) = \zeta(a, \frac{\pi}{2})$

TABLE VI

Angle Between Principal Strain-Rate Axis and Rotor Tangent, and Principal Strain-Rate

ξ	$\beta = 0$		$\beta = \pi/2$		$\beta = \pi$		$\beta = 3\pi/2$	
	η(deg)	E/ω_2	η(deg)	E/ω_2	η(deg)	E/ω_2	η(deg)	E/ω_2
ξ_0	45.0000	-11.9869	45.0000	11.8913	45.0000	-1.3678	45.0000	11.8913
ξ_1	45.0000	-10.3812	45.1553	11.2107	45.0000	-3.2987	44.8446	11.2107
ξ_2	45.0000	-8.8106	45.2684	10.5392	45.0000	-5.7089	44.7315	10.5392
ξ_3	45.0000	-7.2745	45.3414	9.8761	45.0000	-8.0994	44.6585	9.8761
ξ_4	45.0000	-5.7725	45.3610	9.2205	45.0000	-10.4709	44.6447	9.2205
ξ_5	45.0000	-4.3037	45.2840	8.5717	45.0000	-12.8241	44.7160	8.5717
ξ_6	45.0000	-2.8673	45.1387	7.9286	45.0000	-15.1585	44.8612	7.9286
ξ_7	45.0000	-1.4640	44.8680	7.2935	45.0000	-17.4789	45.1319	7.2935
ξ_8	45.0000	-0.0917	44.4773	6.6640	45.0000	-19.7819	45.5284	6.6640
ξ_9	45.0000	+1.2494	43.9020	6.0415	45.0000	-22.0697	46.0979	6.0415
ξ_{10}	45.0000	+2.5707	43.1005	5.4274	45.0000	-24.3429	46.8995	5.4274

TABLE VII

Dimensionless Coordinates

ξ	$\beta = 0$	$\beta = \frac{\pi}{2}, \frac{3\pi}{2}$	$\beta = \pi$
ξ_0	1.000	1.000	1.000
ξ_1	0.905	0.900	0.902
ξ_2	0.809	0.802	0.803
ξ_3	0.711	0.705	0.704
ξ_4	0.613	0.605	0.604
ξ_5	0.514	0.500	0.505
ξ_6	0.413	0.406	0.404
ξ_7	0.311	0.304	0.304
ξ_8	0.208	0.204	0.203
ξ_9	0.104	0.103	0.101
ξ_{10}	0.000	0.000	0.000